Advancing process development for antibody-drug conjugates

Incorporation of high-throughput, analytical, and digital tools

zur Erlangung des akademischen Grades eines

DOKTORS DER INGENIEURWISSENSCHAFTEN (DR.-ING.)

von der KIT-Fakultät für Chemieingenieurwesen und Verfahrenstechnik des
Karlsruher Instituts für Technologie (KIT)

genehmigte

DISSERTATION

von

Dipl.-Ing. Sebastian Andris

aus Herrenberg

Erstgutachter: Prof. Dr. Jürgen Hubbuch

Zweitgutachter: Prof. Dr.-Ing. Michel Eppink

Tag der mündlichen Prüfung: 14.05.2020

Acknowledgments

This thesis would not have been possible without the support of a number of people. In the following, I would like to thank them for their different contributions.

First of all, I would like to thank Prof. Jürgen Hubbuch for giving me the opportunity of doing my PhD in this fascinating field of research within a group of talented and motivated people. He always gave me the right amount of guidance, while leaving a lot of space for developing own ideas.

I also would like to thank Prof. Michel Eppink for taking the time of being the second advisor, his interest in my work, and his positive attitude.

Prof. Hubbuch and Prof. Eppink further made it possible that my defense could be held despite Corona restrictions as the first defense in the faculty partly done via video conferencing.

My work was partially funded by MedImmune, LLC (now AstraZeneca). I would like to express my gratitude, in particular to Michaela Wendeler and Xiangyang Wang, for believing in this collaboration. Thank you, Michaela, for all your efforts and many fruitful discussions.

One publication resulted from a collaboration with my colleague Matthias Rüdt. I always enjoyed working together and I am very grateful you shared your knowledge and experience with me.

Next, I want to thank my office mates Philipp Vormittag and Steffen Großhans. Without your input and the perfect atmosphere in 201, completing this thesis would have been a lot harder and way less fun.

My students Jonas Rogalla, Dennis Weber, Jonathan Seidel, Christopher Berg, Tom Huck, and Jan Kehrbaum did a great job in and out of the lab and I am thankful for their hard work and their ideas.

All my colleagues from MAB, current and former, have contributed to making my time here as memorable as it was. I am happy to have shared with you all the great cakes, long days in the lab, lively discussions, creative events, awesome conferences, amazing defense parties, nice seminars, and the first-time win of the legendary Kaktus Cup.

My roommates, old and new, were always there, when I needed to clear my head after a long day at the office or as an audience for a rehearsal talk. My

brothers and my friends always took care of the necessary diversion and had an open ear for my troubles.

Finally, and most importantly, I am deeply thankful to my parents for their unconditional support in this and all my other endeavors. You truly are the best.

<div align="right">

Sebastian Andris

Karlsruhe, 03.06.2020

</div>

„Eigentlich weiß man nur, wenn man wenig weiß;
mit dem Wissen wächst der Zweifel.“

Johann Wolfgang von Goethe

Abstract

Antibody-drug conjugates (ADCs) have been designed as a combination of monoclonal antibody (mAb) therapy and chemotherapy. From this fact, they draw their potential of uniting the advantages of both strategies in one molecule. mAbs have the ability to specifically bind their target antigen, thus focusing the effect on the target site of action. Due to their size and other biochemical properties, they have a good circulation half-life in the body, which is an important pharmacokinetic property. While mAbs are applied in various therapeutic fields, they form a highly important part of modern oncology. Here, mAbs are used to target antigens that are highly expressed on cancer cells, exhibiting different modes of action to fight the cancer. In order to increase their capacity of killing cancer cells, small cytotoxic molecules, as applied in chemotherapy, can be covalently attached to the mAbs, forming ADCs. Due to the decreased systemic exposure, drug molecules with higher cytotoxicity can be used. Motivated by this potential and the market approval of the first successful products in 2011 and 2013, ADCs gained a lot of attention. By the end of 2019, there were already six products on the market and over 60 candidates in clinical trials. Substantial progress has been made in areas like the development of new cytotoxic drugs, linker chemistries, and conjugation strategies. Despite these successes, the development of new ADCs remains challenging. Unfavorable pharmacokinetic profiles caused by the hydrophobic nature of the drugs and heterogeneity in the degree and site of conjugation are factors which are being improved for current ADCs. Solutions include, for example, site-specific conjugation strategies. Still, the number of parameters for optimization is high for these complex hybrid molecules. Issues range from antibody, drug, and linker over attachment chemistry to the optimal drug-to-antibody ratio (DAR). In order to unlock the full potential of ADCs, efficient, knowledge-based process development is necessary.

Also looking at the current landscape of biopharmaceutical development, it is evident that there is high pressure on process developers to efficiently deliver robust processes while gathering enhanced knowledge on process and product. One reason is the diversification of the product pipeline caused by emerging new modalities like ADCs and other antibody formats or cell and gene therapy. It increases development efforts and hinders the use of platform approaches. In addition, time to market gets more crucial with rising development costs and growing global competition, for example by producers of so-called biosimilars. Finally, it is promoted by regulatory agencies like the U.S. Food and Drug Administration or the European Medicines Agency that the concept of quality by design (QbD) is implemented in pharmaceutical development. Its

goal is for processes to be designed in a way that the desired product performance is robustly achieved in a controlled fashion. It requires increased process understanding and the thorough characterization of the relationship between critical process parameters and critical quality attributes of the product.

The goal of this thesis is to advance the process development of ADCs in the direction of more efficient, systematic, and knowledge-based approaches. As a strategy for the realization of this objective, the establishment of high-throughput, analytical, and digital tools for ADC processes was investigated. High-throughput tools, especially in combination with design of experiments (DoE), can lead to a strong increase in efficiency regarding time as well as material consumption. In order to prevent an analytical bottle neck, high-throughput compatible analytics are crucial. Also analytical techniques for the on-line monitoring of processes have great benefit. They are the basis for implementing process analytical technology (PAT) tools, which give the opportunity for real-time monitoring and control of product quality attributes. Digital tools, such as methods for the mechanistic modeling and simulation of processes, offer many advantages for process development. Apart from granting a deeper understanding of the process fundamentals, mechanistic models can be efficient tools for process optimization and characterization of the design space.
The methods for ADC process development applied or developed in this work did not rely on the highly toxic drugs used in ADCs. Instead, nontoxic surrogate drug molecules, similar in relevant properties like size and hydrophobicity as commonly used cytotoxic drugs in ADCs, were employed. The applied combination of cysteine-engineered mAb and maleimide conjugation chemistry is a strategy for site-specific conjugation with high relevance for ADC development.

In the first part of this thesis, a high-throughput process development platform for site-specific conjugation processes was developed[1]. The multi-step process of making ADCs from cysteine-engineered mAbs was successfully transferred to a robotic liquid handling station. This included a high-throughput buffer exchange step using cation-exchange batch adsorption and the subsequent automated protein quantification with process feedback. As high-throughput compatible analytics, a reversed-phase ultra-high performance liquid chromatography (RP-UHPLC) method without sample preparation was developed, focusing on a short runtime for high efficiency. The final platform was used in a conjugation DoE, showing the capacity of the method for efficient process characterization. Finally, the comparability of the high-throughput results with experiments in a larger scale was demonstrated.

The second part describes the establishment of an on-line monitoring approach for ADC conjugation reactions using UV/Vis spectroscopy[2]. First, a spectral change caused by the conjugation of the maleimide-functionalized surrogate drug to the thiol group of the engineered cysteines was detected. Spectra were recorded during the reaction in two setups with different detectors. Subsequently, the spectral change was correlated to off-line concentration data measured by RP-UHPLC using partial least-squares (PLS) regression. The calibrated PLS models enabled the prediction of the amount of conjugated drug directly from UV/Vis spectra. Both external validation data sets as well as cross-validation were used for model validation. The successful prediction of the reaction progress was shown with two different surrogate drugs in both setups.

After covering high-throughput tools, analytics, and process monitoring in the first and second parts, the third part focuses on applying mechanistic understanding towards conjugation process development. In this section, a kinetic reaction model for the conjugation of ADCs was established and the application of the mechanistic model to process development was investigated[3]. Before model calibration, six model structures were set up based on different assumptions regarding the binding to the two available cysteines. All six models were fit to a calibration data set and the best model was selected using cross-validation. The results suggest that the attachment of a first drug to the mAb influences the attachment to the second binding site. An external data set including data outside the calibration range was used for the successful validation of the model. The validated model was then applied to an *in silico* screening and optimization of the conjugation process, enabling the selection of conditions with efficient drug use and high yield of the target component. Additional process understanding was generated by showing a positive effect of different salts on the reaction rate. Finally, a combination of the kinetic model with the monitoring approach of the second part was investigated.

While the previous parts are primarily concerned with the conjugation reaction itself, the fourth part deals with the subsequent purification of the ADCs. A mechanistic model was established for the separation of ADC species with different DAR using hydrophobic interaction chromatography (HIC)[4]. This separation allows to set the target DAR also post-conjugation. For modeling the transport of solutes through the column and the adsorption equilibrium, the transport-dispersive model and a suitable adsorption isotherm were applied. First of all, a detailed characterization of the chromatography system and column was conducted, which served the calculation of a number of model parameters. The rest of the model parameters were determined by parameter estimation using numerical simulations. For the calibration, nine experiments

with different linear and step gradients were run with varying load compositions. Peak positions as well as peak shapes were accurately described by the model for all components. Applying the final model to process optimization gave step gradients with improved yield, DAR, and concentration in the pool. The successful prediction of yield and DAR in the pool of the optimized gradients was validated with external data. In a first *in silico* study, model-based process control was used to react to variations in the preceding unit operation, ensuring a robust achievement of a critical quality attribute, the target DAR. A second *in silico* study shows that a linkage of the HIC model with the kinetic reaction model developed in the third part of this thesis can be profitably applied to process development. This 'digital twin' widens the system boundaries over two adjacent unit operations, which could enable the establishment of a flexible design space over more than one process step.

In conclusion, the present thesis helps to shape the ADC process development of the future, able to cope with the challenges of a transforming biopharmaceutical industry. The whole process from the preparation of the conjugation sites over the conjugation reaction through to the purification of the conjugates was covered. Efficient characterization of the design space was demonstrated by incorporating tools like high-throughput experimentation combined with DoE, and mechanistic modeling techniques. The implementation of QbD relies on the establishment of suitable tools for acquiring enhanced process knowledge and for process monitoring and control. To this end, a PAT method for conjugation monitoring based on multivariate data analysis, and mechanistic models for conjugation and purification were developed. The presented studies showcase the realization of new ideas for exploiting the potential of digital tools for the specific challenges of ADC process development.

Zusammenfassung

Antikörper-Wirkstoff-Konjugate (*antibody-drug conjugates;* ADCs) wurden als Kombination aus der Therapie durch monoklonale Antikörper (*monoclonal antibodies;* mAbs) und der Chemotherapie entwickelt. Darauf basiert ihr Potential die Vorteile beider Strategien in einem Molekül zu vereinen. mAbs besitzen die Eigenschaft an ihr Zielantigen spezifisch zu binden, wodurch ihr Effekt auf den vorgesehenen Wirkort konzentriert werden kann. Aufgrund ihrer Größe und anderer biochemischer Merkmale weisen sie gute pharmakokinetische Eigenschaften auf, wie beispielweise eine hohe Verweilzeit im Körper. Während mAbs in verschiedenen therapeutischen Feldern eingesetzt werden, kommt ihnen in der modernen Onkologie eine besondere Bedeutung zu. Dort werden mAbs eingesetzt, die spezifisch für bestimmte Antigene sind, die auf Krebszellen stark exprimiert werden, wodurch sie verschiedene Wirkungsmechanismen entfalten können, um den Krebs zu bekämpfen. Ihre Fähigkeit Krebszellen zu töten kann gesteigert werden, indem kleine zytotoxische Moleküle, wie sie in der Chemotherapie eingesetzt werden, kovalent an die Antikörper gebunden werden. Bei dieser sogenannten Proteinkonjugationsreaktion entstehen ADCs. Dank der geringeren systemischen Exposition können hier Wirkstoffe mit höherer Zytotoxizität eingesetzt werden als in der Chemotherapie. Angeregt durch ihr großes Potential für die Krebstherapie und durch die Marktzulassung der ersten erfolgreichen Produkte 2011 und 2013, wuchs die Aufmerksamkeit für ADCs. Ende 2019 waren sechs Produkte zugelassen und über 60 Kandidaten befanden sich in klinischen Studien. Wesentliche Fortschritte wurden in Bereichen wie der Entwicklung neuer zytotoxischer Wirkstoffe, Linker-Chemie und Konjugationsstrategien gemacht. Trotz dieser Erfolge bleibt die Entwicklung neuer ADCs äußerst anspruchsvoll. Ungünstige pharmako-kinetische Profile, verursacht durch die hydrophobe Natur der zytotoxischen Wirkstoffe, und Heterogenität bezüglich des Grads und des Ortes der Konjugation sind Faktoren, die bei aktuellen ADCs verbessert werden. Zu den möglichen Lösungswegen gehören z.B. bindestellenspezifische Konjugations-strategien. Dennoch bleibt die Zahl der zu optimierenden Parameter bei diesen komplexen Hybridmolekülen groß. Von Antikörper, Wirkstoff und Linker über Konjugationschemie bis zum Wirkstoff-Antikörper-Verhältnis (*drug-to-antibody ratio*; DAR) müssen optimale Parameter gefunden werden. Um das volle Potential von ADCs auszuschöpfen, ist eine effiziente, wissensbasierte Prozessentwicklung nötig.

Darüber hinaus wird bei der Betrachtung der aktuellen Landschaft der biopharmazeutischen Entwicklung offenkundig, dass ein großer Druck auf

Prozessentwicklern lastet, auf effiziente Art und Weise robuste Prozesse abzuliefern und gleichzeitig erweitertes Prozess- und Produktwissen zu generieren. Ein Grund dafür ist die Diversifizierung der Produkt-Pipeline, die durch neue Modalitäten wie ADCs, andere Antikörper-Formate oder Zell- und Gentherapie entsteht. Dadurch erhöht sich der Entwicklungsaufwand und eine Anwendung von Plattform-Prozessen wird erschwert. Zusätzlich wird die Markteinführungszeit mit steigenden Entwicklungskosten und wachsendem globalen Wettbewerb, z.B. durch Hersteller sogenannter *Biosimilars*, immer kritischer. Schließlich forcieren die Regulationsbehörden wie die US-amerikanische *Food and Drug Administration* oder die *European Medicines Agency* die Implementierung des Konzepts *Quality by design* (QbD) in der pharmazeutischen Entwicklung. Das Ziel dieses Konzepts ist eine Art der Prozessentwicklung, durch die gewünschte Produkteigenschaften schon durch die Beschaffenheit der Prozesse zuverlässig und kontrolliert erreicht werden. Dies erfordert ein verbessertes Prozessverständnis und eine umfangreiche Charakterisierung der Beziehung zwischen kritischen Prozessparametern und kritischen Produktattributen.

Das Ziel dieser Doktorarbeit ist es, die Prozessentwicklung für ADCs in die Richtung effizienter, systematischer und wissensbasierter Ansätze weiterzudenken und solche Ansätze zu entwickeln. Für die Realisierung dieses Ziels, wurde die Etablierung von Hochdurchsatzanwendungen, analytischen Methoden und digitalen Werkzeugen untersucht. Hochdurchsatz-anwendungen, insbesondere in Kombination mit statistischer Versuchs-planung (*design of experiments;* DoE), können zu großen Effizienzsteigerungen in Bezug auf Zeit- und Materialaufwand führen. Hochdurchsatzfähige Analytikmethoden sind zwingend notwendig, um einen Engpass bei der Analytik zu verhindern. Auch analytische Techniken zur Prozessüberwachung bringen erhebliche Vorteile mit sich. Sie sind die Basis für die Implementierung von prozessanalytischen Technologien (*process analytical technology; PAT*), die wiederum die Möglichkeit zur Echtzeitüberwachung und Kontrolle von Produktqualitätsattributen eröffnen. Nicht zuletzt bieten digitale Werkzeuge, wie Methoden der mechanistischen Modellierung und Simulation von Prozessen große Vorteile für die Prozessentwicklung. Zum einen ermöglichen sie ein tieferes Verständnis der Prozessgrundlagen, zum anderen können sie sehr effizient für die Prozessoptimierung und die Charakterisierung des Parameterraumes (*design space*) eingesetzt werden.

Die Methoden zur ADC-Prozessentwicklung, die in dieser Arbeit angewendet oder entwickelt wurden, basieren nicht auf den äußerst toxischen Wirkstoffen, die für ADCs typisch sind. Stattdessen wurden nicht-toxische Surrogat-Moleküle verwendet. Diese wurden so ausgewählt, dass relevante Eigenschaften wie Größe und Hydrophobizität in der gleichen Größenordnung

lagen wie bei häufig eingesetzten zytotoxischen Wirkstoffen. Des Weiteren wurde für die Konjugation die Kombination aus einem mAb mit zwei rekombinant eingebrachten Cysteinen und der Maleimid-Chemie gewählt, eine Strategie der bindestellenspezifischen Konjugation mit hoher Relevanz für die ADC-Entwicklung.

Im ersten Teil der Arbeit wurde eine hochdurchsatzfähige Prozessentwicklungsplattform für bindestellenspezifische Konjugations-prozesse entwickelt[1]. Der mehrstufige Prozess aus den Cystein-mAbs ADCs herzustellen, wurde erfolgreich in vollem Umfang auf eine automatisierte Liquid Handling-Station transferiert. Dies schloss einen Hochdurchsatz-Pufferaustausch mit ein, der über einen Kationtauscher-Batchadsorptionsschritt realisiert wurde. Außerdem wurde darauffolgend eine automatisierte Proteinquantifizierung mit Prozess-Rückkopplung integriert. Für die hochdurchsatzfähige Analytik wurde analytische Umkehrphasenchromatographie (RPC) eingesetzt. Zur Effizienzsteigerung wurde eine Methode ohne Probenvorbereitung und mit kurzer Laufzeit entwickelt. Mit der finalen Plattform wurde ein Konjugations-DoE durchgeführt, um die Eignung der Methode zur effizienten Prozesscharakterisierung zu demonstrieren. Abschließend wurde die Vergleichbarkeit der Hochdurchsatz-Ergebnisse mit manuell, in einem größeren Maßstab durchgeführten Experimenten gezeigt.

Der zweite Teil der Arbeit beschreibt die Etablierung einer On-line-Überwachungsmethode für ADC-Konjugationsreaktionen unter Verwendung von UV/Vis-Spektroskopie[2]. Zunächst wurde eine Änderung im Spektrum festgestellt, welche durch die Maleimid-Konjugation des Surrogat-Wirkstoffes an die Thiol-Gruppen der rekombinanten Cysteine verursacht wird. Dafür wurden in zwei verschiedenen Setups mit zwei unterschiedlichen Detektoren Spektren während der Reaktion aufgenommen. Die Änderung im Spektrum wurde daraufhin mit off-line bestimmten Konzentrationsdaten aus der RPC korreliert. Verwendet wurde dafür die *Partial least squares* (PLS) Regression. Die kalibrierten PLS-Modelle ermöglichten die Vorhersage der Menge an konjugiertem Wirkstoff direkt aus UV/Vis-Spektren. Sowohl externe Daten, als auch eine Cross-Validierung, wurden für die Validierung des Modells eingesetzt. Die korrekte Vorhersage des Reaktionsfortschritts wurde mit zwei verschiedenen Surrogat-Wirkstoffen in beiden Setups erfolgreich gezeigt.

Nachdem Hochdurchsatz-Methoden, Analytik und Prozessüberwachung im ersten und zweiten Teil bearbeitet wurden, befasst sich der dritte Teil mit der Anwendung von mechanistischem Prozessverständnis auf die Entwicklung von Konjugationsprozessen. In diesem Teil der Arbeit wurde ein kinetisches Reaktionsmodell für die Konjugation von ADCs entwickelt und die Anwendung

des mechanistischen Modells für die Prozessentwicklung untersucht[3]. Vor der Modellkalibrierung wurden sechs Modellstrukturen entworfen, basierend auf verschiedenen Annahmen bezüglich der Bindung an die zwei verfügbaren Cysteine. Alle sechs Modelle wurden an ein Kalibrierdatenset gefittet und das beste Modell wurde mittels Cross-Validierung ausgewählt. Das Ergebnis legt nahe, dass die Bindung des ersten Wirkstoffmoleküls an den Antikörper die Bindung an die zweite Bindestelle beeinflusst. Ein externer Datensatz, einschließlich Daten außerhalb des Kalibrierraumes, wurde für die erfolgreiche Validierung des gewählten Modells verwendet. Das validierte Modell wurde dann für *in silico* Screening und Optimierung des Konjugationsprozesses eingesetzt. Dies ermöglichte die Bestimmung von Bedingungen mit minimalem Wirkstoffverbrauch und hoher Ausbeute der zweifach konjugierten Zielkomponente. Zusätzliches Prozessverständnis wurde dadurch generiert, dass ein positiver Effekt auf die Reaktionsrate durch Zusatz verschiedener Salze zum Puffer gezeigt wurde. Zuletzt wurde noch die Kombination des kinetischen Modells mit der Prozessüberwachungsmethode aus dem zweiten Teil untersucht.

Während in den bisher beschriebenen Teilen primär die Konjugationsreaktion selbst behandelt wird, beschäftigt sich der vierte Teil mit der darauffolgenden Aufreinigung der ADCs. Ein mechanistisches Modell der präparativen Trennung von ADC-Varianten mit unterschiedlichem DAR mittels hydrophober Interaktionschromatographie (HIC) wurde etabliert[4]. Diese Trennung gestattet es noch nach der Konjugation das gewünschte DAR einzustellen. Um den Transport von gelösten Stoffen durch die Säule und das Adsorptionsgleichgewicht zu modellieren, wurde das sogenannte *Transport-dispersive model* und eine geeignete Adsorptionsisotherme verwendet. Zunächst erfolgte eine eingehende Charakterisierung des Chromatographie-systems und der Säule, welche der Berechnung mehrerer Modellparameter diente. Die übrigen Modellparameter wurden durch Parameterschätzung mithilfe numerischer Simulationen bestimmt. Für die Modellkalibrierung wurden neun Experimente mit linearen und Stufengradienten, sowie unterschiedlichen Beladungszusammensetzungen durchgeführt. Die Peakpositionen wie auch die Peakformen wurden für alle Komponenten präzise durch das Modell beschrieben. Prozessoptimierung mithilfe des finalen Modells ergab Stufengradienten mit verbesserter Ausbeute, verbessertem DAR und höherer Konzentration in den gesammelten Produktfraktionen. Die erfolgreiche Vorhersage der Ausbeute und des DAR in den Produktfraktionen der optimierten Gradienten wurde mit externen Daten validiert. In einer ersten *in silico* Studie wurde Modell-basierte Prozesskontrolle eingesetzt, um auf Variationen in vorhergehenden Prozessschritten zu reagieren, wodurch das zuverlässige Erreichen des gewünschten DAR gewährleistet werden kann.

Eine zweite *in silico* Studie zeigt, dass eine Verbindung des HIC-Modells mit dem kinetischen Reaktionsmodell, welches im dritten Teil entwickelt wurde, für die Prozessentwicklung äußerst vorteilhaft eingesetzt werden kann. Dieser „digitale Zwilling" erweitert die Systemgrenzen über zwei aufeinander folgende Prozessschritte, was die Etablierung eines flexiblen *Design space* über mehr als einen Prozessschritt ermöglichen könnte.

Im Ergebnis ist die vorliegende Dissertation ein wertvoller Beitrag dazu, eine ADC-Prozessentwicklung der Zukunft zu gestalten, welche in der Lage ist, die Herausforderungen einer sich transformierenden biopharmazeutischen Industrie zu bewältigen. Der gesamte Prozess von der Vorbereitung der Bindestellen über die Konjugationsreaktion bis hin zur Aufreinigung der Konjugate wurde bearbeitet. Eine effiziente Charakterisierung des Parameterraums (*Design space*) wurde demonstriert, indem einerseits Hochdurchsatz-Prozesse kombiniert mit DoE, andererseits Techniken der mechanistischen Modellierung eingesetzt wurden. Die Implementierung von QbD setzt die Etablierung von geeigneten Werkzeugen voraus, um erweitertes Prozesswissen zu generieren und um Prozesse überwachen und kontrollieren zu können. Mit diesem Ziel wurden sowohl eine PAT-Methode zur Überwachung von Konjugationsreaktionen, basierend auf multivariater Datenanalyse, als auch mechanistische Modelle für Konjugation und Aufreinigung entwickelt. Die vorgestellten Studien präsentieren die Realisierung neuer Ideen, das Potential digitaler Instrumente für die spezifischen Herausforderungen der ADC-Prozessentwicklung auszuschöpfen.

Table of contents

1 Introduction

Availability of essential healthcare, like access to medical services or vaccination of children, is one of the fundamental conditions for a healthy life, next to other important factors like clean water, access to sanitation and sufficient nutrition[5]. Preventive as well as therapeutic medicines form one of the core elements of modern healthcare. While the majority of available products are still so-called small-molecule drugs (chemically synthesized compounds below a molecular weight of 1000 Da), the importance of biopharmaceutical drugs is increasing rapidly. In 2018, there were 316 biopharmaceutical products on the market with 155 approved between 2014 and 2018[6]. These 'biologics' are biological molecules derived from pharmaceutical biotechnology. The advances in the field are fueled by an ever growing scientific and technological knowledge base in biochemistry, genetics, microbiology, molecular biology, engineering, and computer technology, complementing achievements in medicinal chemistry and pharmaceutics[7]. Next to therapeutic proteins and vaccines, the scope of biopharmaceuticals is expanding towards new formats like cell- and gene-therapy to answer unmet medical needs. The majority of approved products, however, are recombinant proteins, with monoclonal antibodies (mAbs) dominating the new approvals (53% between 2015 and July 2018)[6,8]. Besides immunoglobulin G molecules (IgG), there are four other different formats of approved antibody drugs: antibody-drug conjugates (ADCs), radioimmunoconjugates, bispecific antibodies, and antibody-fragments[9]. This increasing diversity of the drug development pipeline is one of the challenges posed to scientists developing biopharmaceutical production processes, because it complicates the use of platform processes. These are very common in IgG production.

ADCs are complex hybrid-molecules comprising mAbs and small cytotoxic molecules that are covalently attached via a linker. On the one hand, this hybrid character holds great potential for cancer therapy, because both specificity of mAbs and efficacy of cytotoxic drugs can be combined. On the other hand, process development for ADCs involves specific challenges arising from the fusion of these two molecule classes. This means that specific solutions have to be investigated in order to efficiently develop suitable processes for the production of ADCs.

Generally, the production of recombinant protein drugs can be divided into

several steps. In the *upstream processing*, the drug substance is produced by fermentation, normally using either a mammalian cell line, *Escherichia coli* or yeast[6]. Also steps preceding the fermentation like cell line development and cell culture and the cell separation following the fermentation are part of *upstream processing*. Next, the drug substance is isolated during *downstream processing*, which can be divided into capture, purification, and polishing. In the case of ADCs, additional steps like the conjugation of the cytotoxic drug to the mAb and further purification steps have to be included. Finally, the drug product is prepared by formulating the active pharmaceutical ingredient (API) together with different excipients supporting long-term stability and administration to the human body. The whole process comprises many different unit operations like filtration and chromatography steps, which are designed during process development. During each molecules' way through toxicology studies, preclinical studies, and clinical studies towards market approval, the production processes must be further and further refined. This is done until a robust and reliable process is able to produce a safe product in a consistent quality. To ensure efficacy and patient safety, regulatory agencies like the U.S. Food and Drug Administration (FDA) and the European Medicines Agency (EMA) have to approve each product before commercial launch, including the production processes with design space, specifications, and manufacturing controls.

For the last decade, regulators have promoted the implementation of a concept called quality by design (QbD) for pharmaceutical development, which implies a more informed, systematic approach for process development[10]. The underlying idea is that quality should be built into products by design rather than trying to test quality into products. This is done by gaining a more profound understanding of product performance over a range of material attributes, manufacturing processes, and process parameters, yielding an expanded design space and at the same time creating opportunities for more flexible regulatory approaches. For acquiring this enhanced knowledge, possible strategies are, for example, multivariate experiments, process analytical technology (PAT), and relating mechanistic understanding to product quality[10]. For complying with these requirements and to support an efficient process development in the setting of diversifying pipelines and immense pressure to minimize time to market, different tools involving a more digitized process development can be applied. While high-throughput approaches in combination with design of experiments (DoE) are already widely spread for some applications[11–14], PAT tools in conjunction with multivariate data analysis and process development based on mechanistic modeling of processes are on their way there[15,16].

In this chapter, some of these methods are introduced in combination with the unit operations that they have been applied to in this thesis. Furthermore, the concept of antibody-drug conjugates and their specific development challenges are described.

1.1 Antibody-drug conjugates

1.1.1 Concept

The idea of creating targeted therapeutics for human diseases is older than a century and was originally brought forward by Paul Ehrlich in his vision of creating 'magic bullets' to attack pathogens but spare healthy tissues[17]. Ehrlich, who is considered the founder of chemotherapy, postulated the existence of different receptors with varying binding groups, based on experiments with different chemical dyes[17,18]. The differential affinities of these compounds for specific biological structures lead to the concept of drugs going directly to their designated targets[17,19]. The first effort to treat cancer with a chemical substance was undertaken by Goodman, Gilman and Linskog in the 1940s, who used a nitrogen mustard anticancer agent on a lymphoma patient[20,21]. Since then, chemotherapy has come a long way and new therapies like monoclonal antibodies have been developed. mAbs, in contrast to polyclonal antibodies, are produced by cells derived from a single B-lymphocyte and are directed against a single epitope. Originally, murine antibodies were used, but for reduced immunogenicity, chimeric, humanized, and even human mAbs have been developed[22,23]. mAbs bind their corresponding antigen with high specificity. Due to the fact that some receptors exist on the surface of tumor cells, which are not or less expressed on the surface of healthy cells, mAbs can be used to target cancer cells[17,24–26]. By specifically binding to these receptors, antibodies can exert different kinds of effects leading to recession of the tumor. The modes of action can be either direct or immune-mediated. Examples for direct action are through receptor blockade or agonist activity, induction of apoptosis, or delivery of a drug to the target cell. Immune-mediated modes of action range from antibody-dependent cellular cytotoxicity (ADCC) over complement-dependent cytotoxicity (CDC) to regulation of T-cell function. Finally, antibodies can have specific effects on tumor vasculature and stroma[24]. Drugs targeted to their site of action in cancer cells using mAbs are usually cytotoxic small-molecules, which are covalently linked to the antibodies, forming antibody-drug conjugates. They constitute a combination of mAbs and chemotherapy, yielding the potential for high specificity as well as high cytotoxicity. As a consequence, a lot of research and development efforts are focused on developing new ADCs. Among the 33 antibody drugs that were

in late-stage clinical development for cancer therapy by the end of 2018, eight were ADCs and many more are in earlier stages of the clinic[27]. Currently, there are seven marketed ADCs, which are described further in Table 1.1. The mode of action of ADCs is based on binding to the target cell and releasing the toxin upon internalization, thus inducing apoptosis. However, there are also ADCs being investigated using non-internalizing receptors[28,29]. Apart from the cytotoxic effect of the toxin, some mAbs can contribute to the cell killing capacity of the ADC by the modes of action described above, e.g. ADCC.

Table 1.1: There are currently seven antibody-drug conjugates on the market. The name in brackets is the trade name.

Name	Companies	Antibody	Indication
Brentuximab vedotin (Adcetris)	Seattle Genetics, Takeda	Chimeric IgG1	Hodgkin lymphoma, systemic anaplastic large cell lymphoma
Ado-trastuzumab emtansine (Kadcyla)	Genentech / Roche	Humanized IgG1	Breast cancer
Inotuzumab ozogamicin (Besponsa)	Pfizer, UCB	Humanized IgG4	Acute lymphoblastic leukemia
Gemtuzumab ozogamicin (Mylotarg)	Pfizer, Wyeth, Takeda, UCB, etc.	Humanized IgG4	Acute myeloid leukemia
Polatuzumab vedotin (Polivy)	Hoffmann-La Roche	Humanized IgG1	Diffuse large B-cell lymphoma
Trastuzumab deruxtecan (Enhertu)	Daiichi Sankyo / AstraZeneca	Humanized IgG1	Breast cancer
Enfortumab vedotin (Padcev)	Astellas / Seattle Genetics	Human IgG1	Urothelial cancer

1.1.2   ADC structure – the three components

ADCs consist of three components, a monoclonal antibody, a drug molecule, and a linker molecule, which has, among other functions, the purpose of covalently attaching the drug to the antibody. In the following, these three parts are covered in more detail.

1.1.2.1 Monoclonal antibody

As described above, the mAb is supposed to bring its payload to the site of action, the target cancer cell. For this to be achieved, a high binding affinity for the target antigen is necessary. Due to their size (no renal clearance of large biomolecules) and other factors, like FcRn-mediated recycling, antibodies exhibit long circulation times in the body (about 18-21 days for IgG1, IgG2, and IgG4), which enhances the chances of reaching their target[30]. Another prerequisite for being applied as a therapeutic is low immunogenicity, which is promoted by using chimeric, humanized, or human IgG. For illustration, the generic mAb structure is shown in Figure 1.1. A chimeric antibody has the antigen-binding variable domains of a mouse mAb and a human constant region. For humanized antibodies the complementarity-determining regions (CDRs) are taken from a mouse mAb. Depending on the humanization technology, additional residues are transferred from the parent mouse mAb[22].

Another important factor for the mAb is antigen selection. The antibody's target antigen should be highly expressed on the surface of target cells, to ensure a sufficient dose of the drug for the cytotoxic effect is delivered. In most cases, an antigen with a suitable internalization mechanism is selected for the drug to reach its intracellular target[31]. The target of the ADC trastuzumab emtansine for example is the HER2 antigen (also ERBB2, HER2/neu or CD340). HER2 stands for human epidermal growth factor receptor and is amplified in human breast cancer cell lines[26]. In addition to the cytotoxic effect of the drug, trastuzumab is able to inhibit HER2 signaling and shedding and also causes ADCC[9].
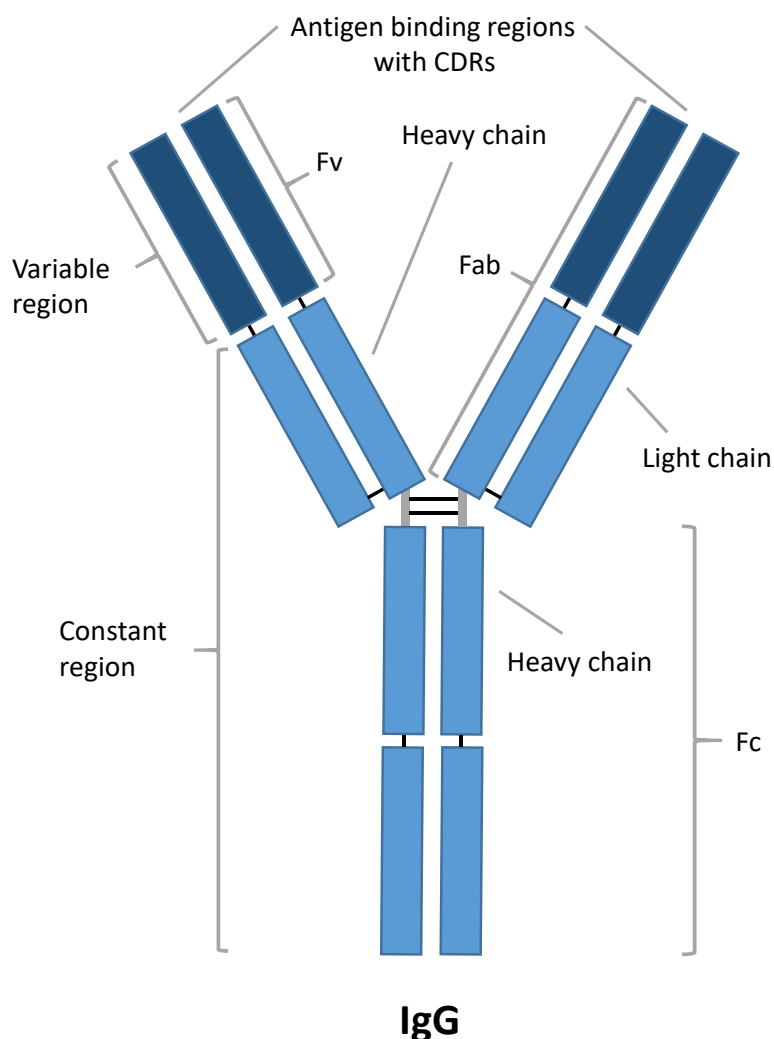
Figure 1.1: Generic structure of Immunoglobulin G.

1.1.2.2 Small-molecule drug

The goal is to use highly potent cytotoxic drugs with physicochemical properties that permit the attachment of several molecules without causing mAb aggregation or unfavorable pharmacokinetics[31,32]. Typical molecular weights of the molecules used range from 500 g/mol to 1300 g/mol. About 60% of ADCs in clinical trials use antimitotic microtubule-disrupting agents[33]. One reason is their lack of cytotoxicity towards less proliferative normal cells, which may lead to a better tolerability profile of ADCs employing these payloads. This is a valuable property, because target antigens are normally not totally tumor-specific and the administered ADC is mostly eliminated from the body by catabolism via the mononuclear phagocyte system[34]. The important molecule classes of tubulin polymerization inhibitors are auristatins and maytansinoids, but also tubulysin is used in a few cases. Despite their widespread use, the success rate is not very high, most probably due to the use of the same mechanism for different target antigens and cancer types[35]. Increasingly, other

types of molecules like DNA-interacting agents are being investigated. Examples are DNA-crosslinking compounds based on pyrrolobenzodiazepine dimers or calicheamicins, showing promising antitumor activity in clinical trials[34,36]. It remains a challenge establishing small-molecule drugs fulfilling the special requirements for application in ADCs like picomolar IC_{50} (half maximal inhibitory concentration) and suitable properties regarding solubility and stability[33,35].

1.1.2.3 Linker

The linkers' essential task is to keep the drug attached to the mAb as long as necessary for it to reach its site of action and then releasing it effectively. This means it has to be stable towards premature release during circulation. Additionally, the cytotoxic drug is in many cases hydrophobic and the linker is used to solubilize it in aqueous conditions. A linker-drug moiety is normally prepared before being conjugated to the antibody[31]. The used linkers can be categorized into cleavable and non-cleavable linkers. Cleavable linkers contain a site that is susceptible to enzymatic or chemical disintegration upon reaching the target cell, while non-cleavable linkers may remain attached to the drug and rely on the degradation of the antibody's peptide backbone to set free the drug-linker moiety. With cleavable linkers, the drug is separated from the linker by peptidases, reducing agents, or the low-pH environment of the lysosomes. Since it can have a huge impact on pharmacokinetics and efficacy, the choice of linker has to be matched to the payload and the target and each ADC will possibly require its own optimization[35,37]. Prevalent among ADCs in clinical trials are the cleavable valine-citrulline dipeptide-linker and the non-cleavable thioether linkage[35,38]. Other cleavable linkers used in a number of ADCs are acid-labile hydrazone linkers and disulfide linkers, which facilitate reductive cleavage of the toxin.

A summary of the most important ADC component properties is given in Figure 1.2.

mAb	Linker	Payload
- Selectivity and affinity - Low immunogenicity - Stability - Long circulation time - Target: abundant cancer antigen	- Stable in circulation - Stable in product storage - Releasing active payload - Optimized for target and payload	- Potency - Stability - Low immunogenicity - Amenable to conjugation - Good pharmacokinetics
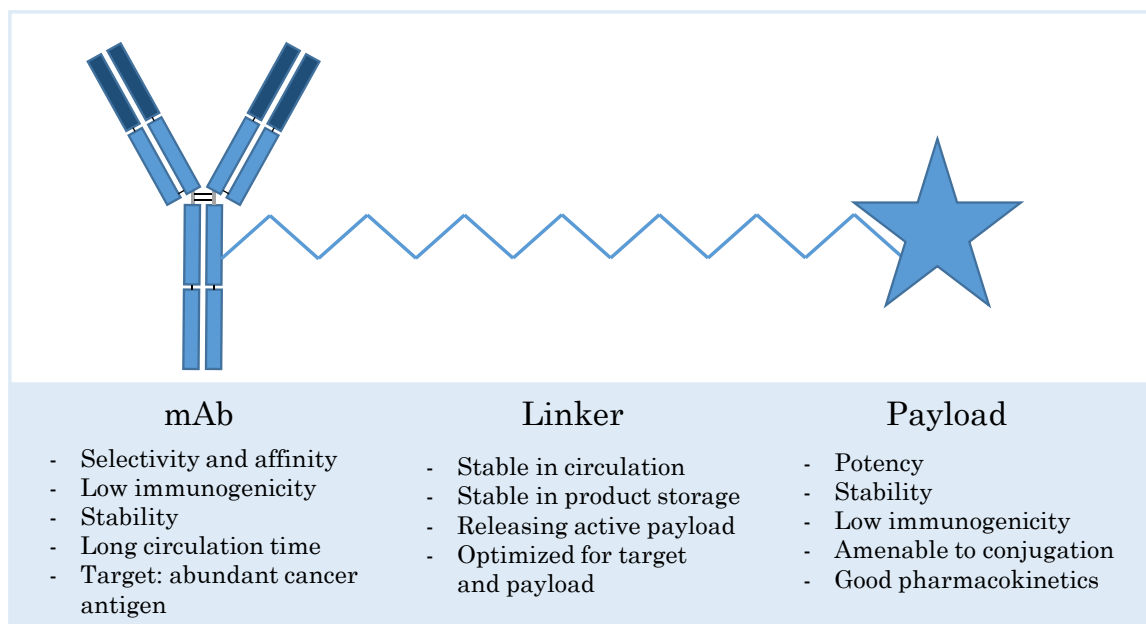
Figure 1.2: Overview of some of the important requirements for the three ADC components mAb, linker, and payload (cytotoxic drug). Figure adapted from Bakhtiar[39] and Gébleux and Casi[40].

1.1.3 Conjugation process

Protein conjugation means the attachment of other (non-polypeptide) chemical groups to a protein, in the case of ADCs via a covalent bond. Different amino acids contain various functional groups like primary amines, carboxylates, sulfhydryl, or phenolate groups, which provide reactive sites within proteins. In addition, mAbs possess an N-glycosylation site in the Fc region offering the possibility of glycoconjugation. Traditionally, lysine amines or cysteine sulfhydryl groups are employed for making ADCs, as can also be seen from the commercial ADCs (see Table 1.1). Trastuzumab emtansine (Kadcyla) for example is produced by attaching an amino-specific N-hydroxysuccinimide (NHS) ester to lysine amines forming an amide bond. Brentuximab vedotin (Adcetris) on the other hand is based on the attachment of the payload to interchain cysteines via a thiol-specific maleimide-linker. This requires a prior reduction of the interchain disulfides yielding reactive thiol groups, which can be achieved by addition of a reducing agent like tris(2-carboxyethyl)phosphine (TCEP). A drawback of these techniques is their limited site-specificity. The mAb of trastuzumab contains 88 lysines and 4 N-terminal amines of which 70 were identified having drug molecules attached to them, although the average drug-to-antibody ratio (DAR) is 3.5 [41]. In the case of brentuximab and the conjugation to interchain disulfides, there are 8 possible sites. For ADCs produced with these stochastic conjugation approaches, this leads to a highly heterogeneous mixture of conjugates with different amounts of drugs attached to different sites. These molecules potentially have varying pharmacokinetic

and therapeutic properties. For reducing heterogeneity, numerous strategies for site-specific conjugation have been developed and are being applied to the new generation of ADCs[42]. Techniques range from the incorporation of non-natural amino acids over enzyme-directed conjugations to the functional re-bridging of native disulfides[42,43]. In this introduction, only the conjugation to engineered cysteines will be covered due to its relevance to this work. It was introduced by Junutula *et al.*, who recombinantly inserted one cysteine on each heavy-chain of a mAb affording conjugates with predominantly two drugs per antibody[44]. These showed comparable efficacy but a lower toxicity compared to conventionally produced ADCs, leading to an improved therapeutic index [1]. As for the conjugation to interchain disulfides, a prior reduction step is needed to uncap the engineered cysteines, which are blocked by glutathione or cysteine[44]. In order to reform the interchain disulfides, which are also affected by the reduction, a partial re-oxidation using dehydro-ascorbic acid (DHA) can be performed. Then, the linker-drug is added and the conjugation occurs.

Selecting a conjugation chemistry and developing the conjugation reaction are essential parts of ADC development since important properties like DAR and conjugation sites are defined that directly influence pharmacokinetics, efficacy, and safety of the final product. Sun *et al.* studied this influence for maytansinoid ADCs with different DARs and showed that DARs between 2 and 6 lead to a better therapeutic index than conjugates with high DARs of 9-10 [45]. They interpret their data towards a use of DAR 3-4 for maytansinoid ADCs, but suggest the investigation of higher and lower DAR depending on target antigen biology. Regarding the conjugation site, it was shown that there is an effect on *in vivo* stability, pharmacokinetics, and therapeutic activity and approaches were developed for selecting suitable binding sites[46–49]. The objectives of selecting appropriate conjugation chemistries and conjugation sites, and of achieving the optimal DAR contribute to the complexity of ADCs and their process development. It adds to the general challenges of developing a biopharmaceutical, because the starting material for the conjugation reaction is the purified mAb. After being isolated from the harvested cell culture fluid in a number of unit operations, the mAbs used in ADCs are the product of a complete biopharmaceutical production process.

1.2 Strategies for process development of biologics

While a new molecule makes its way from candidate selection through clinical studies towards the market, different stages of process development are taking

---

[1] Toxic effect versus efficacy; e.g. toxic dose in 50% of subjects divided by efficacious dose in 50% of subjects

place. The later the stage, the more material is needed and the higher are the requirements for yield and productivity. Time constraints are ubiquitous, because time to market is crucial and a diversifying biopharmaceutical product pipeline brings new challenges. At the same time, robust processes have to guarantee product quality and safety. In the following, current strategies to overcome these challenges are described.

1.2.1 Quality by design

The International conference on harmonization of technical requirements for registration of pharmaceuticals for human use (ICH) provides a guideline for pharmaceutical development, which, since 2008, contains a part describing the principles of quality by design (QbD)[10]. In this part, important concepts and tools for pharmaceutical development from the parent Q8 guideline are further elaborated. Quality by design essentially means a more systematic approach to development, which can imply, for example, "the incorporation of prior knowledge, results from studies using design of experiments (DoE), use of quality risk management, and use of knowledge management (see ICH Q10) throughout the lifecycle of the product"[10]. A great incentive of applying such concepts is that an increased understanding of the product and the process can facilitate science- and risk-based regulatory approaches, which can increase regulatory flexibility. In the following, the most important elements of pharmaceutical development, according to the ICH guideline, will be described. First of all, a quality target product profile (QTPP) has to be established, covering aspects like intended clinical use, route of administration, dosage form, and appropriate drug product quality criteria (e.g. sterility, purity, stability). From the QTPP and from prior knowledge, potential critical quality attributes (CQAs) of the drug product can be derived. These potential CQAs guide process development and can be adjusted with increasing product knowledge and process understanding. A prioritization of CQAs can be done using quality risk management. Part of quality risk management is risk assessment, where process parameters and material attributes are linked to CQAs. Since the list of potential parameters can be long, key parameters have to be identified and then further studied to reach a high degree of process understanding. DoE and mechanistic models are important tools that can be applied in this procedure. The so-called design space is then used to characterize the connection between process inputs and CQAs. It can be represented in the form of ranges of process inputs or by more complex mathematical relationships. Also, it can be described for single unit operations, or, in order to achieve increased operational flexibility, for multiple operations. To guarantee consistent product quality, a control strategy is necessary, including in-process controls and controls of input materials, intermediates,

container closure system, and drug products. Of particular importance is the control of critical process parameters (CPP), which have an influence on critical quality attributes. Process analytical technologies are a key tool for enhanced process control approaches and will be discussed separately in Section 1.3. The enhanced process understanding and control generated by the application of these methods could support a trend from end-product testing towards in-process or real-time release testing, which means that CQAs are measured and controlled already during the process. Finally, it is advisable to implement product lifecycle management to assess means of improving product quality during the lifecycle of the product.

Implementation of these principles in the biopharmaceutical field and the corresponding need for enhanced process understanding and control is prompting research in areas like model-based process development (statistical and mechanistic) and the development of PAT tools[16,41,50–59]. These topics will be covered in the subsequent sections.

1.2.2 High-throughput process development and design of experiments

The high numbers of drug candidates and conditions that have to be tested and the narrow time frames especially in manufacturability assessment and early stage development call for efficient ways of data generation[60,61]. Here, one suitable tool is high-throughput experimentation, which is characterized by a large amount of automated, parallel experiments in very small scale. These are facilitated by using robotic liquid handling stations, which are usually equipped with arms for automated pipetting and for the handling of microplates. Often, they have integrated capabilities for mixing, centrifugation and analytics, which enable fully automated experimentation. In downstream process development, high-throughput tools are for example used for the screening of chromatographic separations, either in 96-well batch experiments or also with mini columns that are compatible with automation[62–65]. Important parameters like pH, salt, and protein concentration can be screened for different resins and different salts in an efficient manner compared to potentially dozens of chromatographic column runs[62]. Also in upstream process development, high-throughput tools can be applied, for example in micro-scale cultivations for the optimization of cultivation conditions[66]. For formulation development, information on the phase behavior of biopharmaceuticals is essential. It is strongly influenced by different factors like pH, salt type and salt concentration, which can also be screened using high-throughput methods[67,68]. Recently, high-throughput ADC conjugation approaches started gaining attention since screening of multiple linker-payload combinations on different conjugation sites at different conditions represents a practical

application[69,70]. When using these types of techniques, of course it has to be shown, that the small-scale results are representative for the process scale data.

Despite the use of high-throughput experimentation, it is still advisable to reduce the amount of data that is necessary for process development by experimental design. DoE means the "process of planning, designing and analyzing the experiment so that valid and objective conclusions can be drawn effectively and efficiently"[71]. Essentially, the dependence of relevant process outputs on inputs like process parameters is to be investigated for a specified range of inputs. DoE defines the number and type of experiments that are conducted to cover this range efficiently. Using statistical models, the relationship between inputs and outputs can then be described inside the design space. One element of DoE is randomization of experiments, in order to reduce experimental bias[71]. Another is replication, which is the repetition of an experiment or a part of it to obtain an estimate of the experimental error. Finally, it can make sense to group the experiments into blocks of experiments that share a certain property like a batch of raw materials or different operators. This is a way to eliminate variability between blocks from the experimental error.

1.2.3 Model-based process development

As touched upon in the previous parts of this section, it can be advantageous to use models in the support of process development. In all phases of the implementation of QbD, for example, different types of models can be employed[54]. By embodying a representation of the underlying process, they can help reducing experimental effort, increase process understanding, and facilitate process optimization leading to a better process and product[16,54]. There are different ways to describe a process with a model, depending on the available data and the degree of process understanding. Empirical or statistical models derived from DoE data as mentioned in the previous section are also called 'black box' models, since only a mathematical relationship between process input and output is computed. Here, a comparably low degree of process understanding is necessary, which can be helpful for very complex processes[54]. On the other side, there are mechanistic models, by analogy called 'white box' models, trying to capture the physicochemical properties of the system. This approach requires more process understanding. Equations describing the underlying processes have to be set up and suitable model parameters determined. Due to their mechanistic nature, they have the advantage that a good model is valid outside its calibration range. Finally, there are also 'grey box' models with both mechanistic and empirical features. In fact, mechanistic

models always have some empirical aspects and empirical models always have a mechanistic part[54].

An example for 'grey box' models are models based on quantitative structure-activity relationships (QSAR). These models use structure-based molecular descriptors, which are correlated to parameters of interest like chromatographic behavior or precipitation propensity[72,73]. Empirical models are for example used for the development of PAT tools, like correlating the signals of process analyzers with product data (see Section 1.3)[50,53,74]. Typical applications for mechanistic models can be computational fluid dynamics (CFD) models for bioreactor selection or modeling the chromatographic behavior of proteins (see Section 1.4)[59,75,76].

1.3 Process analytical technology

In its 2004 guidance for industry the FDA defined PAT as a "system for designing, analyzing, and controlling manufacturing through timely measurements (i.e., during processing) of critical quality and performance attributes of raw and in-process materials and processes with the goal of ensuring final product quality"[77]. The U.S. regulatory agency promotes the implementation of PAT tools with the purpose of supporting a trend towards enhanced process understanding and control in development, manufacturing, and quality assurance. The motivation is that this could move the strategy from batch processing with laboratory testing in the direction of exploiting more advanced, innovative approaches for product and process development and analysis. Well understood, monitored and controlled processes and products are in line with the QbD framework and might be able to mitigate quality risks and regulatory concerns and at the same time improve efficiency for example by facilitating continuous processing and real-time release[77].

Besides process analyzers and process control tools, also multivariate tools for design, data acquisition and analysis are necessary for the implementation of PAT. In the following, the principles of the multivariate methods applied in this work are described.

1.3.1 Principle component analysis

The principle component analysis (PCA) forms the basis for partial least squares regression (PLS, Section 1.3.2) and is thus briefly touched upon in this section. Its goal is to reduce many variables describing a set of objects to a couple of so-called latent variables or principal components (PCs) that are easier to interpret without losing important information. This often serves to

identify groups within the objects and can yield insight on which properties affect the classification[78]. For determining a PCs of the data matrix X, which consists of n observations and m variables (for example n samples with their corresponding UV absorption spectra of m wavelengths), one way is to calculate the directions or axes of greatest variance in the data. The a PCs, which are linear combinations of the original variables, then represent a new coordinate system that is able to describe the data more effectively. Every observation is projected on every axis in the new coordinate system, yielding the scores matrix T (n x a) with a score values for each observation. The scores are thus the new coordinates of the observations. The loadings matrix P (a x m) contains m loadings for each of the a PCs, constituting the 'directions' from the old coordinate system to the new. The loadings state how much each PC is influenced by each of the m old variables. Since a data reduction is performed by reducing the number of variables, there is also a residual matrix E. The PCA is consequently characterized by the following equation:

$$X = TP^{\mathrm{T}} + E \qquad (1.1)$$

Before conducting the PCA, it is often necessary to standardize the variables because otherwise variables with high absolute values would dominate the results. For that, the variables can be centered by subtracting their average and scaled by dividing by their standard deviation. When working with spectra, this step is in many cases omitted to not overemphasize regions with a low signal and by that increase noise[78]. Its capability for data and noise reduction, outlier detection and classification make it a typical method for exploratory data analysis[79].

1.3.2 Partial least squares regression

A regression problem is characterized by the goal of modeling one or more dependent variables or responses based on a set of predictor variables. Regression models are often used to predict target variables Y that are otherwise more difficult to determine by relating them to more easily accessible variables X. A very common example is relating analyte concentration to absorbance. Partial least squares (PLS) regression in its basic form is a linear multivariate regression method, which is capable of handling a large number of noisy, collinear X-variables, and also several dependent variables Y (in contrast to multiple linear regression)[80]. A schematic description of the principle of PLS regression is displayed in Figure 1.3. Essentially, in PLS regression, two PCAs are performed, one on the X-data and one on the Y-data, and the two PCAs influence each other[78]. Depending on the presence of one or multiple Y-variables, either the y-vector or the vector u_1 with the greatest Euclidean norm out of the columns of Y is used as first estimate for the scores

vector t_1 of the first PC of the PCA on the *X*-data (subscript 1 refers to the first PC). With this scores vector, a weighted loadings vector w_1 is determined by minimizing the residual *E* in the following equation:

$$X_1 = u_1 w_1^T + E \qquad (1.2)$$

After then determining the actual scores t_1 and loadings p_1 of the first PC of the *X*-data, the information is transferred to the *y*-data by using t_1 to calculate the loadings q_1 of the *Y*-data. For several *Y*-variables, this process has to be performed iteratively until t_1 converges towards u_1, which is updated in every iteration based on q_1. After calculating the first PC, its information has to be deducted from *X* and *Y* and the procedure is repeated for the next PC. After determining all PCs, the regression coefficients can be calculated from the scores and loadings matrices. These form the linear multivariate regression model, which can then be used to predict the response variables for new *X*-data. PLS regression is one of the most common multivariate data analysis (MVDA) tools used in PAT[53]. One important application is the use of spectroscopy in PAT, because the recorded spectra can result in a great number of predictor variables (e.g. wavelengths). Brestrich *et al.*, for example, used it for the selective in-line quantification of co-eluting proteins in chromatography[81].
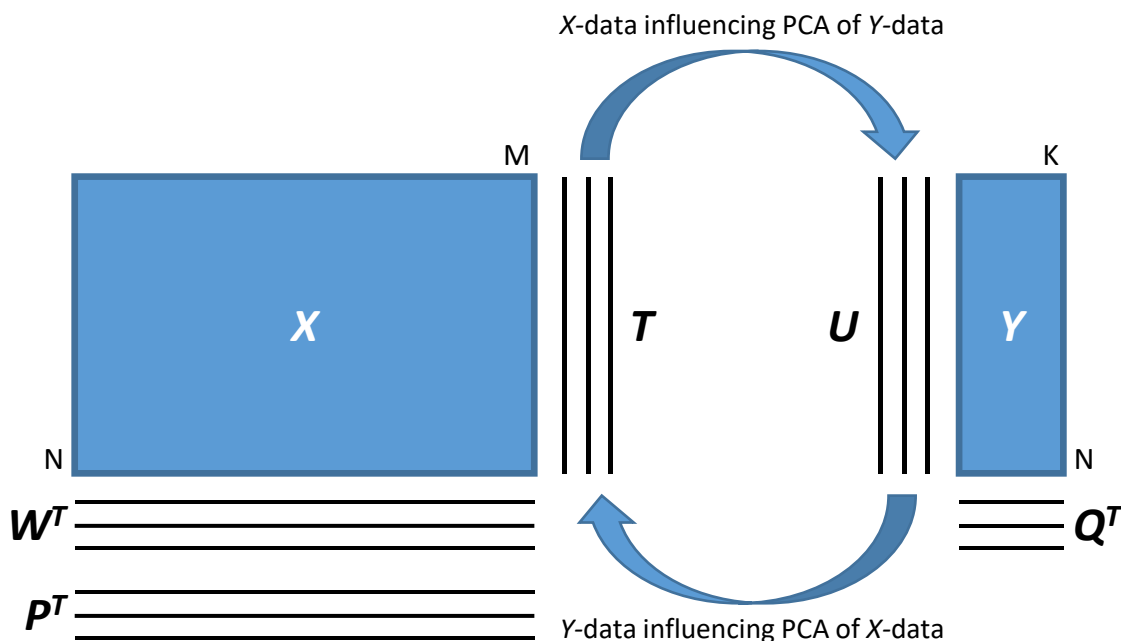
*Figure 1.3: Principle of PLS regression. A PCA is performed for predictor data X as well as response data Y. These two PCAs influence each other, resulting in a regression model for the response. T and P^T are the scores and loadings matrix for X, respectively, while W^T are the weighted loadings for X. U functions as the scores and Q^T as the loadings matrix of Y. Figure adapted from Kessler[78].*

1.4 Mechanistic modeling of liquid chromatography for large biomolecules

1.4.1 Process chromatography for biologics

Chromatography is by definition a thermal separation process applied to separating homogeneous, molecularly disperse mixtures. These mixtures constitute a fluid phase, in the case described in this section a liquid. Separation is achieved by introducing a second phase, which exhibits a differential interaction with different molecules of the first phase. This means the transfer of mass and energy between the phases, caused by a deviation from thermodynamic equilibrium[82]. By then separating the phases, a separation of the molecules from the mixture can be obtained. The second phase can be solid or liquid, here only chromatography with a solid stationary phase is described. It is called stationary, because it is fixed, in contrast to the first phase, which is called mobile phase. In liquid chromatography (LC), the stationary phase is usually packed into a cylinder, the system being called a chromatography column. While the mobile phase is pumped through the column, the molecules to be separated are retained by the solid phase by reversible, physical adsorption processes. For process chromatography of biologics, the adsorbent usually consists of a porous medium of packed beads or also membranes. Here, only columns with porous bead packing will be regarded. Components of the mobile phase with a higher affinity to the stationary phase have a higher mean adsorption time and thus a lower migration speed through the column. This can be exploited by collecting different fractions at the column end containing the separated components. The process is usually monitored at the column end, for example with UV absorption and conductivity detectors. In so-called chromatograms, the detector signal is displayed and analyzed regarding parameters like retention time of the components and resolution of the separation. Furthermore, they can be used for quantification of the processed components, given a suitable absorption profile.

In biopharmaceutical downstream processing, liquid chromatography is a very common unit operation. Most purification processes contain between one and three chromatography steps. Compared to small molecules, the processing of biologics entails a number of different requirements. For example, biopolymers like proteins are substantially bigger and thus have around 100 times smaller diffusion coefficients, which impacts mass transfer characteristics[83]. Their tertiary structure, vital for their intended function, can be negatively influenced by solution conditions or physical effects like shear stress or temperature. Consequently, preparative chromatography for biomolecules is conducted with aqueous buffers avoiding extreme conditions (pH, salt,

temperature etc.). Moreover, separation can in most cases only be achieved by running linear or step gradients of varying solution properties, because of highly different retention times[82]. A typical bind-and-elute process is composed of at least an equilibration, load, wash, and elution step. In the first step, the column is equilibrated to conditions that facilitate optimal binding of the target, before the product solution is loaded. A wash step can for example serve to remove weakly bound contaminants. In the elution, the solution conditions are changed in order to ensure the complete removal of the product from the column, which can then be collected at the column outlet, ideally separated from impurities. In flow-through mode, the impurities are bound instead of the product.

Three important techniques for the purification of biologics based on different kinds of interactions between adsorbent and solutes are affinity (AC), ion exchange (IEX), and hydrophobic interaction chromatography (HIC). In AC, the adsorption is based on specific interactions between ligand and target. The Protein A ligand used in mAb purification, for example, is a protein isolated from *Staphylococcus aureus,* which specifically binds to the Fc region of the antibodies. IEX exploits different charges between products and contaminants. The charges strongly depend on the eluent pH and the isoelectric point of the components. Retention is modified by varying the salt concentration of the eluent, a high salt content effecting weaker binding.
HIC is of interest in the ADC field due to the hydrophobic nature of the drugs that are used and is thus described in greater detail. For this type of chromatography, hydrophobic ligands like phenyl or alkyl groups are used. Like the name suggests, adsorption is caused by hydrophobic interactions between hydrophobic patches of the protein and these hydrophobic ligands. Kosmotropic salts, in contrast to chaotropic salts, promote hydrophobic interactions by the way they interact with water molecules, influencing the chemical potential of the protein in solution[84,85]. Due to this effect, a high concentration of rather kosmotropic salts is generally used for equilibration buffers in HIC. Elution is then induced by lowering the salt content. HIC is a common step for mAb polishing, but it is also applied to the separation of antibody-drug conjugates with different levels of conjugation (preparatively as well as analytics)[70,86–88].

When developing a chromatography step for a biopharmaceutical product, it is crucial to optimize the process for yield, purity, and productivity, while keeping in mind high adsorber costs and strict timelines. The parameter space is large and thus process development time-consuming and costly. This is why high-throughput tools, DoE, and increasingly also mechanistic models are applied to efficiently design robust and high-quality processes[12,14,15,63,65,89–92]. The next

section gives an introduction to the mechanistic modeling of column chromatography.

1.4.2 Mechanistic chromatography modeling

The function of a mechanistic model for a chromatography process is to describe mathematically what is happening inside the column, from fluid dynamics over mass transfer to adsorption. A calibrated model can then be used in different ways, for example to generate process understanding, for process optimization, or even root-cause investigations[89,90,93,94].

For a time and space dependent process, dynamic and microscopic balances have to be used[94]. Common models for chromatographic columns are usually based on one-dimensional mass balances as shown in Figure 1.4. This is based on assuming a homogeneous bed of equal and spherical particles, constant fluid density and viscosity, negligible radial distributions, and no convection inside the particles[94]. Furthermore, an isothermal process and inert eluents are assumed. With a set of different, connected models, it is possible to describe the adsorption equilibrium between fluid and solid phase, the components' resistance to mass transfer, and the fluid dynamics inside the column. Depending on their complexity, chromatography models may include different numbers of the effects displayed in Figure 1.4 in addition to convective transport.
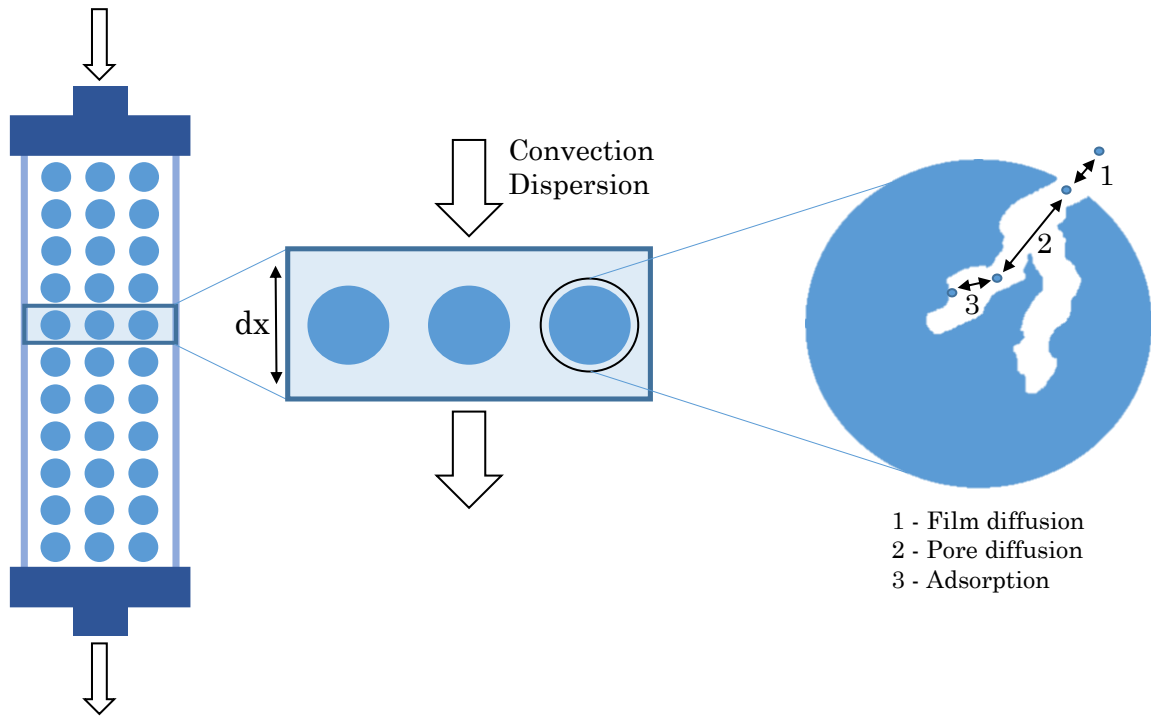
Figure 1.4: Processes in chromatographic columns, which can be modeled by setting up differential mass balances. Not included in the figure is surface diffusion, which can also contribute to mass transfer inside the pores. Figure adapted from Seidel-Morgenstern et al.[94].

For calibrating the models, a number of parameters and properties of the system have to be determined. Some are usually provided by manufacturers, some are accessible experimentally, and some need to be estimated numerically. Basic parameters like volumes and porosities can be determined by injections of non-interacting tracers[94]. The column volume V_c is split into the interstitial volume V_{int} (mobile phase) and the volume of the stationary phase V_{ads}, which consists of the solid part V_{sol} and the pore volume V_{pore}. In Equation 1.3, 1.4, and 1.5 the porosities calculated from these volumes are displayed. ε_{int} is the interstitial porosity, ε_p the porosity of the stationary phase, and ε_{tot} the total column porosity.

$$\varepsilon_{int} = \frac{V_{int}}{V_c} \tag{1.3}$$

$$\varepsilon_p = \frac{V_{pore}}{V_{ads}} \tag{1.4}$$

$$\varepsilon_{tot} = \frac{V_{int} + V_{pore}}{V_c} = \varepsilon_{int} + (1 - \varepsilon_{int})\varepsilon_p \tag{1.5}$$

The interstitial porosity is used to determine the interstitial velocity of the mobile phase u_int in Equation 1.6. $\dot{V}$ is the volumetric flow rate and d_c the inner diameter of the column.

$$u_\text{int} = \frac{\dot{V}}{\varepsilon_\text{int} \cdot \pi \cdot \frac{d_\text{c}^2}{4}} \tag{1.6}$$

In this work, the transport-dispersive model (TDM), a lumped-rate model, was used. It comprises an axial dispersion term D_ax, covering the influence of hydrodynamic effects on band broadening (e.g. quality of the packing). Inside the beads, concentration distribution is not taken into account. Instead, the TDM includes a lumped coefficient, the effective film transfer coefficient, k_eff, which combines external and internal mass transfer resistances (film diffusion, pore diffusion, and surface diffusion). A balance for the mobile phase (Equation 1.7) and a balance for the stationary phase (Equation 1.8) are necessary to describe the system. Equation 1.7 gives the change of the concentration $c_i(x,t)$ of component i in the mobile phase. The first term, describing the convective transport, is affected by the interstitial velocity u_int. In the middle is the mass transfer term, containing $k_{\text{eff},i}$, which is also influenced by ε_int, the particle radius r_p, and the difference between c_i and the pore concentration $c_{\text{p},i}$. The last term is the axial dispersion term.

$$\frac{\partial c_i}{\partial t} = -u_\text{int} \cdot \frac{\partial c_i}{\partial x} - \frac{1 - \varepsilon_\text{int}}{\varepsilon_\text{int}} \cdot \left(k_{\text{eff},i} \cdot \frac{3}{r_\text{p}} \cdot (c_i - c_{\text{p},i})\right) + D_\text{ax} \cdot \frac{\partial^2 c_i}{\partial x^2} \tag{1.7}$$

$$\varepsilon_\text{p} \cdot \frac{\partial c_{\text{p},i}}{\partial t} + (1 - \varepsilon_\text{p}) \frac{\partial q_i}{\partial t} = k_{\text{eff},i} \cdot \frac{3}{r_\text{p}} \cdot (c_i - c_{\text{p},i}) \tag{1.8}$$

The balance for the particle phase (Equation 1.8) is strongly dependent on the particle porosity ε_p and it relates the pore concentration $c_{\text{p},i}$ to the concentration adsorbed to the solid phase q_i and the concentration in the mobile phase c_i. The concentration loaded to the adsorber is a function of the pore concentration. In the case of the transport-dispersive model, no adsorption kinetics are considered and the equilibrium is given by an isotherm equation. Apart from common isotherms like Langmuir, various isotherms have been published for different types of adsorbers[75,95–97]. Depending on the isotherm, they take into account factors like salt content, concentration dependent parameters, and shielding of binding sites by bound proteins.

2 Thesis outline

2.1 Research proposal

Antibody-drug conjugates for cancer treatment are one of the recent, promising modalities taking to the growing biopharmaceutical market. Together with other new formats, they contribute to a diversifying product pipeline. While this diversification results in new solutions for so far unmet medical needs, it also poses challenges to biopharmaceutical process development by impairing the use of platform approaches. At the same time, the pressure to minimize time to market is intensified by immense development costs and growing competition. Another great challenge for process development is the implementation of the 'quality-by-design' concept, called for by regulatory agencies. It requires enhanced process and product understanding and control in order to move away from mostly heuristic approaches in process development.

Being composed of monoclonal antibodies and cytotoxic small molecule drugs, ADCs are hybrid molecules with inherent development challenges regarding, for example, product heterogeneity and pharmacokinetics. These specific characteristics have to be handled, while at the same time meeting the general challenges of biopharmaceutical process development given above. This requires the application of new tools facilitating an efficient, systematic, and knowledge-based process development. The focus of this thesis is the establishment of high-throughput, analytical, and digital methods for the purpose of advancing process development of ADCs in this direction.

A key area of ADC research is the development of site-specific conjugation strategies with the goal of increasing homogeneity and reducing drug deconjugation of next generation ADCs. The different approaches for site-specific conjugation often require multiple reaction steps that comprise many parameters to be screened and optimized. Examples are different conjugation chemistries, types and concentrations of reactants, reaction times, and solution conditions like the pH and buffer. For an efficient characterization of the design space, high-throughput tools combined with DoE approaches are highly suited. However, especially when intermediate buffer exchange steps and protein quantification are needed, it is not straightforward to perform such complex processes in a fully automated fashion. In a first study, the challenge of

21

transferring a multi-step conjugation process for site-specific conjugation of antibodies to a robotic liquid handling station is faced. The high-throughput platform needs to include an intermediate high-throughput buffer exchange and automated determination of the protein concentration with process feedback. Another challenge is the development of high-throughput compatible analytics for assessing the result of the reaction. Once developed, the applicability of the platform will be investigated in a parameter screening based on DoE and the comparability to a different scale will be evaluated.

Naturally, it is not only of interest to determine parameters like the protein concentration after process steps are completed. In order to implement process control strategies, new ways of monitoring critical process parameters (CPPs) and critical quality attributes (CQAs) have to be included in process development. An important CQA of ADCs is the drug-to-antibody ratio (DAR), which strongly influences efficacy and safety of the product. It is generally determined by analytical chromatography after stopping the reaction, which is not very feasible for an application as part of a PAT tool for reaction monitoring. This requires a method for assessing the progress of ADC conjugation reactions on-line, which will be the focus of the second study[2]. The goal will be the establishment of a fast analytical method for determining the degree of conjugation without the need for any sample handling. UV/Vis absorption spectroscopy is widely used in biopharmaceutical manufacturing and will be investigated as a fast, quantitative, and noninvasive technique. To this end, it will be examined, if the conjugation reaction of a small surrogate drug molecule to an antibody causes a spectral change. This change could then possibly be correlated to the amount of conjugated drug in the solution and thus the reaction progress. Multivariate data analysis will be applied to establish this correlation. One important part of the study will be underlining the validity of the approach by using different surrogate drug molecules and different experimental setups with different detectors. The final method may help reduce an analytical bottleneck in ADC process development and allow for real-time process monitoring, a prerequisite for the implementation of PAT approaches.

Another essential part in transforming conjugation process development towards more QbD-focused approaches is addressing it from a mechanistic angle. A kinetic model of the conjugation reaction, a central step in making ADCs, would facilitate the prediction of the product composition at any point of the reaction, enabling *in silico* parameter screening and optimization, possibly outside the calibration range. At the same time it could yield information on the underlying mechanism and thus benefit process and product understanding. Since no such models exist for ADC conjugations, the

third study will have the goal of creating a kinetic reaction model for a site-specific conjugation to a mAb[3]. For achieving an accurate model of the underlying process, different model structures will be set up and tested. The relevance for ADC process development will be demonstrated by optimizing the modeled process towards low consumption of drug and a short reaction time. Efficient drug use is crucial due to its high cost and toxicity. The need for better process understanding will be further addressed by investigating the influence of different salts on reaction kinetics. Finally, a combination of the kinetic model with the reaction monitoring approach developed in the second study is intended, which could expand its capabilities for on-line process assessment.

As elaborated above, the DAR is critical for the quality of the final ADC product. Initially, the DAR is set by the conjugation, which will be addressed in the other studies outlined in this proposal. It is also possible, however, to adjust the DAR post conjugation. To do so, it might be necessary to remove unconjugated mAb or components with unfavorable degrees of conjugation. For achieving this separation, hydrophobic interaction chromatography is the most suitable method due to additional hydrophobicity introduced by the conjugated drugs. For a critical quality attribute like the DAR, it is important to understand the relationship between process and product performance and to ensure the robust achievement of a specified range. Fulfilling these requirements usually involves extensive experimental effort. In order to reduce the lab work and possibly widen the design space and increase robustness, mechanistic models can be applied. After establishing a model for the conjugation reaction, it will thus be the goal of a forth study to develop a mechanistic HIC model for the separation of different ADC components. First, an adsorber exhibiting sufficient separation of the components will be identified, before a suitable column model and a model for the adsorption equilibrium are selected. In case of successful model calibration, it will be important to validate the capability of the model to calculate optimized HIC conditions for different load compositions. The accurate prediction of process outcomes like yield and DAR in the HIC pool needs to be validated. Finally, a combination with a mechanistic model for the conjugation reaction could be beneficial since both steps influence the final DAR.

2.2 Outline and author statement

In Chapter 4, first authorship was shared (contributed equally) among my colleague Matthias Rüdt and me. This was undertaken to elevate the quality of our common publication. A detailed listing of author contributions signed by the respective authors is given in the Appendix of the examination copy. In general, work connected to antibody conjugation reactions as put forward in Abstract and Research proposal has been performed by myself. Fundamentals for techniques concerning PAT used throughout the study, have been laid by the thesis of Rüdt, M. (2018) 'Spectroscopy as process analytical technology for preparative protein purification'.

Chapter 3: Multi-step high-throughput conjugation platform for the development of antibody-drug conjugates

S. Andris, M. Wendeler, X. Wang, J. Hubbuch

Journal of Biotechnology (2018), Volume 278, Pages 48–55

In Chapter 3, an automated high-throughput platform for antibody conjugation reactions was developed on a robotic liquid handling station. Site-specific approaches for the generation of antibody-drug conjugates often require multiple steps including an intermediate buffer-exchange. The proposed method contains all typical steps for the site-specific conjugation to engineered cysteine residues and facilitates a buffer-exchange using a batch cation-exchange step. A subsequent automated protein quantification with process feedback provides the means for accurate adjustment of reagent concentrations in the following steps. For showcasing the application of the platform towards efficient process characterization, a high-throughput conjugation DoE was conducted. Finally, the high-throughput platform showed comparable results in a comparability-study with a mL-scale manual conjugation approach.

Chapter 4: Monitoring of antibody-drug conjugation reactions with UV/Vis spectroscopy

S. Andris*, M. Rüdt*, J. Rogalla, M. Wendeler, J. Hubbuch
(*contributed equally)

Journal of Biotechnology (2018), Volume 288, Pages 15-22

In this article, the real-time monitoring of an antibody-drug conjugation reaction using UV/Vis absorption measurements and PLS regression is demonstrated. Conjugation experiments with two maleimide-functionalized surrogate drugs were conducted in a microplate setup as well as in 20 mL scale. A change in the UV/Vis absorption spectra was recorded with a Tecan microplate reader and a diode array detector (DAD), respectively. This change was correlated to the course of the reaction i.e. the amount of conjugated drug. To this end, PLS regression models were generated for the different drug molecules and the different setups and subsequently validated using cross-validation. The microplate models were additionally validated with an external test data set.

Chapter 5: Kinetic reaction modeling for antibody-drug conjugate process development

S. Andris, J. Seidel, J. Hubbuch

Journal of Biotechnology (2019), Volume 306, Pages 71-80

Chapter 5 investigates the mechanistic modeling of the reaction kinetics of antibody-drug conjugations and its application to process development. Six model structures with different assumptions regarding the mechanism were set up in the form of ordinary differential equations (ODEs). For model calibration, selection, and validation, 21 experiments with varying starting concentrations of the reactants were conducted and kinetics were recorded. After model calibration with 12 experiments, the best model was selected using cross-validation. The best model was additionally validated with an external test data set containing 9 experiments. To further enhance process understanding, the influence of different salts on the reaction rate was studied. Next, the application of the model to *in silico* process screening and optimization was demonstrated. Finally, the combination of the kinetic model with the reaction monitoring tool established in Chapter 4 was investigated.

Chapter 6: Modeling of hydrophobic interaction chromatography for the separation of antibody-drug conjugates and its application towards quality by design

S. Andris, J. Hubbuch

Journal of Biotechnology (2020), Volume 317, Pages 48-58

In Chapter 6 the application of mechanistic modeling to the preparative separation of ADC components using HIC was investigated. After thoroughly characterizing the system and the column, linear and step gradient runs with different load compositions were conducted for model calibration. The model parameters of the transport-dispersive model and a suitable adsorption isotherm were either determined experimentally or through parameter estimation. Using the model, optimized step gradient conditions were calculated and the successful prediction of peak profiles, yield and DAR was validated. Next, an *in silico* case study was conducted demonstrating the capabilities of the model to increase robustness in achieving the target DAR by reacting to variations in the conjugation. In the last part, the HIC model was combined with the kinetic reaction model established in Chapter 5, in order to study the interplay between conjugation and HIC purification in reaching the target DAR.

3 Multi-step high-throughput conjugation platform for the development of antibody-drug conjugates

Sebastian Andris[a], Michaela Wendeler[b], Xiangyang Wang[b], Jürgen Hubbuch[a] *

[a] Institute of Process Engineering in Life Sciences, Section IV: Biomolecular Separation Engineering, Karlsruhe Institute of Technology, Fritz-Haber-Weg 2, 76131 Karlsruhe, Germany

[b] MedImmune LLC, Gaithersburg, Maryland 20878, United States

* Corresponding author

Abstract

Antibody drug conjugates (ADCs) form a rapidly growing class of biopharmaceuticals which attracts a lot of attention throughout the industry due to its high potential for cancer therapy. They combine the specificity of a monoclonal antibody (mAb) and the cell-killing capacity of highly cytotoxic small molecule drugs. Site-specific conjugation approaches involve a multi-step process for covalent linkage of antibody and drug via a linker. Despite the range of parameters that have to be investigated, high-throughput methods are scarcely used so far in ADC development.

In this work an automated high-throughput platform for a site-specific multi-step conjugation process on a liquid handling station is presented by use of a model conjugation system. A high-throughput solid-phase buffer exchange was successfully incorporated for reagent removal by utilization of a batch cation-exchange step. To ensure accurate screening of conjugation parameters, an intermediate UV/Vis-based concentration determination was established including feedback to the process. For conjugate characterization, a high-throughput compatible reversed-phase chromatography method with a runtime of 7 min and no sample preparation was developed. Two case studies

illustrate the efficient use for mapping the operating space of a conjugation process. Due to the degree of automation and parallelization, the platform is capable of significantly reducing process development efforts and material demands and shorten development timelines for antibody-drug conjugates.

3.1 Introduction

Antibody-drug conjugates (ADCs) constitute a class of therapeutic molecules inspiring high hopes for patients as well as pharmaceutical companies on the basis of their potential for cancer treatment. Around 60 ADCs in clinical trials in the beginning of 2017 indicate the amount of resources that is currently and has previously been invested in their development[98]. Until 2017, the only two ADCs on the market were Seattle Genetics's brentuximab vedotin (Adcetris) and Genentech and Immunogen's trastuzumab emtansine (Kadcyla), approved in 2011 and 2013, respectively. In August 2017, inotuzumab ozogamicin (Besponsa) by Pfizer was approved for relapsed or refractory B-cell precursor acute lymphoblastic leukemia. The highly complex compounds consist of three components: a monoclonal antibody (mAb), a cytotoxic drug and a linker between the two. The intention is to combine the specificity of the mAb and the cell-killing capacity of the small molecule drug in one compound, potentially widening the therapeutic window compared to the individual cytotoxic drug.
Induced by the currently limited success of conjugation procedures where random lysines or hinge cysteines are targeted, a generation of more homogeneous ADCs with site-specific conjugation strategies is currently in development. These strategies enable control of drug-to-antibody ratio (DAR) and conjugation site, both of which heavily influence efficacy, stability and pharmacokinetics[46,49,88,99,100]. Site-specific conjugation to engineered cysteines instead of hinge cysteines has been shown to improve the therapeutic index[44]. To pave the way for this third generation of ADCs more than 40 site-specific drug conjugate technologies have been developed, often in combination with novel conjugation chemistries[98]. Many of these technologies require multi-step conjugation processes, in which a range of parameters can be varied. For the case of engineered cysteine mAbs, this usually involves a reduction step to uncap engineered cysteines and a partial re-oxidation step to reform interchain cysteines. Additionally, the residual reduction agent has to be removed before oxidation and conjugation. This adds further development challenges to the existing ones being the selection of the best target antigens and cytotoxic drugs and the development of a linker system and a suitable conjugation chemistry. Parameters like protein, reagent and drug concentrations have to be screened as well as process conditions like temperature, reaction time and mixing.
As an appropriate measure to speed up the development process, high-

throughput tools seem to be the logical choice. Yet they are only scarcely used in ADC process development, judged by the amount of literature that is available on the topic. In other biotechnological fields like the development of chromatographic separations for downstream processes, high-throughput screenings are widely used in academia and industry[63,66,101–103]. One of the reasons is that for many multi-step conjugation processes an intermediate buffer exchange or reagent removal step is necessary[44,87,99,104,105], which is more complicated to realize in a high-throughput way than simple pipetting and mixing steps. The other issue can be, that in order to achieve defined process conditions, concentration determination is necessary between steps, which is also challenging to perform in an automated, high-throughput fashion.

Vink *et al.* transferred a dialysis step, which is widely used for buffer exchange, to high-throughput scale in their 96 well crystallization block[106]. The challenge with this approach is that the dialysis time lies in the range of several days, which makes it less applicable to high-throughput conjugations. Source 30RPC reversed-phase media was successfully used for buffer exchange in a platform for high-throughput characterization of mAbs, but this strategy is suitable only for analytical applications as elution was done with 50% acetonitrile and 0.1% TFA at 50 °C [107].

With regard to antibody drug conjugation, three approaches for high-throughput platforms were found in the literature. The first one by Zimmerman *et al.* combines the cell free expression of azide amino acid containing antibodies with their purification and conjugation[108]. The purification was done using IMAC Phytips (Phynexus Inc, San Jose, USA) which require His-tagged proteins. The buffer exchange after conjugation was performed with special gel filtration plates. Since the conjugation was a single-step process, no protein quantification was integrated. Catcott *et al.* proposed a microscale platform for a single-step conjugation process where 30 kDa filter plates are used for reagent removal by repeated centrifugation and buffer addition, resulting in a diafiltration type buffer exchange[69]. They demonstrated the applicability to ADC lead selection. A solid-phase site-specific conjugation methodology was developed by Puthenveetil *et al.* consisting of a multi-step conjugation to engineered cysteines where each step is conducted with the antibody bound to Protein A/L beads[70]. This facilitates the removal of reagents or the exchange of buffers by washing the beads with the desired buffer but raises the question of the comparability to solution-phase conjugations.

What becomes apparent is the absence of an automated high-throughput platform for a multi-step solution-phase conjugation process with broad applicability to site-specific conjugations. This work proposes, at the example of the multi-step conjugation to engineered cysteine antibodies, the transfer of the complete sequence of steps needed for this reaction to a robotic liquid handling station. The 96-well high-throughput process includes an automated

intermediate buffer exchange, using a cation-exchange resin, with subsequent protein quantification. Instead of cytotoxic payloads, non-toxic fluorophores are used as surrogate drugs. The suitability of the approach to screen conjugation reaction conditions is demonstrated and the comparability to reactions in milliliter scale is investigated.

3.2   Materials and Methods

3.2.1   Chemicals

For reduction of disulfides tris(2-carboxyethyl)phosphine hydrochloride (TCEP, Sigma-Aldrich, St. Louis, USA) was used. (L)-dehydroascorbic acid (DHA, Sigma Aldrich) was used for re-oxidation of interchain disulfides. As substitute for a cytotoxic drug 7-Diethylamino-3-(4'-Maleimidylphenyl)-4-Methylcoumarin (CPM, Sigma-Aldrich) was selected. Dimethyl sulfoxide (DMSO, Sigma Aldrich) was necessary to dissolve DHA and CPM. N-acetyl cysteine (NAC, Sigma Aldrich) was applied as quenching reagent. For buffer preparation NaH_2PO_4 x 2 H_2O and K_2HPO_4 were obtained from VWR International GmbH (Darmstadt, Germany) and NaCl and KCl from Merck KGaA (Darmstadt, Germany). All buffers were titrated to the desired pH with 4 M NaOH (Merck KGaA) and filtered through a 0.2 µm cellulose acetate membrane filter (Sartorius AG, Göttingen, Germany).

3.2.2   Model system and conjugation process

Purified IgG1 mAb with two engineered cysteines as conjugation sites was provided at a concentration of 12.4 mg/mL in PBS (+5 mM EDTA, pH 7.2) by MedImmune, LLC. CPM was used as a non-toxic maleimide-functionalized surrogate drug and conjugated to the antibody's engineered cysteines via its maleimide linker. The reaction scheme is shown in Figure 3.1. The initial step in the conjugation process was a mild reduction with TCEP to uncap engineered cysteine residues. To re-establish interchain disulfides, reduction was followed by partial re-oxidation. The conjugation reaction was stopped by addition of excess NAC. Detailed process and reagents are described in the following section.
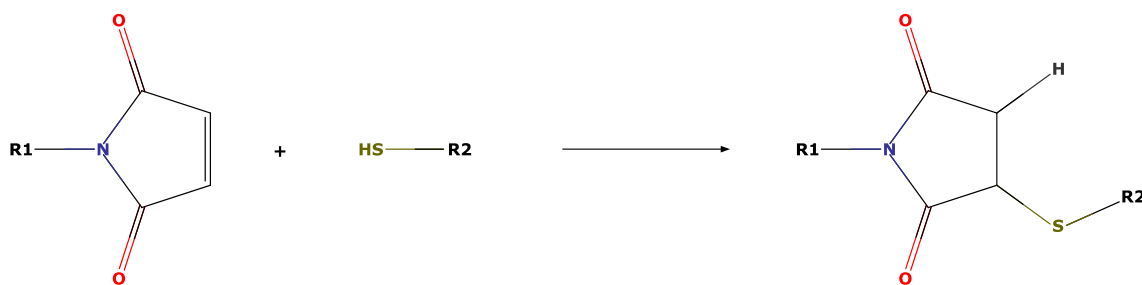
Figure 3.1: Reaction scheme for the conjugation reaction. The maleimide functionality of the CPM molecule reacts with the thiol group of the two engineered cysteine residues of the antibody, forming a stable thioether bond.

3.2.3 Multi-step high-throughput conjugation

An overview of the process is shown in Figure 3.2. Automated liquid and microplate handling was done on a Freedom EVO 200 platform (Tecan Group Ltd., Männedorf, Switzerland) with an integrated Infinite 200 PRO multimode plate reader (Tecan Group Ltd.). The platform was controlled via the Freedom EVOware software (Tecan Group Ltd.). All steps were performed at a temperature of 22 °C. For all incubation steps, the microplate was covered by a lid to minimize evaporation.

The purified antibody was transferred to a 96 well U-bottom polypropylene (PP) microplate (#650201, greiner bio-one GmbH, Frickenhausen, Germany) and diluted to the desired concentrations with 50 mM sodium phosphate buffer at pH 7.2 ("equilibration buffer"), resulting in a volume of 245 µL per well. For global reduction of disulfides 40 molar equivalents of TCEP in equilibration buffer were added. The plate was incubated for 2 h 15 min on the integrated orbital shaker (Te-Shake™; Tecan Group Ltd) at 700 rpm. During the reduction, a 96 well 0.2 µm GHP filter plate (#8082, AcroPrep™ Advance; Pall Corporation, New York, USA) was manually prefilled with a strong cation-exchange resin (POROS™ XS; #4404338, Life technologies, Foster City, USA). Each well was filled with 65 µL of 56% slurry in 18% ethanol. The filter plate was placed inside the liquid handling station for further processing. First, the storage solution of the resin was removed using the integrated Te-VacS™ vacuum filtration system (Tecan Group Ltd.). Next, the resin was equilibrated three times with 200 µL of equilibration buffer. To prevent the resin from drying out, the equilibration was programmed to be finished shortly before the end of the reduction step. The equilibrated resin was used to remove TCEP after the reduction, conducting a solid phase buffer exchange. 225 µL of reduced mAb solution were transferred to the filter plate to be loaded onto the resin. After 15 min of orbital shaking at 1000 rpm, the load solution was removed and the resin with bound mAb was washed once with 150 µL of equilibration buffer. The first elution step was done by adding 112.5 µL of 50

mM sodium phosphate buffer with 500 mM NaCl ("elution buffer") and incubating for 10 min while shaking at 1000 rpm. The eluate 1 was removed by vacuum filtration and collected in a 96 well F-bottom PP microplate (#655201, greiner bio-one), before conducting the second elution in the same way. Eluate 1 and 2 were mixed at 1000 rpm for 80 s. With 25 µL of the resulting 225 µL of eluate a concentration determination was conducted (see next paragraph) and the pipetting volumes were updated accordingly by Matlab (Mathworks, Natick, USA). Then, the re-oxidation of interchain disulfides was started by addition of 20 molar equivalents of DHA dissolved in DMSO. The plate was incubated for 1-4 h with mild mixing (700 rpm). For the conjugation reaction, the surrogate drug CPM was dissolved in DMSO and added to the re-oxidized antibody in molar excess depending on the application. After 45 min, a molar excess of 12 equiv of NAC over CPM dissolved in ultrapure water was added to quench the reaction.
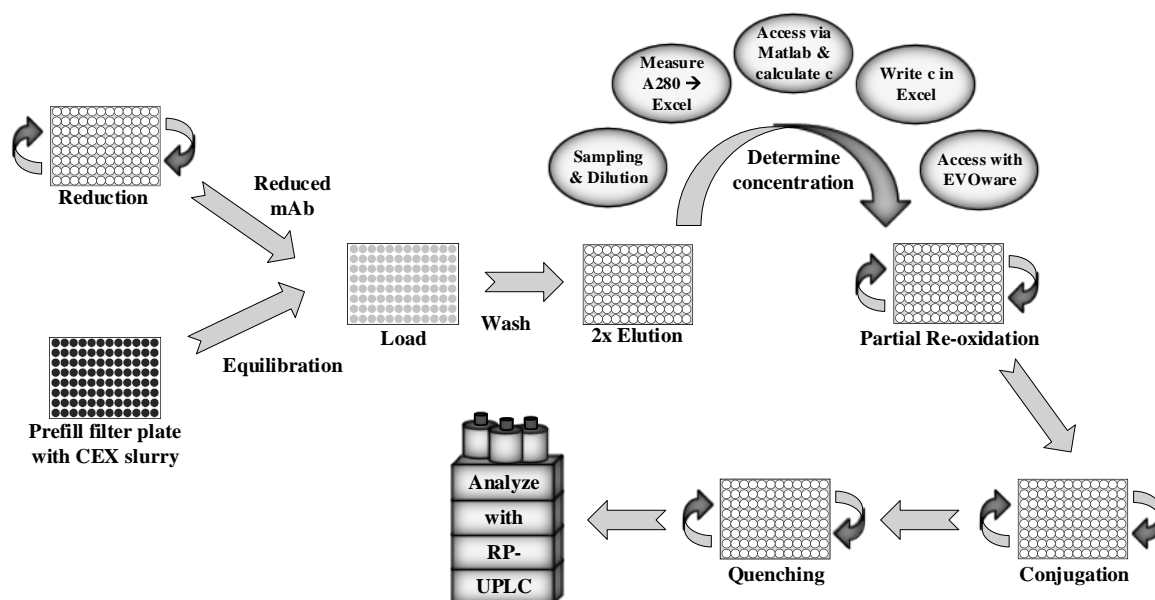
Figure 3.2: High-throughput platform for conjugation process development on automated liquid handling station. The concentration c stands for the mAb concentration after the buffer exchange step, which is determined to calculate reagent concentrations for the following steps.

3.2.4 Protein quantification

This step is part of the Freedom EVOware script which was created for the whole process. After the buffer exchange step, the resulting protein concentration in the eluate has to be determined. For this purpose, a 25 µL sample is taken from each well and diluted with 175 µL of elution buffer in a 96 well UV-Star microplate (#655801, greiner bio-one). With the integrated plate reader, absorption at 280 nm is measured and the resulting excel file is automatically accessed by Matlab. With a previously determined calibration

factor the protein concentration is calculated and entered into the source excel file, from which EVOware receives the pipetting volumes. This way, the mAb concentration is updated during the process to achieve accurate molar ratios for oxidation and conjugation.

3.2.5 Optimization and characterization of CEX buffer exchange step

In the experiments conducted to optimize slurry volume and determine yield and reproducibility, the buffer exchange procedure was generally as described in the high-throughput conjugation section. To be able to determine the yield of the steps, load, wash and elution were collected in UV-Star microplates and the concentrations were determined with the Tecan plate reader. For concentrations over 2 mg/mL, samples were diluted with elution buffer for the measurement. The slurry volume study was run with a starting mAb concentration of 10 mg/mL, which equals a loading of 53-73 g per liter of resin for the investigated slurry volumes of 55-75 µL. To reduce material consumption, the reproducibility study was run at 2 mg/mL.

3.2.6 Analytics

To assess the result of the conjugation, reversed-phase ultra-high performance liquid chromatography (RP-UHPLC) was applied. A Dionex Ultimate 3000 system was used, equipped with pump unit, RS autosampler, RS column compartment and diode array detector (Dionex Softron GmbH, Germering, Germany). No sample preparation like reduction was required for this method as the native mAbs were analyzed. An Acquity UPLC Protein BEH C4 column (#186004495, Waters Corporation, Milford, USA; 300 Å, 1.7 µm, 2.1 mm x 50 mm) was used with a flow rate of 0.45 mL/min at a temperature of 80 °C. Solvent A consisted of 0.1% trifluoroacetic acid (TFA) in ultrapure water, solvent B was 0.1% TFA in acetonitrile. Equilibration and injection were done at 26% B. After 0.2 min, % B was raised to 30%. Then, a 4.8 min gradient from 30% to 38% B was run for separation of the conjugated samples. Including the following strip at 95% B and 1.2 min of re-equilibration the entire method had a runtime of 7 min. UV signals at 280 nm and at the corresponding absorption maximum of the used surrogate drug were recorded (384 nm for CPM). Concentrations of ADC species were calculated using a calibration curve for mAb concentrations and the ratio of CPM absorption at 280 nm and 384 nm. To determine monomer content, a TSK Gel SuperSW mAb HTP 4.6x150 mm column (#22855, Tosoh Bioscience, Griesheim, Germany) was used with isocratic flow of SEC-buffer (200 mM K2HPO4, 250 mM KCl, pH 7) for a runtime of 8 min (0.3 mL/min).

3.2.7   High-throughput conjugation DoE

A central composite face-centered design with 3 center points was created with the statistics software MODDE 10.1 (Sartorius Stedim Data Analytics AB) to test the high-throughput approach with the mAb and CPM model system. mAb concentration and CPM excess were varied as factors in the DoE. mAb concentration range was set between 2 and 6 mg/mL and CPM excess between 2 and 10 equiv. All runs were performed at once according to the high-throughput conjugation procedure described above, except reduction was run for 3 h and oxidation for 4 h. Samples were analyzed using RP-UHPLC.

3.2.8   Comparability study

To showcase the potential of the high-throughput platform and at the same time show comparability with a standard mL-scale procedure, the reaction kinetics of the model conjugation system were investigated once using the described high-throughput approach and once in mL-scale. For the mL-scale, conjugation reactions were conducted manually in 2 mL centrifuge tubes (Eppendorf AG, Hamburg, Germany), reduction and oxidation in 50 mL centrifuge tubes (VWR). The same conditions, reagents and incubation times were used as for the high-throughput conjugation. During all incubation steps, light mixing was applied with Thermo Mixer MKR 13 (HLC BioTech, Bovenden, Germany). After reduction, a buffer exchange was performed by dialysis to remove residual TCEP. For this, Slide-A-Lyzer dialysis cassettes (#66807, Thermo Fisher Scientific) with a 10,000 Da molecular weight cut off (MWCO) were used in 2.0 L of equilibration buffer at 4 °C (overnight). For concentration determination after buffer exchange, a NanoDrop 2000c spectrometer (Thermo Fisher Scientific) was used. The model system consisted of the engineered antibody and CPM which was used as a surrogate drug and conjugated to the antibody's engineered cysteines.

2 and 4 mg/mL of antibody were selected as starting concentrations and duplicates were run for both concentrations. To assess the kinetics, the reaction was quenched at different time points up to 20 min. For the HTC, a separate well was assigned to each time point and quenched accordingly. In mL-scale, 100 µL samples were drawn from the tubes at each time point and added to a prepared quenching plate containing NAC. All samples were analyzed by RP-UHPLC, the ones from the HTC also with size-exclusion chromatography (SEC).

3.3 Results and Discussion

3.3.1 Implementation of high-throughput conjugation process on liquid handling station

The model process utilized for this work consisted of the site-specific attachment of a maleimide-functionalized fluorophore (surrogate drug) to two engineered cysteine residues in a mAb. This process involves multiple steps: reduction with TCEP to remove capping groups from the engineered cysteines; removal of reducing agent via buffer exchange; re-oxidation of interchain disulfide bonds with DHA; conjugation with the maleimide-functionalized surrogate drug; quenching of residual free drug by addition of NAC. To obtain a fully automated, high-throughput, microscale conjugation process, every part of the multi-step conjugation process had to be transferred to the liquid handling station, with the most challenging being the high-throughput buffer exchange. Weight-based liquid classes were generated for pipetted solutions to assure high accuracy in pipetting (data not shown). To reduce loss when transferring samples, U-bottom microplates were used. This way, all but < 20 μL of a sample can be transferred from one plate to another.

Several methods were assessed regarding the high-throughput TCEP removal, the first one being the commercially available Immobilized TCEP Disulfide Reducing Gel (Thermo Scientific). The rationale was to conduct the reaction in a filter plate and afterwards remove the reduced mAb solution via vacuum filtration. This concept was abandoned due to insufficient reduction and unspecific adsorption of the mAb to the agarose beads, which could not be improved sufficiently by addition of low amounts of salt. Next, a size-exclusion type approach was studied. Zeba Spin Desalting Plates (40 kDa MWCO, ThermoFisher Scientific) were used to exchange the buffer and remove TCEP. Here, the main drawback was the low maximal sample volume of 100 μL which decreases flexibility or increases complexity for the application in the high-throughput conjugation process. Also the use of ultrafiltration plates (Acroprep Advance Omega 30 kDa, Pall) with repeated centrifugation and buffer addition was discarded due to low reproducibility. The issues with all of these methods could be eliminated by developing a buffer exchange step based on cation exchange (CEX). To facilitate this high-throughput CEX-step, a high capacity CEX-resin was pipetted into a 0.2 μm filter plate. As described in the methods section, the reduced mAb was loaded onto the CEX-beads at low salt content and pH 7.2, washed with equilibration buffer to ensure effective TCEP removal and then eluted with high salt buffer also at pH 7.2 (500 mM NaCl). The possibility to keep the pH constant is a great advantage compared to using a Protein A resin like Puthenveetil *et al.* in their solid-phase conjugation

process[70], as no neutralization is necessary. The other issue with Protein A could be that certain linkages like acid-labile cleavable hydrazone linkers might be sensitive to low pH exposure during elution. The advantage of the solid-phase conjugation approach is that removal of residual free drug can be done by repeatedly washing the solid support before elution without further steps. In the present approach this feature could possibly be included by adding another CEX buffer exchange step after conjugation.

The CEX step was initially optimized regarding protein yield, which is predominantly depending on binding characteristics and the volume of resin slurry used per well. Slurry volume was optimized with the goal of finding the optimum between insufficient binding capacity and large carryover volume. An excess of slurry results in a higher carryover volume after elution, because part of the liquid stays in the pores and the interstitial volume due to capillary forces. Different amounts of slurry between 55 µL and 75 µL were tested and the yield of the buffer exchange step was determined. As can be seen in Figure 3.3, left panel, the loss during the load step decreased from 10.5% to 4.9%, when the slurry volume was increased from 55 µL to 75 µL. However, the yield after elution did not increase accordingly, which is shown in the right panel of Figure 3.3. For lower amounts of resin, the yield is lower due to insufficient binding capacity. It reaches a maximum between 65 µL and 70 µL, before it starts falling again at 75 µL. This can be attributed to the effect of the higher carryover volume, which starts to outweigh the effect of binding capacity. The mAb concentration in this study was 10 mg/mL and the achieved yield was above 85%. In order to decrease complexity, the slurry volume was set constant at 65 µL for the final platform, although yields vary for different protein concentrations. This is practical for a screening method, where maximum yield is not the primary objective. To further lower the protein loss, two elution steps with half the volume were included in the process instead of one. In accordance with Coffman *et al.*[62], 60% of the resin bed volume was assumed as liquid carryover volume. With this assumption, a resin bed volume of 36.4 µL and a filter plate hold up of 12 µL, the calculated yield can be improved by about 8% for two elutions with 112.5 µL compared to one elution with 225 µL. The maximum theoretical yield in this scenario would be 94.7%. The actual impact was tested with a mAb solution at 4 mg/mL and the yield was improved by 8.5% for two elutions compared to one elution.

It is important to show that the buffer exchange step is reproducible for the different wells of the microplate. If not, it would lead to varying starting conditions when the subsequent oxidation and conjugation steps are investigated. Different factors can influence the reproducibility of the approach. Among these are for example the usage of different pipetting tips of

the liquid handling arm for different rows of the plate, inhomogeneity of the vacuum filtration unit or the filter plate itself or inaccurate pipetting of the slurry volume. For this reason, a reproducibility study was performed for the CEX buffer exchange step with 18 wells at equal conditions in different parts of the plate. The relative standard deviation of the mAb-concentration after buffer exchange was at 1.6% for the different wells. This means that the developed step is a robust way for a high-throughput buffer exchange performed automatically by a liquid handling station without the need for expensive commercial solutions or pH neutralization. Compared to dialysis, which is often used for reagent removal or buffer exchange for smaller volumes[70,109,110] time savings are significant.

After TCEP removal, the next steps are re-oxidation and conjugation. For both steps, reagents are added at a fixed molar ratio to antibody. This means that before continuing the process, the protein concentration has to be determined in order to calculate the correct amounts of DHA and surrogate drug to add. For this purpose, an absorption-based protein quantification step was successfully incorporated into the EVOware script, using Matlab to calculate the new concentration and update the pipetting volumes in the excel source file loaded by EVOware (see Methods section). In a single-step process like the conjugation platform developed by Catcott et al.[69], this in-process control is less essential. For a multi-step process like site-specific cysteine conjugation however, it contributes to guarantee defined process conditions for parameter screenings during oxidation and conjugation.
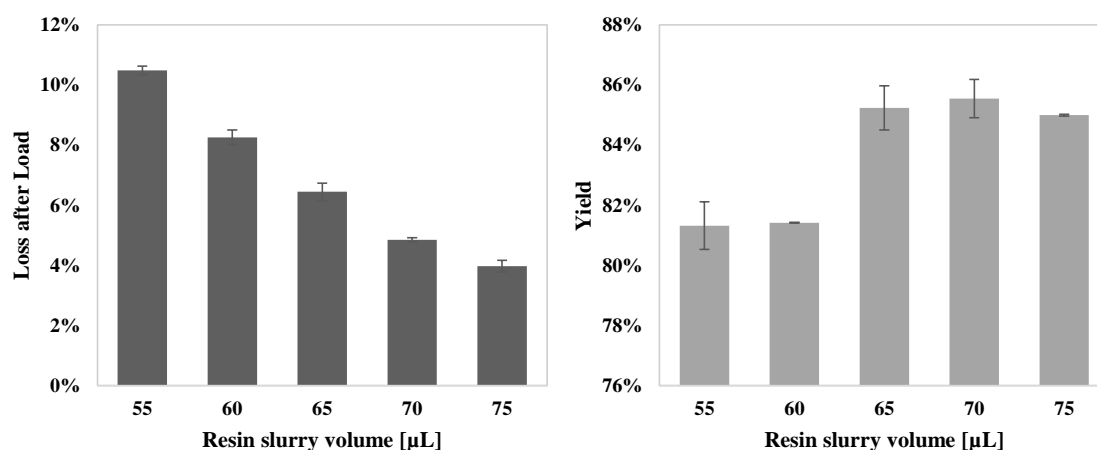

Figure 3.3: Results of slurry volume study for TCEP removal step at 10 mg/mL of antibody. Left: Protein loss during load for different resin slurry volumes. Right: Protein yield of total buffer exchange step for different resin slurry volumes.

3.3.2 Analytics

A high-throughput method is not functional without high-throughput compatible analytics. To analyze the result of an antibody conjugation reaction, conjugate species with different drug loading have to be separated and detected. For this reason, a chromatographic separation assay was developed with the focus on low method runtime. With the RP-UHPLC assay, sufficient separation between unconjugated mAb, mono-conjugated mAb und di-conjugated mAb was achieved with a total runtime of 7 min and no lengthy sample preparation. An example chromatogram from the comparability study is shown in Figure 3.4. The starting concentration was 2 mg/mL and the conjugation was stopped after 45 s to have enough un- and mono-conjugated mAb in the samples. The residual free drug is well separated from the conjugate species. Between mAb and mono-conjugated mAb, resolution was 1.38, between mono- and di-conjugated mAb resolution was 1.56 (calculated according to EP-Norm). Taking into account that in this case a small molecule surrogate drug of about 400 Da is attached to a 150 kDa antibody and that method runtime was of primary concern, separation was satisfactory. Due to higher hydrophobicity of the real payloads used for ADCs, separation will be improved. From the resulting peak areas, concentrations of the different species and DAR can be calculated. Compared to methods in literature separating ADC conjugate species with runtimes up to 50 min, this method should be well suited to characterize ADCs in HTS applications[70,111,112]. A quick size-exclusion based method would have the advantage that monomer content and DAR can be determined at the same time[69], but the amounts of different conjugate species, which play a defining role for pharmacokinetics and efficacy[111], cannot be assessed.
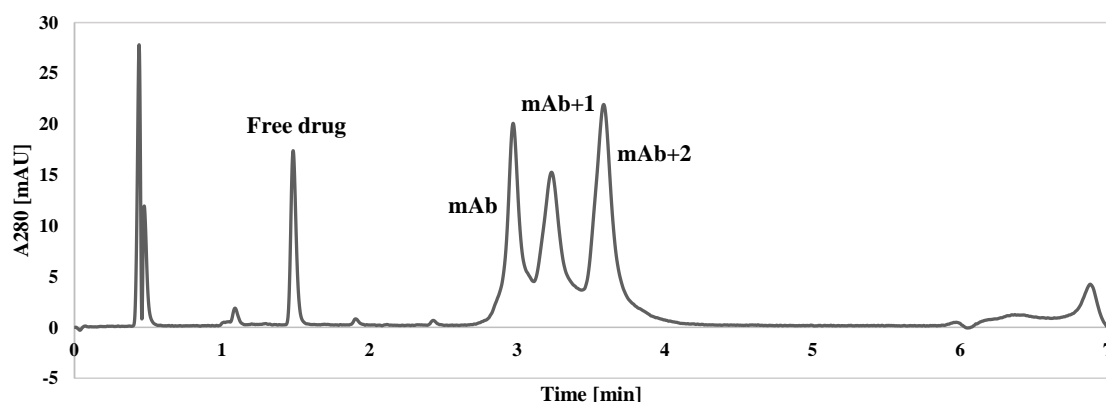

Figure 3.4: Reversed-phase chromatogram of the analytical separation of unconjugated, mono-conjugated, di-conjugated antibodies and residual free CPM. This example was taken from the comparability study. The starting concentration was 2 mg/mL and the conjugation was stopped after 45 s.

3.3.3 High-throughput conjugation DoE

In order to test the established platform and to show that a model conjugation process can be characterized efficiently, a DoE for the conjugation step was run. mAb starting concentration and excess surrogate drug were varied as factors. A multiple linear regression model (MLR) was calibrated for three responses being the relative amounts of un-, mono- and di-conjugated mAb. R^2 values were all at 0.96 or above and Q^2 by cross-validation was 0.92, 0.96 and 0.93, respectively. The experimental data and the response surfaces of the MLR-models are shown in Figure 3.5. The dominating factor was CPM excess, with the tendency of more CPM resulting in more conjugation. For the mAb concentration, an influence towards lower conjugation could be determined, but model coefficients were around the significance barrier (95% confidence interval). In the samples with 2 equiv of CPM, over 30% of unconjugated mAb was left, while almost no residual CPM was detected. This means the amount of CPM was insufficient for complete conjugation, although 2 equiv should be enough to attach 2 CPM molecules per antibody. The reason is probably unspecific adsorption of CPM molecules to the walls of the PP reaction vessels due to their hydrophobicity.

Efficient characterization of the conjugation step using the high-throughput platform was demonstrated. The excess of CPM needed for efficient conjugation can be drawn from the model. This information can help to limit the use of the cytotoxic drugs to a minimum. To obtain a more clear and reliable picture of the factor effects, the design space should be extended and covered with more samples. This underlines the suitability of high-throughput tools for conjugation process development, as 'numbering up' of experimental conditions is possible with low use of resources.
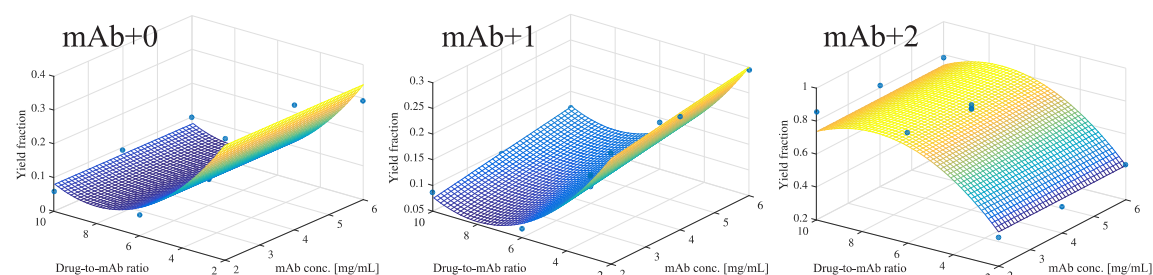

Figure 3.5: MLR-Results for conjugation DoE of engineered cysteine mAb with surrogate drug CPM. Dots: Experimental data of DoE. Mesh: Response surface of MLR-models. mAb+0: Yield fraction of un-conjugated antibody. mAb+1: mono-conjugated antibody. mAb+2: di-conjugated antibody.

3.3.4 Comparability with mL-scale reaction

To illustrate the potential and the comparability of the high-throughput conjugation (HTC) with conjugations in conventional centrifuge tubes, a comparability study for the conjugation step was conducted with both set-ups at two different protein concentrations in duplicates. For the HTC, TCEP removal was achieved via the CEX buffer exchange step. One reaction was run for each time point and stopped at the corresponding time with NAC. For the mL-scale reactions, TCEP removal was done via dialysis overnight. At each time point, samples were taken from the reaction mixture and quenched by adding them to a microplate containing NAC stock solution. Apart from the reaction vessel, this was the main difference between both approaches. The results of the conjugation were determined by RP-UHPLC and are shown in Figure 3.6. In general, the reaction is slower for the mL-scale, where the steady state is reached later for both concentrations. This difference can likely be attributed to different mixing parameters. The reaction is taking place very rapidly, so that small differences in quenching efficiency have a strong influence on the curve. The immediate mixing with the NAC stock solution is more efficient for the mL-scale approach due to the fact that the microplate shaker used in the HTC system was programmed to stop very briefly for the quenching step.

The conjugation reactions were faster for the higher protein concentration. In Figure 3.6A (2 mg/mL) steady state is not completely reached within the 20 min that were monitored. In Figure 3.6B (4 mg/mL), steady state is almost reached after 6 min. This trend can also be seen for the HTC, although it is less pronounced due to the higher reaction rate. However, the final outcome of the reaction is the same for all four experiments: 90 ($\pm$2)% of di-conjugated mAb and 5 ($\pm$2)% for mono- and unconjugated mAb. This results in an average DAR of 1.84 and 1.86 for HTC and mL-scale, respectively. Also, monomer content for the HTC was at about 99% as seen for the mL-scale conjugations (data not shown). These are the essential physicochemical properties for the comparability of the high-throughput conjugation to larger scale approaches. It shows successfully that the high-throughput platform results can be compared to mL-scale reactions. Further scale-up studies are needed to validate the approach with large scale data. With respect to the buffer exchange step it can be stated that the amount of salt used for elution (500 mM NaCl) does not disturb the following reaction steps.

Regarding the efficiency of data generation, there are several advantages for the automated HTC compared to the manual approach. First of all, the total duration of the process is reduced substantially by elimination of the slow dialysis step, which is usually done overnight. After preparation, the liquid handling station performs all process steps independently without any user

input. This means the operator can focus on other tasks until transferring the microplate to a UHPLC for analysis. Finally, there is the obvious advantage of any high-throughput screening approach, which is that the number of screened conditions can be increased without significant increase in workload and material demand. For the present study only 32 wells were used in order to save material for further studies.
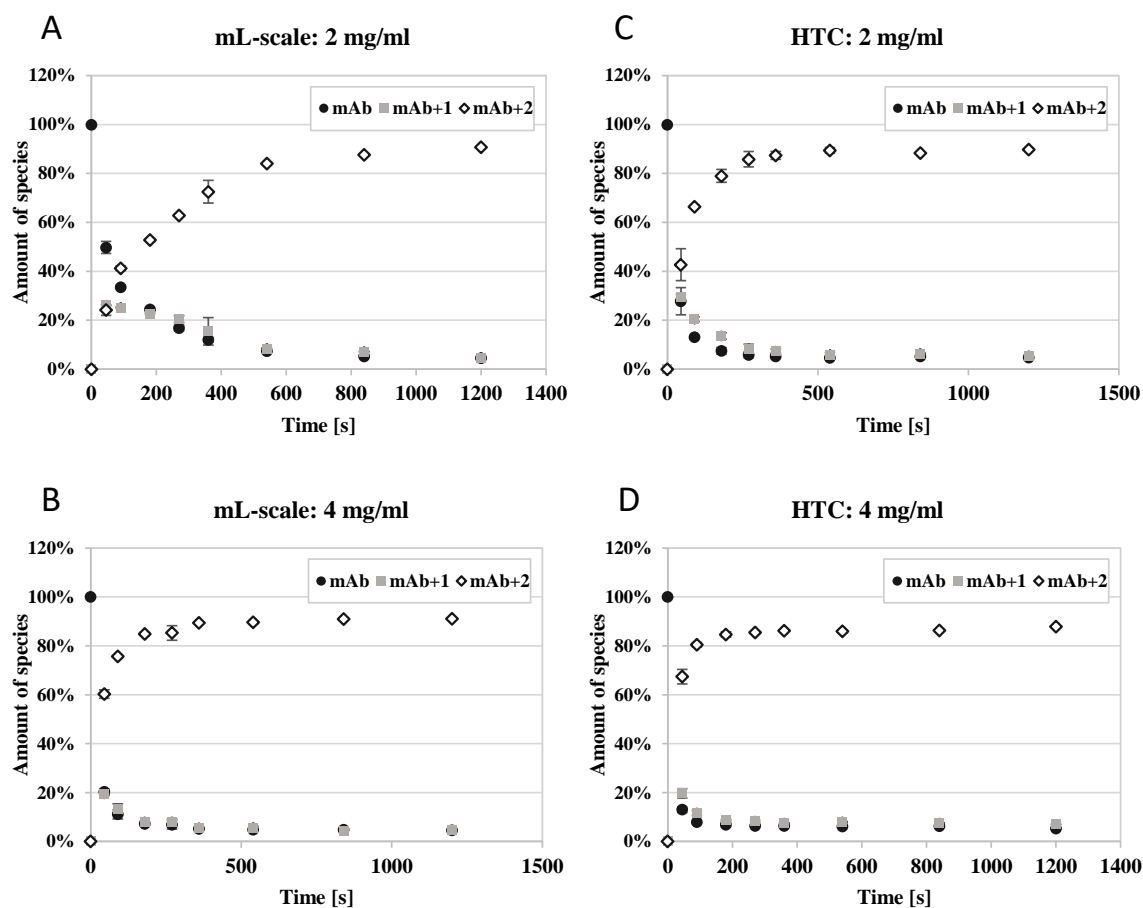
Figure 3.6: Comparability study with 2 and 4 mg/mL starting antibody concentration. Comparison of reactions in mL-scale process (A, B) and 200 µL-scale automated high-throughput process (C, D). The amount of each conjugate species (unconjugated, mono-conjugated, di-conjugated) is depicted as a function of reaction time.

3.4 Conclusion

A fully automated high-throughput platform for solution-phase site-specific conjugation of small molecules to antibodies was successfully established. Due to the high-throughput buffer exchange step and the intermediate concentration determination, it is applicable to multi-step processes that, in many cases, require a removal of reagents between reaction steps. The proposed method for buffer exchange using CEX can be performed with high

yields around physiological pH for IgG1 conjugations and no neutralization is necessary after elution as for Protein A. Automated protein quantification with process feedback facilitates addition of reagents in subsequent steps in correct molar ratios. To complete the platform a high-throughput compatible analytical RP-UHPLC method was developed, suitable for determination of DAR and concentration of conjugate species which are relevant parameters for ADC efficacy and pharmacokinetics. In two case studies for site-specific engineered cysteine conjugation using the non-toxic fluorophore CPM as a surrogate drug, the potential of the approach to efficiently characterize conjugation reactions was demonstrated. It was shown that the amount of salt needed for elution does not affect conjugation efficiency compared to a mL-scale reaction with dialysis buffer exchange. The final outcome of the conjugation reaction was not influenced by the smaller scale or different mixing characteristics. A more detailed study on scaling-up conjugation reactions from microscale to lab- or pilot-scale would be worthwhile to be able to transfer detailed process parameters after mapping the design space. Obviously a direct transfer of reaction conditions determined with surrogate drugs to real-drug conjugations is not practical without prior validation, but process parameters like mixing and pipetting settings should be mostly independent from the payload. This means the platform can be applied to ADC process development without significant further development effort. Especially because all steps before conjugation were developed only with the antibody and the relevant reagents. This way, the platform could play an important role in establishing high-throughput tools in antibody-drug conjugation development and thus more efficiently address the challenges posed by the complexity of site-specific conjugation procedures. A crucial thrust for the development of next-generation ADCs could be achieved by framing certain design guidelines derived from the extensive screening of different target antigens, drug-linker moieties, conjugation sites, reaction conditions and other parameters significant for next-generation ADCs.

Acknowledgments

4 Monitoring of antibody-drug conjugation reactions with UV/Vis spectroscopy

Sebastian Andris[ac], Matthias Rüdt[ac], Jonas Rogalla[a], Michaela Wendeler[b], Jürgen Hubbuch[a] [*]

[a] Institute of Process Engineering in Life Sciences, Section IV: Biomolecular Separation Engineering, Karlsruhe Institute of Technology, Fritz-Haber-Weg 2, 76131 Karlsruhe, Germany

[b] Department of Purification Process Sciences, MedImmune LLC, Gaithersburg, Maryland 20878, United States

[c] These authors contributed equally to the work.

[*] Corresponding author

Abstract

The conjugation reaction of monoclonal antibodies (mAbs) with small-molecule drugs is a central step during production of antibody-drug conjugates (ADCs). The ability to monitor this step in real time can be advantageous for process understanding and control. Here, we propose a method based on UV/Vis spectroscopy in conjunction with partial least squares (PLS) regression for non-invasive monitoring of conjugation reactions. In experiments, the method was applied to conjugation reactions with two surrogate drugs in microplate format as well as at 20 mL scale. All calibrated PLS models performed well in cross-validation ($Q^2 > 0.975$ for all models). In microplate format, the PLS models were furthermore successfully validated with an independent prediction set ($R^2_{\mathrm{pred}} = 0.9770$ resp. 0.8940). In summary, the proposed method provides a quick and easily implementable tool for reaction monitoring of ADC conjugation reactions and may in the future support the implementation of process analytical technologies (PAT).

4.1 Introduction

ADCs are among the most promising new formats in the biopharmaceutical industry[98]. More than 60 candidates are currently evaluated in clinical trials. ADCs gain their potential from combining the high selectivity of monoclonal antibodies (mAbs) with the high cytotoxicity of small-molecule drugs. Next to specificity and cytotoxicity, ADCs also inherit other attributes of both species, such as the absorption bands of both protein and drug and an often increased hydrophobicity compared to unmodified mAbs due to the non-polar character of the drugs[113–115].

One of the most central steps during ADC production is the conjugation reaction which links the drug to the mAb via a linker. The conjugation reaction may either be site-specific or unspecific, with next-generation ADCs mainly focusing on site-specific conjugation reactions with well-defined drug-to-antibody ratios (DARs)[31,116,117]. The conjugation yield and DAR are generally measured off-line by analytical hydrophobic interaction chromatography (HIC) or reversed-phase chromatography (RPC), often in combination with mass spectrometry[118]. This is, however, time-demanding and needs manual sample handling. If only the DAR needs to be measured without the concentration of each conjugate species, a simple method relying on UV/Vis absorption measurements can be applied[118]. It requires the drug to have an absorption band different from the one of the protein (≈ 280 nm). Using the absorption at both maxima and the respective extinction coefficients, the concentrations of protein and drug can be mathematically determined without further analytical methods. The technique has been used for conjugations with different drugs like the maytansinoid DM1 and dipeptide-linked auristatins (e.g. vcMMAE)[111,119], but is limited to purified conjugates, as residual free drug and other possibly UV-active contaminants have to be removed. As a consequence, this approach as well as analytical chromatography are not very well suited for fast and prompt characterization of ADC conjugation reactions. Therefore, only complex analytical solutions are found so far for the monitoring of these reactions. Size-exclusion chromatography (SEC) with a post-column reaction was proposed for DAR determination of cysteine-conjugated ADCs[51]. Tang *et al.* present an approach for rapid DAR measurement by fast deglycosylation and LC-MS detection[120].

It would be highly beneficial to establish a fast analytical method for monitoring the progress of conjugation reactions without any sample processing. Ideally, such a method would also provide the means for application as a process analytical technology in accordance with the PAT initiative by the Food and Drug Administration (FDA). For this, the applied method needs to be

fast, without manual sample handling, and robust[121]. To monitor the process, the method should be sensitive to the progress of protein conjugation reactions. UV/Vis absorption spectroscopy is a rapid, noninvasive, and quantitative method which is widely established in biopharmaceutical manufacturing. It has previously been applied to process monitoring of proteins and small molecules[53,81,122–124]. Hansen *et al.* showed the potential of UV/Vis spectroscopy to distinguish between different proteins based on their content of aromatic amino acids and their solvatization[124]. The method was later transferred to chromatographic separations by Brestrich *et al.*[81]. There are some examples of UV/Vis spectroscopy in reaction monitoring applications. Quinn *et al.* followed a small-molecule reaction in lab scale using fiber-optic UV/Vis spectroscopy[125]. Gurden *et al.* employed a model based on UV/Vis absorption data to detect and diagnose process variations in a non-protein biochemical conversion reaction [126].

Drugs used in ADCs frequently feature delocalized electron systems thus providing absorption bands in the UV/Vis range [118] besides the ones of the aromatic amino acids of the mAbs. Spectral shifts of UV/Vis absorption may not only be caused by a structural change in the UV/Vis active compounds, they can also occur as a result of changes in the local environment of the chromophores[127,128], e.g. a change in solvent composition. If the conjugation reaction thus causes a change in the environment of the aromatic amino acids or the drug, it will cause spectral shifts which in turn may help to monitor this type of reaction.

This work investigates a new and easily applicable method for on-line conjugation reaction monitoring. Monitoring was accomplished by a combination of UV/Vis spectroscopy and partial least squares (PLS) modeling. Spectra were recorded and analyzed during conjugation reactions in two different scales with different UV/Vis detectors. Based on the results, a method was established for small-scale screening in 96-well plates which provides an estimate of the amount of drug conjugated to the antibody by PLS regression. Two different surrogate drugs, 7-diethylamino-3-(4'-maleimidylphenyl)-4-methylcoumarin (CPM) and N-(1-pyrenyl)maleimide (NPM), were applied in both setups. Additional variability was introduced by changing the concentrations of the reactants. The method was then adapted to a lab-scale conjugation reaction with an on-line diode array detector (DAD) to show applicability as a PAT tool.

4.2 Materials and Methods

4.2.1 Chemicals

For disulfide reduction, tris(2-carboxyethyl)phosphine hydrochloride (TCEP, Sigma-Aldrich, #C4706) was used. (L)-dehydroascorbic acid (DHA, Sigma Aldrich, #261556) was used as oxidation agent for re-oxidation of interchain disulfides. As nontoxic substitutes for cytotoxic drugs, 7-diethylamino-3-(4'-maleimidylphenyl)-4-methylcoumarin and N-(1-pyrenyl)maleimide (both Sigma-Aldrich, #C1484 and #P7908) were selected. Their structural formulae are shown in Figure 4.1. Dimethyl sulfoxide (DMSO, Sigma Aldrich) was used to dissolve DHA, CPM and NPM. N-acetyl cysteine (NAC, Sigma Aldrich, #A7250) was applied to quench residual free drug. For buffer preparation, Na-H_2PO_4 x 2 H_2O was obtained from VWR International GmbH. The buffers were titrated to the desired pH with 4 M NaOH (Merck KGaA) and filtered through a 0.2 µm cellulose acetate membrane filter (Sartorius AG, Göttingen, Germany).
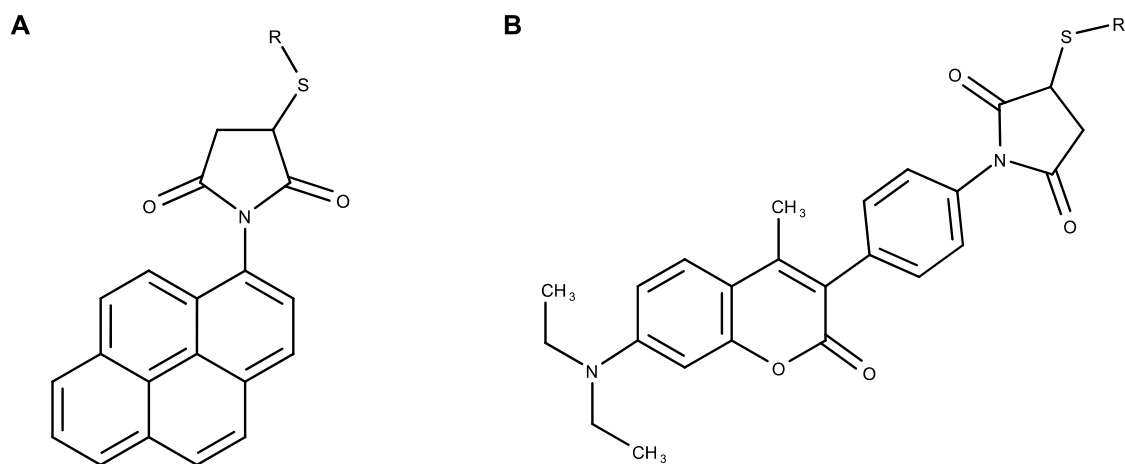
Figure 4.1: The structures of conjugated NPM (A) and conjugated CPM (B) are shown. R denotes the protein.

4.2.2 Model system and conjugation process

Purified IgG1 mAb with two engineered cysteines as conjugation sites was provided at a concentration of 12.4 mg/mL in PBS (+5 mM EDTA, pH 7.2) by MedImmune, LLC. CPM and NPM were used as non-toxic maleimide-functionalized surrogate drugs and conjugated to the antibody's two engineered cysteines via their maleimide linker. For the conjugation experiments, aliquots of the engineered mAb stock solution were thawed and diluted to the desired concentration (2 mg/mL) with 50 mM sodium phosphate buffer (pH 7.2). The resulting mAb concentrations were determined with a

Nano Drop 2000c spectrometer (ThermoFisher Scientific, Waltham, USA).

The following mAb preparation steps (reduction and re-oxidation) were conducted in 50 mL centrifugation tubes (VWR International GmbH). A reduction step was performed to uncap engineered cysteine residues. For this purpose, a 40-fold molar excess of TCEP (over mAb concentration) was added to the mAb solution. After 3 h of incubation at room temperature, the reduced mAb solution was transferred into a dialysis cassette with a 10 kDa molecular weight cut-off to remove TCEP. The dialysis was performed in a volume of 1.7 L of 50 mM sodium phosphate buffer at 5 °C over night (approx. 19 h). The mAb concentration after dialysis was determined with the Nano Drop spectrometer.

For re-oxidation of the interchain disulfide bonds, 20-fold molar excess of DHA (3 mM stock solution in DMSO) was added. The mixture was incubated at room temperature for 4 h. Through addition of the DHA solution, DMSO content was increased to around 8.5%. To remove potential precipitate before spectroscopic conjugation monitoring, the mAb solution was filtered through a 0.2 µm polyethersulfone syringe filter (VWR International GmbH). The final mAb concentration for the conjugation experiments was set via dilution with 50 mM sodium phosphate buffer containing 10% of DMSO. Conjugation experiments were executed with mAb concentrations in the range of 1.0 mg/mL to 2.0 mg/mL.

The conjugation reaction in the different experimental setups was started by addition of the surrogate drug (NPM or CPM) to the re-oxidized mAb solution. The molar ratio (drug to mAb) was set to 2 for the NPM conjugations and to 3 for CPM. The concentration of the surrogate drug stock solutions was varied (2 - 6 mM) depending on the mAb concentration to result in a final DMSO content of approximately 10%. This content of DMSO was maintained to ensure solubility of the hydrophobic surrogate drugs in the water-based solution. The conjugation reaction was quenched by addition of a 12-fold molar excess of NAC (over the applied amount of surrogate drug) to ensure the immediate termination of the conjugation reaction.

4.2.3   High-throughput on-line monitoring experiments in microplate format

The high-throughput conjugation experiments were conducted in 96-well UV-transparent microplates (UV-STAR®, Greiner bio-one GmbH, Frickenhausen, Germany). The reaction was monitored by the acquisition of UV/Vis absorption spectra of the reaction mixture in the range from 250 nm to 450 nm with an Infinite M200 microplate spectrometer (Tecan Group Ltd., Männedorf, Switzerland). To allow for the correlation of UV/Vis absorption data with the progress of the conjugation reaction, spectra had to be recorded while different time points of the reaction were sampled. The used experimental setup is

depicted in Figure 4.2. The UV-microplate was divided into *monitoring wells* designated for UV/Vis absorption measurements and *quenching wells* designated for off-line analytics. In the latter, the reaction was quenched at different time points to generate samples for off-line analysis. The six monitoring wells contained 200 µl of liquid and were further separated into two blank wells and four reaction wells. One blank well contained buffer solution, the other one re-oxidized mAb. The remaining monitoring wells were used for reaction monitoring in duplicates under two different conditions. There were 16 quenching wells for each of the two screened conditions, containing 100 µL of the corresponding reaction mixture. In this study, the mAb concentration was varied in the range of 1.0 mg/mL to 2.0 mg/mL while all other process conditions were kept constant for all experiments. This resulted in 6 calibration and 2 prediction runs for NPM and 5 calibration and 2 prediction runs for CPM.

The conjugation reaction was started by adding the surrogate drug to the re-oxidized mAb solution in a 50 mL centrifugation tube. After short mixing, aliquots were transferred immediately to the microplate. The reaction in the first quenching well was instantly stopped by addition of NAC solution before placing the microplate into the reader and starting the on-line monitoring procedure. The UV/Vis spectra acquisition was controlled by the software Magellan (Tecan Group Ltd.) according to the following process: Prior to each measurement, the plate was shaken for 15 s (orbital shaking, 1.5 mm amplitude, 335.8 rpm). For the first 22 min or 25 min, single spectra were recorded and after each measurement, one well was quenched. At later time points more spectra were acquired between each quenching step, resulting in quenching time intervals of 4 min to up to 10 min. The spectral range for the conjugation reaction with NPM was defined at 250 nm to 390 nm and for CPM at 250 nm to 450 nm (step size: 4 nm, 5 reads) to cover the characteristic absorption maxima of the surrogate drugs. The conjugation reaction was monitored over a run time of 50 min. Afterwards, the microplate was centrifuged (1789 g, 7 °C) to remove potential precipitate prior to off-line analysis. The supernatants were measured by reversed-phase ultra-high performance liquid chromatography (RP-UHPLC).
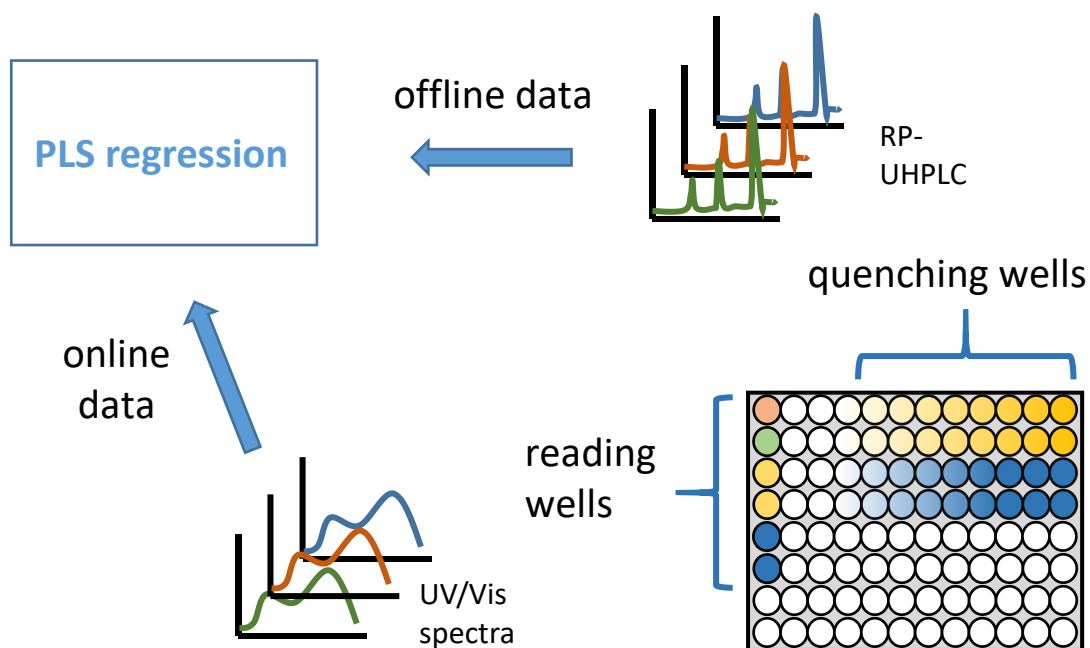
Figure 4.2: Experimental setup used for high-throughput on-line monitoring in microplate format. UV/Vis spectra were recorded during the conjugation reaction using the integrated Tecan plate reader. Reactions in the quenching wells were stopped at different time points and analyzed by RP-UHPLC. On-line and off-line data was used for the generation of PLS regression models.

4.2.4   20 mL lab-scale on-line monitoring experiments

Preparation of the mAb was conducted as described above in the conjugation process section. The re-oxidized mAb solution at a concentration of 2 mg/mL was used for the experiments. Here, the acquisition of UV/Vis spectra was performed with an Ultimate 3000 DAD (Dionex Softron GmbH, Germering, Germany) with a semi-preparative flow cell (volume 0.7 μL, 0.4 mm path length) at a spectral resolution of 1 nm. The experimental setup consisted of a 50 mL beaker glass as reaction vessel, a peristaltic pump (Minipuls 3, Gilson, Villiers de Bel, France) with marprene pump tubing, and the DAD. All elements were connected via PEEK tubing (0.5 mm diameter). By attaching the beaker glass to a thermal shaker (HLC BioTech, Bovenden, Germany), the solution was continuously mixed at 200 rpm and the temperature was kept constant around 23 °C. The reaction mixture was circulated from the reservoir via the peristaltic pump through the DAD flow cell and back into the reservoir. In- and outlet were placed below the liquid surface. The flow rate was approximately 3 mL/min which equaled the maximum speed of the peristaltic pump (48 rpm).

Prior to monitoring the reaction, the DAD was equilibrated with sodium phosphate buffer for 2 h and with re-oxidized mAb solution for 15 min. Autozero of the DAD signal was performed either with re-oxidized mAb (NPM

experiments) or with sodium phosphate buffer (CPM experiments). After DAD 'warm-up', the reactions were started by addition of the surrogate drugs in the molar ratio of 2 for NPM and 3 for CPM. Three runs were performed for each surrogate drug.

The conjugation reactions were monitored over 30 min while UV/Vis spectra were acquired by the DAD every 0.2 s. To reduce noise, the spectra were then averaged over 10 s. The recorded spectral range was 250 nm to 390 nm for NPM experiments and 250 nm to 450 nm for CPM experiments.

Over the runtime of 30 min, 21 samples were taken and transferred to a 96-well microplate for off-line analysis. The wells were previously loaded with NAC stock solution to facilitate immediate quenching of the reaction upon sampling. After termination of the experiment, the microplate was centrifuged (1789 g, 7 °C). The supernatant was analyzed by RP-UHPLC.

4.2.5 Reversed-phase chromatography

To assess conjugation results, RP-UHPLC was applied as described previously[1]. An Ultimate 3000 system was used, equipped with pump unit, RS autosampler, RS column compartment and diode array detector (Dionex Softron GmbH). Reduction or different sample preparation was not required. An Acquity UPLC Protein BEH C4 column (Waters Corporation, Milford, USA; 300 Å, 1.7 µm, 2.1 mm x 50 mm) was run at a flow rate of 0.45 mL/min. The column oven was heated to 80 °C. Solvent A consisted of 0.1% trifluoroacetic acid (TFA) in ultrapure water, solvent B was 0.1% TFA in acetonitrile. After equilibration and injection at 26% B, content of B was raised to 30%. Next, a 4.8 min gradient from 30% B to 38% B was used for separation of the conjugate species. Including strip at 95% B and re-equilibration, the runtime was 7 min. UV signals at 280 nm and at the corresponding absorption maximum of the used surrogate drug were recorded (384 nm for CPM and 338 nm for NPM). The resulting chromatograms yielded peak areas of unconjugated, mono-conjugated and di-conjugated mAb, as well as of the remaining free drug. Using the areas at 280 nm and 384 nm or 338 nm, concentrations of the different conjugate species could be calculated with a previously determined calibration curve for the mAb peak area. From these concentrations, the amount of conjugated drug was calculated to be used as response for PLS modeling.

4.2.6 Data analysis

All data analysis was performed in Matlab R2016a (The MathWorks). For lab-scale experiments, the spectral band shifts were additionally analyzed by interpolation similar to methods proposed in the literature[129]. First, the spectra were smoothed with a 5th order Savitzky-Golay filter with a 9-point window.

Subsequently, the 1 nm resolved spectral data was interpolated with a cubic spline to a final resolution of 0.01 nm. The wavelength of the maximal absorbance λ_{max} was obtained from the interpolated data.

In the case of microplate experiments, the experiments were split into calibration runs (performed at mAb concentrations of 1.0 mg/mL, 1.5 mg/mL and 2.0 mg/mL; NPM 86 samples, CPM 75 samples) and prediction runs (performed at mAb concentrations of 1.28 mg/mL and 1.7 mg/mL; NPM 28 and CPM 30 samples). The prediction runs were excluded from model calibration and only used for evaluating the model prediction and calculating root mean square errors of prediction (RMSEP) values. No prediction runs were performed in case of the lab-scale experiments.

For model calibration, the spectroscopic data was first preprocessed and subsequently fitted with a PLS-1 model by the SIMPLS algorithm[130]. Parameters for preprocessing and model fitting were selected based on an optimization as proposed previously by Großhans et al.[50]. Preprocessing consisted of multiple steps. First, a baseline was subtracted from each spectrum to reduce possible effects of baseline drifts. For NPM and CPM, 390 nm, respectively 450 nm, were selected as reference wavelength. Subsequently, a Savitzky-Golay filter with a second-order polynomial was applied to the spectra, and, optionally, the first or second derivative was taken [131]. Finally, and only for the lab-scale experiments, the spectra were normalized by a 1-norm to further decrease instrumental drifts.

For all models, cross-validation was performed by successively excluding each batch, calibrating a PLS model based on the remaining runs, and calculating a residual sum of squares for the excluded batch. All residual sums of squares of the different submodels were summed yielding the Predictive Residual Sum of Squares (PRESS). The PRESS was scaled according to Wold et al. by the number of samples and latent variables used in the PLS model[80]. Based on the scaled PRESS, an optimization was performed using the built-in genetic algorithm of Matlab for integers[132]. The genetic algorithm optimized the window width of the Savitzky-Golay filter, the order of derivative, as well as the number of latent variables for the PLS-1 model. The root-mean-square error of cross-validation (RMSECV) was calculated from the PRESS by dividing through the total number of samples. The Q^2 values were calculated by dividing the PRESS through the summed squares of the response corrected to the mean [80]. The coefficient of determination for the prediction R^2_{pred} was calculated in the same way for the prediction set.

4.3 Results

4.3.1 Analysis of UV/Vis absorption spectra

In Figure 4.3, the measured spectra of two of the six lab-scale calibration runs are shown (spectra of all experiments, both microplate and lab scale, are shown in the supplementary data). The different spectra are colored according to the reaction progress (blue to red). The autozero for NPM was performed while already flushing the DAD with mAb and, thus, the protein band does not show in the spectra. For comparison, pure component spectra of mAb, NPM and CPM are supplied in the supplementary material. In both experiments, a baseline drift is visible at all wavelengths.

NPM features a structured absorption band between 300 nm and 360 nm; CPM a broad band between 330 nm and 450 nm. During NPM conjugation reaction (Figure 4.3 top), a small bathochromic (red) shift (up to 2 nm) of all NPM bands upon conjugation can be observed. Looking at the bottom graph in Figure 4.3, a bathochromic shift is also observed for CPM. The maximum around 390 nm is shifted by more than 2 nm. On the right side of Figure 4.3, the location of the band maxima over time is compared to conjugated drug concentrations from off-line analytics. The two curves show a high degree of correlation for both NPM and CPM (Pearson correlation coefficient > 0.97). This is also true for the remaining lab-scale runs, except for the CPM run 1 which reached a correlation coefficient of 0.92.
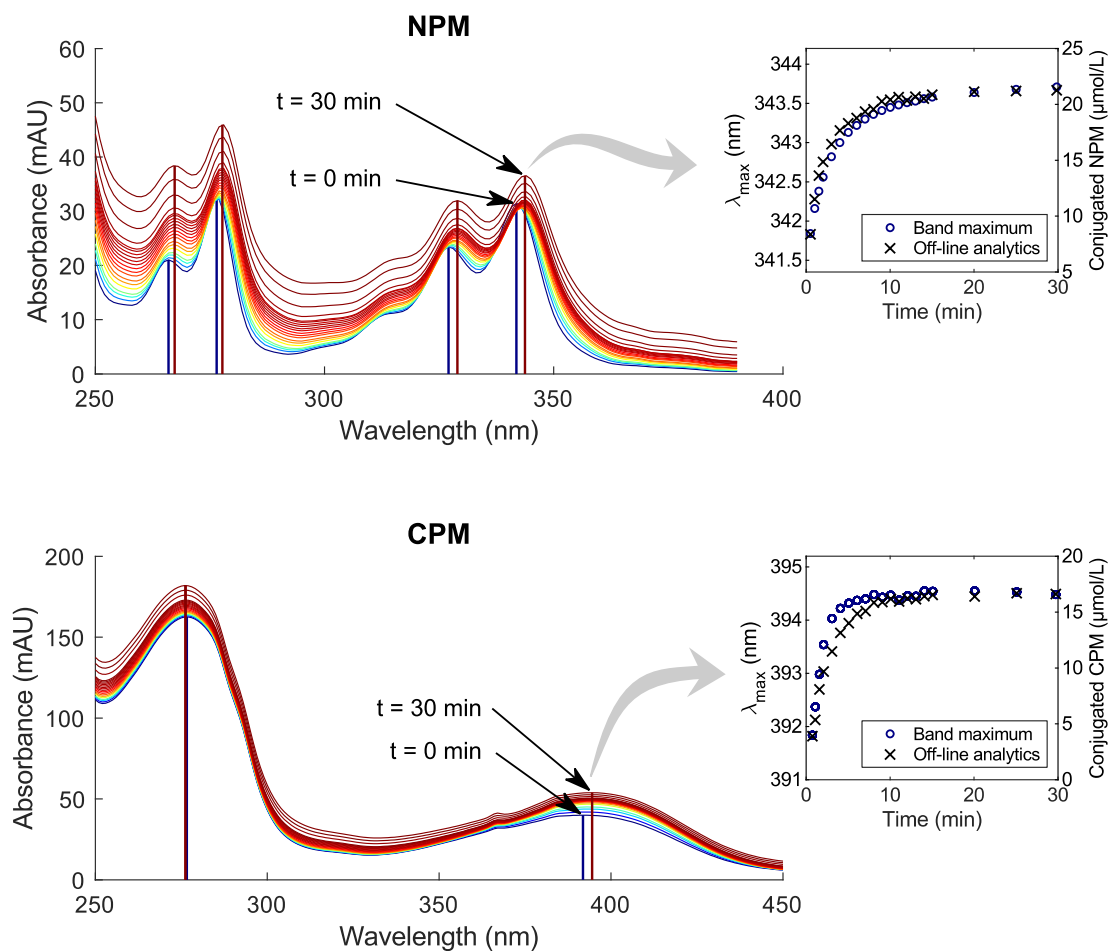
*Figure 4.3: The raw spectra of two lab-scale experiments for NPM (top) and CPM (bottom) are shown. The spectra are colored according to the reaction progress from blue to red. The location of the band maxima of the first (0 min) and the last spectrum (30 min) are marked by vertical lines. On the right side, the time evolution of the band maxima location is compared to the amount of conjugated drug measured by off-line analytics.*

4.3.2 PLS model calibration and validation for microplate experiments

For the microplate experiments, the data was split into a calibration set and an independent prediction set. Multiple parameters were set during model calibration (Savitzky-Golay window width, derivative, number of latent variables). As a systematic approach, a numerical optimization was chosen with the scaled PRESS from cross-validation as an objective. Figure 4.4 shows the calibrated model for the NPM and CPM experiments. For all experiments, the measured concentration of conjugated drug first increases quickly and approximates a limit after 10 min to 20 min. For all calibration experiments, the PLS prediction follows the concentrations from off-line analytics. Table 4.1 summarizes the optimized parameters. For NPM and CPM, RMSECV values of 0.60 µmol/L ($Q^2 = 0.9856$) and 0.56 µmol/L ($Q^2 = 0.9875$), respectively, were reached.
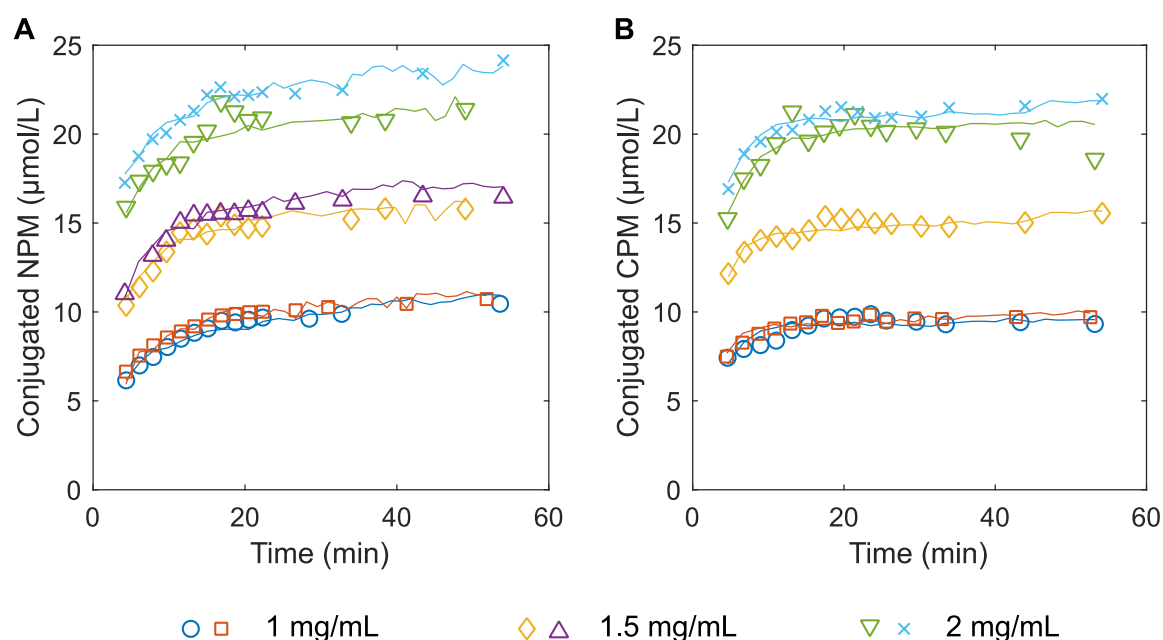
Figure 4.4: PLS model calibration for the microplate experiments is shown for NPM (Figure 4A) and CPM (Figure 4B). The nominal mAb concentrations of the different experiments are 1 mg/mL (red and blue), 1.5 mg/mL (yellow and violet), and 2 mg/mL (green and cyan).

The calibrated PLS models were then validated by applying them to a prediction set (Figure 4.5). The shape of the conjugated drug concentration is similar to the calibration set and captured by the PLS prediction in all experiments. In the case of CPM, the PLS prediction is offset for both experiments to higher concentrations. RMSEPs of 0.57 µmol/L ($R^2_{pred} = 0.9770$) and 0.90 µmol/L ($R^2_{pred} = 0.8940$) were reached for NPM and CPM, respectively.
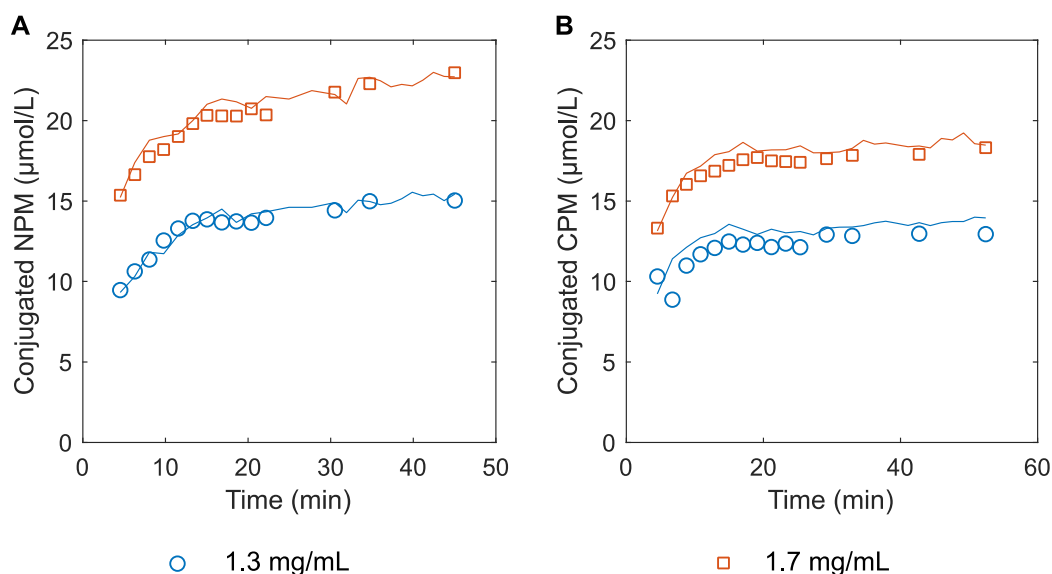
Figure 4.5: PLS model prediction for the microplate experiments is shown for NPM (A) and CPM (B). The nominal mAb concentrations of the different experiments are 1.3 mg/mL (blue), and red 1.7 mg/mL (red).

4.3.3 PLS model calibration for lab-scale experiments

PLS model calibration for lab-scale experiments was optimized in the same way as the calibration for experiments in microplates (Table 4.1). Due to material limitations, no experiments were designated for a prediction set. Instead, the PLS models were assessed only by cross-validation. For NPM, an RMSECV of 0.56 µmol/L ($Q^2 = 0.9792$) was reached. For CPM, the RMSECV was 0.57 µmol/L ($Q^2 = 0.9755$). For ADCs, the degree of conjugation is commonly expressed as DAR. By normalizing the conjugated drug concentration by the initial mAb concentration, the DAR was derived and used for plotting (Figure 4.6).

Table 4.1: Summary of optimized parameters for the spectral preprocessing and PLS model as well as the performance of each model in cross-validation and on independent prediction sets.

	Microplate		Lab scale	
	NPM	CPM	NPM	CPM
No. of calibration samples	86	75	60	58
No. of cross-validation groups	6	5	3	3
No. of prediction samples with off-line analytics	28	30	0	0
No. of prediction samples without off-line analytics	118	84	476	512
No. of latent variables	6	5	4	2
Window for Savitzky-Golay	17	13	35	71
Derivative	1	0	1	1
Q^2	0.9856	0.9875	0.9792	0.9755
RMSECV (µmol/L)	0.60	0.56	0.56	0.57
R^2_{pred}	0.9770	0.8940	-	-
RMSEP (µmol/L)	0.57	0.90	-	-
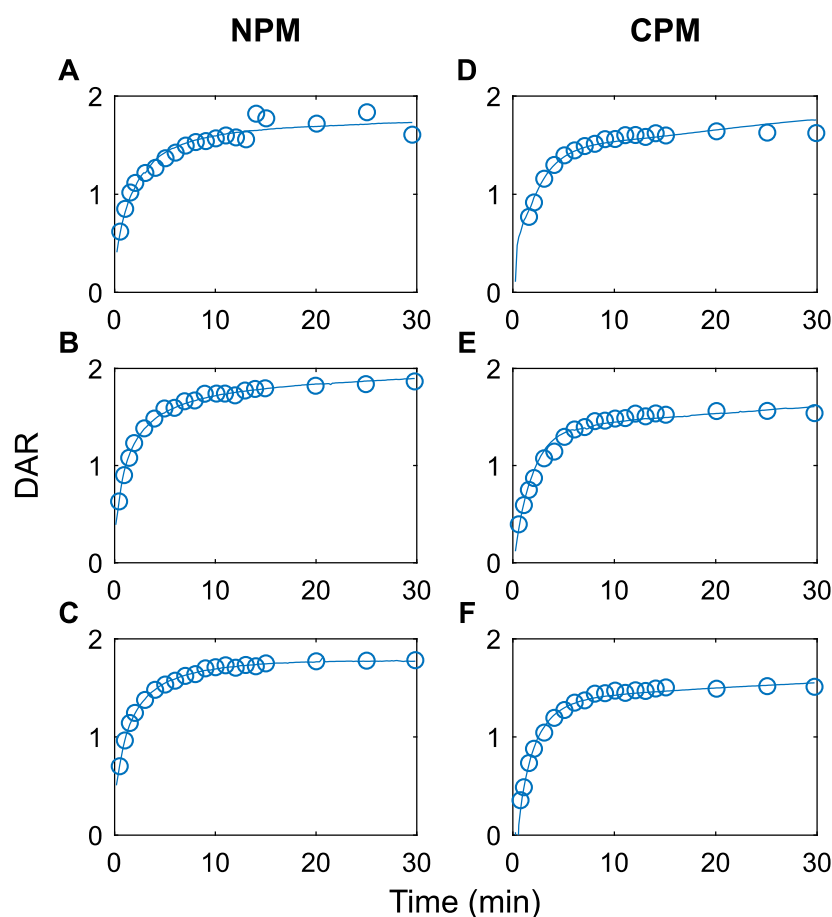
Figure 4.6: PLS model calibration for the lab-scale experiments is shown for NPM (A, B, C) and CPM (D, E, F). Each model was calibrated on 3 replicates shown in the different subplots. The DAR was used for plotting as it is frequently used to specify the conjugation degree of ADCs. For calculating the DAR, a constant protein concentration was assumed over the course of the reaction.

4.4 Discussion

To correlate the progress of conjugation reactions with changes in the UV/Vis absorption spectra, reactions were performed in microplate format as well as in a lab-scale setup while measuring absorption spectra. First, the spectra were interpreted qualitatively to justify the assumption that the conjugation reaction affects the absorption spectra of the protein/drug mixture. Subsequently, the obtained datasets were used to calibrate four PLS models predicting the concentration of conjugated drug for CPM or NPM in the two different setups.

During the conjugation reaction, UV/Vis absorption spectra are expected to change for multiple reasons. While reacting, the drug moves from an aqueous to the proteinaceous environment. Due to solvatochromism, the absorption bands of the drug thus may shift[128]. Second, the proximity of the drug to

aromatic amino acids can change the local hydrophobicity which in turn impacts the absorption spectra of aromatic amino acids [129,133,134]. Finally, maleimide has been reported to generate a relatively weak absorption band around 273 nm[135]. During the conjugation reaction, the double bond in maleimide is reduced and the band at 273 nm is expected to disappear. For the used surrogate drugs (NPM and CPM, cf. Figure 4.1), the maleimide linker is coupled to the chromophores of pyrene and phenylcoumarin. Thus, they may not have the same absorption bands as free maleimide, and the conjugation reaction may also influence the chromophore intramolecularly.

Based on the spectral changes clearly correlated to the reaction progress observed in Figure 4.3, it was concluded, that the conjugation reactions of both NPM and CPM indeed affect the respective absorption spectra. For further verification, experiments with previously quenched NPM and CPM were conducted, and spectra were recorded over 15 min. Here, no spectral shift was detected, since no reaction was taking place. The resulting spectra are shown in the supplementary material. As a consequence of the spectral change caused by the conjugation reaction, predicting the reaction progress from the spectra should be possible. Further data analysis focused on establishing quantitative PLS models for each setup and drug.

For each model, parameters for Savitzky-Golay smoothing and derivative as well as the number of latent variables were optimized. We decided to rely on a numerical optimization with an integer-based genetic algorithm to implement a systematic selection of model parameters. For the optimization, the scaled PRESS served as an objective function. In more detail, cross-validation was performed by iteratively excluding a complete run from PLS model calibration. The reasoning was to make cross-validation representative of the prediction of future runs and thereby maximize the predictive power of the PLS model. This batch-wise approach was rather conservative, excluding 1/6 (MWP experiments with NPM) up to 1/3 (lab-scale experiments) of the calibration data for cross-validation. The so calibrated models were able to predict most of the variations in the measured concentrations based on the spectral data ($Q^2 >$ 0.9750).

For the microplate setup, it is worth noting that the calibration data spans a range from 1 mg/mL to 2 mg/mL of mAb with the corresponding surrogate drug concentrations. As the external validation shows, the model is able to predict the reaction course for different concentrations in the calibration space. Interestingly, the RMSEP for NPM lies below the corresponding RMSECV. For CPM, the RMSEP is noticeably higher than the RMSECV. This seems to be related to a slight offset in the PLS prediction (Figure 4.5B). Nevertheless, the results show that it is possible to quantitatively monitor conjugation reactions

of NPM and CPM to an IgG1 antibody in the microplate format by UV/Vis spectroscopy. The results furthermore show that the chosen way of model optimization did not cause a strong overfit.

Lab-scale experiments led to RMSECV and Q^2 values similar to those found in the microplate experiments. The smooth prediction of the PLS models indicates that the error of the model is mainly related to systematic errors and not to the measurement noise. For reactions with varying protein concentration, it would be possible to estimate the concentration by a PLS model. The DAD experiments successfully show the ease of implementation of the approach in a lab-scale format. As the DAD measurements are very fast, the approach facilitates real-time monitoring, which may be beneficial for kinetic studies or process monitoring and control.

4.5 Conclusion

In summary, we established a novel spectroscopic PAT approach for monitoring ADC conjugation reactions. In two experimental setups, with two different detectors, the conjugation process of surrogate drugs to a mAb was monitored by UV/Vis absorption spectroscopy and PLS regression. The results show that UV/Vis spectroscopy allows to monitor conjugation reactions in microplates as well as in lab scale. The method may thus simplify process development by reducing the analytical bottle neck. This may be especially interesting in combination with High-throughput Process Development (HTPD) on liquid handling stations for ADCs[1,69]. In lab scale, the method allows for real-time process monitoring. Due to the flexibility and ease of implementation, the method may be further developed to a PAT approach for conjugation monitoring at commercial scale.

Future steps should focus on testing the method with cytotoxic drugs. While common drugs contain chromophores, the solvatochromic behavior of those drugs is unknown. Furthermore, the position of the engineered cysteines may have a strong impact on the solvent exposure of the drug and, thus, the change in hydrophobicity in the environment of the drug upon conjugation. Other techniques more sensitive to solvatochromism (e.g. fluorescence spectroscopy) or the changing of covalent bonds (e.g. vibrational spectroscopy) could be evaluated. Due to the simplicity of UV/Vis absorption spectroscopy, it is still a reasonable first choice for future studies.

Acknowledgments

Appendix A: Supplementary data

The supplementary data associated with this chapter contain the following information:

- Spectra of all microplate and lab-scale experiments
- Pure component spectra of mAb, NPM, and CPM
- Spectra of experiments with quenched drugs

5 Kinetic reaction modeling for antibody-drug conjugate process development

Sebastian Andris[a], Jonathan Seidel[a], Jürgen Hubbuch[a] *

[a] Institute of Process Engineering in Life Sciences, Section IV: Biomolecular Separation Engineering, Karlsruhe Institute of Technology, Fritz-Haber-Weg 2, 76131 Karlsruhe, Germany

* Corresponding author

Abstract

By combining the specificity of monoclonal antibodies (mAbs) and the efficacy of cytotoxic drugs in one molecule, antibody-drug conjugates (ADCs) form a promising class of anti-cancer therapeutics. This is emphasized by around 65 molecules in clinical trials and four marketed products. The conjugation reaction of mAbs with small-molecule drugs is a central step during production of ADCs. A detailed kinetic model for the conjugation reaction grants enhanced process understanding and can be profitably applied to process optimization. One example is the identification of the optimal amount of drug excess, which should be minimized due to its high toxicity and high cost.

In this work, we set up six different kinetic model structures for the conjugation of a cysteine-engineered mAb with a maleimide-functionalized surrogate drug. All models consisted of a set of differential equations. The models were fit to an experimental data set, and the best model was selected based on cross-validation. The selected model was successfully validated with an external validation dataset (R^2 of prediction: 0.978). Based on the modeling results, process understanding was improved. The model shows that the binding of the second drug to the mAb is influenced by the attachment of the first drug molecule. Additionally, an increase in reaction rate was observed for the addition of different salts to the reaction. In a next step, the model was applied to an *in silico* screening and optimization which illustrates its potential for

making ADC process development more efficient. Finally, the combination of the kinetic model with a PAT tool for reaction monitoring was demonstrated. In summary, the proposed modeling approach provides a powerful tool for the investigation of ADC conjugation reactions and establishes a valuable *in silico* decision support for process development.

5.1 Introduction

With four marketed products and around 65 molecules in clinical trials, antibody-drug conjugates (ADCs) are among the most important formats for the future of cancer treatment[136]. They combine the targeting specificity of monoclonal antibodies (mAbs) with the potent cytotoxicity of chemotherapy. The approval of gemtuzumab ozogamicin in 2001 (withdrawn in 2010, re-introduced to US market in 2017), brentuximab vedotin in 2011 and ado-trastuzumab emtansine in 2013 has set off substantial research and development efforts in that field, and a variety of new technologies are emerging and are making their way to the clinic.

Regarding the design of enhanced ADCs, areas of focus include new linker chemistries, site-selective conjugation strategies, the selection of adequate binding sites, and the development of new payloads alongside new ways of analyzing and purifying ADCs[117,137–140]. The manufacturing of ADCs poses several unique challenges, most notably the requirement to control product homogeneity and drug-to-antibody stoichiometry. Even with the new generation of site-directed conjugation approaches, the conjugation processes are unlikely to result in a single species. It is imperative to understand sources of ADC heterogeneity, as it can significantly impact safety and efficacy of the product. Process development of ADCs has many variables, and no platform process is available. Furthermore, the implementation of quality by design (QbD) for pharmaceutical development is encouraged by regulatory agencies, promoting a more informed, systematic approach to process development[10]. Apart from these challenges, process development for biologics in general has to handle a diversifying product pipeline. For facilitating efficient process development in this framework, an adaptable process development platform with a broad range of applicability would be highly beneficial. In this setting, further digitization of process development is a key factor. On the one hand, the knowledge of process experts and lab experiments, including high-throughput tools for efficient data generation, will keep forming the basis. On the other hand, it is becoming increasingly important to support the decision making with *in silico* tools. One group are structure-based approaches like molecular dynamics and quantitative structure-activity relationships (QSAR).

The second group is formed by statistical models and design of experiments (DoE). The third group and focus of this research are mechanistic process models, which can support process development in a number of ways. Here, the challenge is to develop high-quality models and to apply them in a beneficial way.

For facilitating efficient process development of ADCs, high-throughput tools are currently applied to screen a lot of conditions with little use of time and material. Ohri *et al.* applied a high-throughput method to scan different conjugation sites on trastuzumab[47]. To facilitate high-throughput screenings of conjugation process parameters, different platforms were developed to conduct the process in microplates[1,69,70]. DoE can be used to further improve efficiency by reducing the number of necessary experiments. In a next step, empirical models can be deduced, e.g. to give correlations between process parameters and critical quality attributes (CQAs). An example of a statistical model applicable to ADC process development shows a correlation between drug-to-antibody ratio (DAR) and drug load distribution on trastuzumab emtansine [41]. The reasoning is that measuring and controlling DAR could be indirectly used to control drug load distribution. Gikanga *et al.* supported their investigation of product quality attributes of ADCs by a molecular dynamics simulation, showcasing the application of a structure-based *in silico* tool for ADC process development[141]. There are also several examples of the use of process analytical technology (PAT) tools in combination with ADC processes[2,51,120]. They generally revolve around monitoring the DAR of the reaction.

In the ADC field, opposed to other fields like preparative chromatography, examples of the use of mechanistic modeling techniques for process development and understanding are limited[89,90,92,142]. A central step in making ADCs is the conjugation reaction, where the drugs are covalently attached to the antibody via a linker. Hu *et al.* used computational fluid dynamics (CFD) as a tool to evaluate multiple reactor designs and evaluate the use of a disposable reactor for the conjugation reaction[76].

Another interesting possibility to mechanistically model the conjugation reaction would be to develop a kinetic model, enabling the prediction of concentrations of different conjugate components at different times of the reaction. At least inside the calibration range, such a model could also be used to optimize input parameters like starting concentrations to achieve the target drug load distribution in the most efficient way. To the best of our knowledge, no such model has been developed for ADC conjugation reactions. For PEGylation of lysozyme, a kinetic model was proposed with the goal of optimizing the process towards maximal production of the mono-PEGylated form[58]. Factors varied were the ratio of PEG to protein and the pH. Moosmann

et al. also simulated PEGylation reactions of lysozyme and a scFv using numerically solved differential equations[143]. In addition to the rate laws for the PEGylation reaction, they introduced an additional term for the inactivation of mPEG-aldehyde in order to achieve a better fit of their data. Using the modeling results, they were able to gain process understanding and optimize the PEGylation process. These examples showcase the ability of kinetic reaction models to be applied to development and optimization of bioconjugation reactions in addition to yielding profound knowledge about the system at hand. With these characteristics, a kinetic modeling approach can be applied as an *in silico* decision support for the development of bioconjugation processes and advance the implementation of QbD. Given the costly and highly toxic reagents used for ADC production, there is additional motivation to minimize their use through process optimization. Improved process understanding could also benefit the selection of suitable binding sites and conjugation chemistries and spark ideas for better processes.

In this work, we use a kinetic reaction model to describe the site-specific attachment of maleimide-functionalized surrogate drugs to two thiol groups in a mAb. Six different model structures were proposed and fit to an experimental data set with varying protein and drug concentrations. The best model was selected using cross-validation (CV) and then validated with an external test data set containing data in- and outside the calibration range. Next, the resulting rate constants and the impact of different salts on the rate constants were examined to enhance process understanding. An *in silico* screening and process optimization was performed, applying the validated model. Finally, a combination of the model with a previously developed PAT tool was investigated.

5.2 Materials and Methods

5.2.1 Chemicals

The reduction of disulfides was done with tris(2-carboxyethyl)phosphine hydrochloride (TCEP, Merck KGaA, #C4706). (L)-dehydroascorbic acid (DHA, Merck KGaA, #261556) was used to re-oxidize the antibodies' interchain disulfides. Cytotoxic drugs used in ADCs were substituted by the nontoxic surrogate N-(1-pyrenyl)maleimide (NPM, Merck KGaA, #P7908). The structural formula is shown in Figure 5.1. Due to low water solubility, dimethyl sulfoxide (DMSO, Merck KGaA, #472301) was used to dissolve NPM. For stopping the reaction, remaining free drug was quenched with N-acetyl cysteine (NAC, Merck KGaA, #A7250). Standard buffers were made with Na-H_2PO_4 x 2 H_2O from VWR International GmbH. The buffers were titrated to

the desired pH with 4 M NaOH (Merck KGaA) and filtered through a 0.2 µm cellulose acetate membrane filter (Sartorius AG, Göttingen, Germany). For buffers with additional salts, ammonium sulfate (AS, #A1032) and guanidine hydrochloride (GuHCl, #A4014) were purchased from AppliChem GmbH and sodium chloride (NaCl) from Merck KGaA.

For analytics, acetonitrile from Carl Roth GmbH + Co. KG (#8825) was used, and trifluoroacetic acid (TFA) was supplied by Thermo Scientific (#28904).
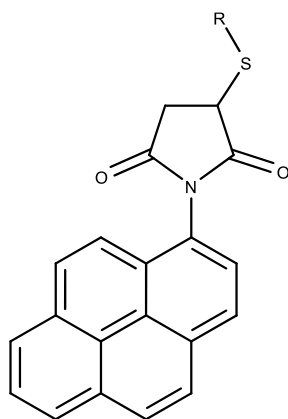
Figure 5.1: The structure of conjugated NPM is shown. R denotes the protein.

5.2.2   Model system, conjugation process and sampling of kinetic data

A stock solution of purified IgG1 mAb in PBS (+5 mM EDTA, pH 7.2) with two engineered cysteines as conjugation sites was generously provided by AstraZeneca. The two additional cysteines were inserted into the heavy chains in constant regions of the antibody. NPM served as non-toxic maleimide-functionalized surrogate drug and was conjugated to the antibody's two engineered cysteines. Aliquots of the engineered mAb stock solution were thawed and diluted with 50 mM sodium phosphate buffer (pH 7.2) for each conjugation experiment. The mAb concentration was determined with a Nano Drop 2000c spectrometer (Thermo Scientific, Waltham, USA).

For activation of the reaction site on the antibody, a reduction and partial re-oxidation were conducted in 2 mL Safe-Lock tubes (Eppendorf AG, #0030120094). The reduction step is performed to uncap engineered cysteine residues. The mAb concentration was set to 6.2 g/L and a 40-fold molar excess of TCEP (over the mAb concentration) was added before incubating for 3 h at room temperature and a 350 rpm orbital shaking rate (Thermo Mixer C, Eppendorf AG, Hamburg). The reduced mAb solution was then transferred into a dialysis cassette with a 10 kDa molecular weight cut-off (Thermo Scientific, #87730) to remove TCEP. The dialysis was performed in a volume of 0.95 L of 50 mM sodium phosphate buffer pH 7.2 at 5 °C. The dialysis buffer was replaced after 4 h, the total duration was around 19 h. The mAb concentration

65

after dialysis was determined using the Nano Drop spectrometer.

To reform interchain disulfide bonds, a partial re-oxidation with a 20-fold molar excess of DHA (8 mM stock solution in sodium phosphate buffer pH 7.2) was conducted for 4 h at room temperature. The mAb concentration was then adjusted with 50 mM sodium phosphate buffer containing 10% of DMSO.

The conjugation reaction was started by addition of the surrogate drug (NPM in DMSO) to the re-oxidized mAb solution. Through addition of the surrogate drug solution, the DMSO content was set to 10% and the mAb concentration to the desired value between 1 g/L and 2.5 g/L. The concentration of the stock solution was varied accordingly. The molar ratio (drug to mAb) was set between 2 and 4 for all conjugations (called NPM ratio from here on). The reaction was stopped by providing a 12-fold molar excess of NAC (over the applied amount of surrogate drug) to ensure the immediate termination of the conjugation reaction. For recording the reaction kinetics, 100 µL samples of the reaction were taken at different time points and mixed with a prepared volume of 20 mM NAC stock solution in sodium phosphate buffer pH 7.2.

All runs conducted with NPM for model calibration and validation are summarized in Table 5.1. The runs at 1.75 g/L and 2.5 g/L were used for validation, the rest for calibration.

Table 5.1: Conjugation experiments conducted with NPM for model calibration and validation. The experiments at 1.75 g/L and 2.5 g/L were used for model validation.

mAb concentration [g/L]	1	1.5	1.75	2	2.5
NPM:mAb 2:1	1x	2x	2x	1x	1x
NPM:mAb 3:1	1x	2x	2x	1x	1x
NPM:mAb 4:1	1x	2x	2x	1x	1x

For investigating the effect of different salts on the rate constants, several runs were conducted where ammonium sulfate, sodium chloride or guanidine hydrochloride were added to the regular buffer. The concentrations 0.2 M, 0.6 M and 1 M were tested for each salt. mAb concentration was set to 1.5 g/L and the NPM ratio was 3 for all salt runs.

5.2.3 Reversed-phase analytical chromatography

The conjugation results were assessed using reversed-phase ultra-high performance liquid chromatography (RP-UHPLC) as described previously[1]. This assay was optimized to measure the conjugation states of the intact ADC. No sample preparation was required. The same device and type of column (Acquity UPLC Protein BEH C4, Waters Corporation, 300 Å, 1.7 µm, 2.1 mm x 50 mm) were used. UV signals at 280 nm and at the absorption maximum of NPM (338 nm) were recorded. The peak areas of unconjugated, mono-conjugated and di-conjugated mAb were determined. From the areas at 280 nm and 338 nm, concentrations of these conjugate species could be calculated with a previously determined calibration curve for the mAb peak area.

5.3 Model construction and development

The first step in creating a process model is developing a model structure. The model parameters can then be determined by fitting the model to experimental data. In this work, six different model structures were proposed and the best one was determined in the model selection. The models were based on the following reaction pathway:

$$mAb + NPM \rightarrow mAbNPM_1 \tag{5.1}$$

$$mAbNPM_1 + NPM \rightarrow mAbNPM_2 \tag{5.2}$$
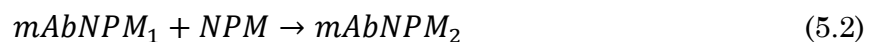
mAb is the unconjugated monoclonal antibody, *NPM* the surrogate drug, *mAbNPM₁* is the mono-conjugated mAb and *mAbNPM₂* is the bi-conjugated form. No higher-order conjugates were detected in previous RP-UHPLC measurements. The rate of these second-order reactions depends on their rate constants and the concentrations of the reactants. The two conjugation sites are located in mirroring positions in the constant region of the heavy chains of the mAb. Model 1 assumes that both binding sites share the same relevant properties and thus have the same rate constant k. Model 2 also assumes no influence of the binding sites on the reaction rate, but uses k_1 for the first attachment and k_2 for the second attachment of a drug to the antibody. Model 3 assumes that the binding sites have inherently different characteristics influencing the reaction rate and thus uses k_1' for the attachment to binding site 1 and k_2' for the attachment to binding site 2. Due to drug inactivation and depletion, for example by wall adsorption, the concentration of drug available for reaction can decrease independently of the conjugation reaction. For incorporating this into the model structures, models 4 to 6 were created by adding a lumped drug sink term with rate constant k_3 to models 1 to 3. A schematic explanation of this model construction is shown in Figure 5.2.
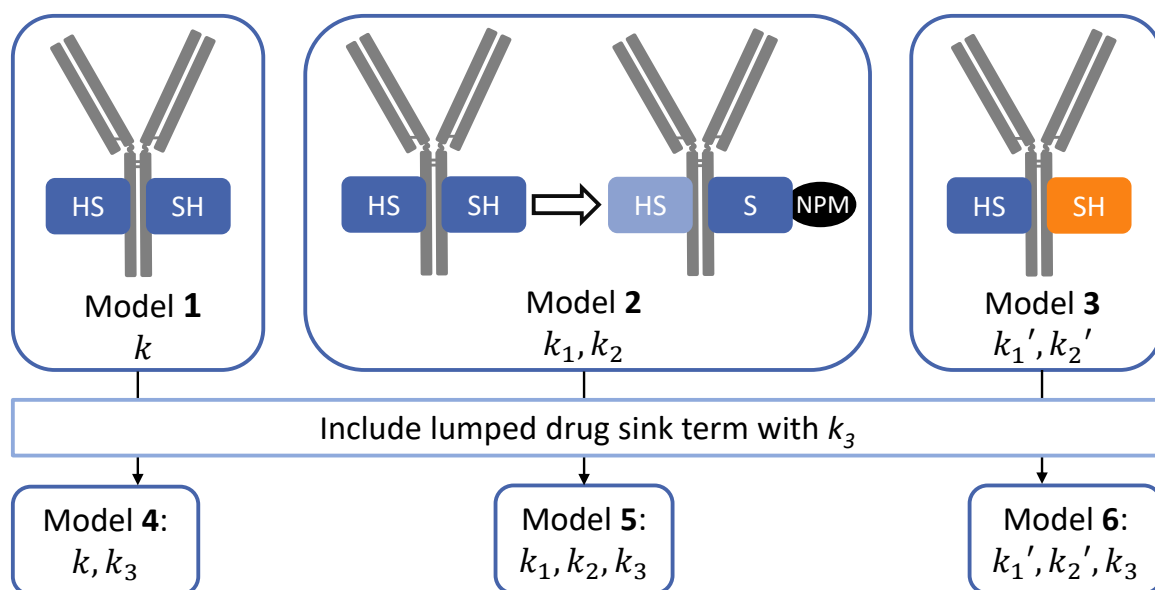
Figure 5.2: Schematic explanation of assumed model structures. Model 1 assumes two equal binding sites on the mAb and one rate constant k. Model 2 includes a second rate constant for the second attachment of drug, which implies an impact of the first binding on the environment of the second binding site (light blue color). Model 3 assumes two different binding sites with two different rate constants (different colors). Models 4 to 6 are deduced from models 1 to 3 by adding a lumped drug sink term with rate constant k_3.

Finally, it had to be incorporated into the models, that not all mAbs possess two active binding sites. In the starting material, there are mAbs with two, one or zero binding sites available for maleimide conjugation. This can be explained by an incomplete reduction of the engineered cysteines. The resulting components were included in the rate laws, which were formulated as a set of ordinary differential equations (ODEs). As an example, the rate laws of model 5 are listed in the following (Equations 5.3-5.9). Rate laws of the other models can be found in the supplementary material. $C_{\mathrm{mAb_{2c}}}$, $C_{\mathrm{mAb_{1c}}}$ and $C_{\mathrm{mAb_{0c}}}$ are the concentrations of mAbs with two, one or zero binding sites available. C_{NPM} is the NPM concentration. $C_{\mathrm{mAb_{1c}NPM}}$ stands for the concentration of mAbs with one NPM attached and one free binding site, while $C_{\mathrm{mAb_{0c}NPM}}$ has one NPM attached and zero free binding sites. Accordingly, $C_{\mathrm{mAb_{0c}(NPM)_2}}$ means the concentration of mAb with two attached NPM and no free binding site.

$$\frac{dC_{\mathrm{mAb_{2c}}}}{dt} = -k_1 \cdot C_{\mathrm{mAb_{2c}}} \cdot C_{\mathrm{NPM}} \tag{5.3}$$

$$\frac{dC_{\mathrm{mAb_{1c}}}}{dt} = -k_1 \cdot C_{\mathrm{mAb_{1c}}} \cdot C_{\mathrm{NPM}} \tag{5.4}$$

$$\frac{dC_{\mathrm{mAb_{0c}}}}{dt} = 0 \tag{5.5}$$

$$\frac{dC_{\mathrm{mAb_{1c}NPM}}}{dt} = k_1 \cdot C_{\mathrm{mAb_{2c}}} \cdot C_{\mathrm{NPM}} - k_2 \cdot C_{\mathrm{mAb_{1c}NPM}} \cdot C_{\mathrm{NPM}} \tag{5.6}$$

$$\frac{dC_{\mathrm{mAb_{0c}NPM}}}{dt} = k_1 \cdot C_{\mathrm{mAb_{1c}}} \cdot C_{\mathrm{NPM}} \tag{5.7}$$

$$\frac{dC_{\mathrm{mAb_{0c}(NPM)_2}}}{dt} = k_2 \cdot C_{\mathrm{mAb_{1c}NPM}} \cdot C_{\mathrm{NPM}} \tag{5.8}$$

$$\frac{dC_{\mathrm{NPM}}}{dt} = -k_1 \cdot C_{\mathrm{mAb_{2c}}} \cdot C_{\mathrm{NPM}} - k_1 \cdot C_{\mathrm{mAb_{1c}}} \cdot C_{\mathrm{NPM}} - k_2 \cdot C_{\mathrm{mAb_{1c}NPM}} \cdot C_{\mathrm{NPM}} \\ - k_3 \cdot C_{\mathrm{NPM}} \tag{5.9}$$

5.3.1 Component starting concentrations

While mAb and NPM starting concentrations were set with the reaction conditions, the ratio of mAb with two, one or zero active binding sites had to be estimated from the calibration data. These values could be deduced from the ratio of di-, mono-, and unconjugated mAb in the experiments, where the reaction reaches a steady state, since here all the available binding sites are conjugated. This applies to the runs with NPM ratios of 3 and 4, hence the average values from all calibration runs with these criteria were taken to calculate the component starting concentrations.

5.3.2 Model fitting, selection and validation

All data analysis was performed in Matlab R2017b (The MathWorks). The experimental data was split into a calibration and a validation set. The data at 1 g/L, 1.5 g/L, and 2 g/L were used for model calibration and those at 1.75 g/L and 2.5 g/L were used for model validation. This equals 12 runs for calibration and 9 runs for validation. All formulae used for model evaluation can be found in the supplementary material.

5.3.2.1 Model fitting (parameter optimization)

Each model consisted of a set of ODEs containing between 1 and 3 rate constants. These rate constants represent the model parameters which were optimized using the nonlinear least squares solver *lsqnonlin* in Matlab with the default algorithm *trust-region-reflective*. Inside the optimization, the ODEs were numerically solved using the *ode45* solver. The difference between the kinetic models and the experimental data was minimized and an optimal parameter set was determined for each of the six models. As start values for the parameter optimization, $k = k_1 = k_2 = k_1' = k_2' = 1$ (mM·s)$^{-1}$ and $k_3 = 0.01$ s^{-1} were selected. In the next step, the best model in the set was selected.

5.3.2.2 Model selection

Model selection was done by cross-validation and comparison of Q^2 and RMSECV values. The calibration data was split into CV groups. Each CV group was left out of model calibration once and predicted by the resulting model. Cumulative Q^2 and RMSECV values were calculated to rank model quality. Different amounts of CV groups (2-12) were tested for a more robust model selection.

5.3.2.3 Model validation

For the best model, parameter uncertainty was assessed by calculating 95% confidence intervals using the Matlab function *nlparci*. Then, the model was validated by predicting the conjugations in the validation data set at 1.75 g/L and 2.5 g/L. R^2 of prediction and RMSEP were calculated.

5.3.3 Model application

5.3.3.1 Investigation of salt effects on rate constants

To investigate the influence of different salts on the rate constants, the selected model structure was also fit to the data of the experiments with salts added to the buffer. The resulting rate constants were compared to the ones of the final calibrated model.

5.3.3.2 *In silico* screening and optimization

The selected model was used to perform *in silico* optimizations of the conjugation process at different conditions. mAb concentrations between 1 g/L and 2.5 g/L with a step size of 0.0015 g/L and NPM ratios of 2 to 4 with a step size of 0.01 were screened. The process was optimized at each combination of mAb and NPM concentration for a short reaction time and maximal amount of the bi-conjugated mAb. During the optimization, the reaction time was varied, while both the reaction time and the amount of bi-conjugated mAb were part of the objective function. This allows that both parameters are weighted appropriately. Hence, the model was evaluated for each point until an optimal reaction time was found that best satisfied the objectives. Here, the amount of bi-conjugated mAb was weighted stronger to get as close to the highest degree of conjugation as possible with the shortest possible reaction time.

5.3.3.3 Combination of models to support process monitoring

To illustrate the possibility of a combination of a kinetic reaction model with a PAT tool, the selected model structure was combined with a reaction monitoring tool described by us previously[2]. It records UV/Vis spectra during the reaction and calculates the amount of conjugated drug via a PLS model.

Data generation and processing was handled as described in the publication. Spectra and off-line data from three runs of a 20-mL scale conjugation reaction at 2 g/L with a NPM ratio of 2 were used. The data was divided into two calibration runs and one validation run. With the calibration data, the PLS model for reaction monitoring as well as the kinetic model were fit. Then, the kinetic model was used to predict the concentration of conjugated drug over the reaction time, which was then used to assess if the concentration monitored by the PLS model is in the specified range.

5.4 Results

5.4.1 Model selection

After setting up different model designs, the goal was to evaluate which model best fits the underlying mechanism of the investigated reaction. Table 5.2 gives RMSECV and Q^2 values of the cross-validation, which was conducted to select the best model. The amount of CV groups was varied in order to achieve a more robust model selection. For all different amounts of CV groups, model 5 consistently gave the best results. With 4 CV groups, RMSECV equals 0.0007 mM and Q^2 is 0.963. Model 5 contains k_1 and k_2 for the first and the second attachment of a drug molecule and k_3 for drug depletion. The models with drug sink term (models 4, 5, 6) are always better than the respective models without sink term (models 1, 2, 3), with one exception (models 3 and 6 with 2 CV groups). The models where two inherently different binding sites are assumed (models 3 and 6) consistently result in the worst RMSECV and Q^2 values. The described trends and the selected best model are the same for all different amounts of CV groups, but absolute values differ.

Table 5.2: Results of model selection by cross-validation based on calibration data set. Different amounts of CV groups were tested to provide for a more robust model selection. RMSECV (in mM) and Q² were calculated for all models.

Model #	2 CV groups		3 CV groups		4 CV groups	
	RMSECV	Q^2	RMSECV	Q^2	RMSECV	Q^2
1	0.0012	0.8861	0.0015	0.8271	0.0010	0.9296
2	0.0010	0.9171	0.0013	0.8652	0.0008	0.9559
3	0.0017	0.7851	0.0020	0.6891	0.0014	0.8446
4	0.0012	0.8908	0.0012	0.8868	0.0009	0.9340
5	0.0010	0.9237	0.0008	0.9490	0.0007	0.9630
6	0.0017	0.7845	0.0020	0.7130	0.0014	0.8456

Model #	6 CV groups		12 CV groups	
	RMSECV	Q^2	RMSECV	Q^2
1	0.0013	0.8701	0.0012	0.8971
2	0.0011	0.9016	0.0010	0.9262
3	0.0018	0.7505	0.0017	0.7871
4	0.0011	0.9085	0.0010	0.9239
5	0.0007	0.9591	0.0007	0.9681
6	0.0018	0.763	0.0017	0.7947

5.4.2 Calibration and parameter uncertainty

After model selection, model 5 was fit to the complete calibration data set consisting of 12 experiments, and the rate constants were calculated. They are shown in Figure 5.3 with their respective parameter uncertainties. The rate constant for the first attachment to the mAb is $k_1 = 0.797$ (mM·s)$^{-1}$, for the second attachment $k_2 = 1.476$ (mM·s)$^{-1}$. The rate constant of the drug sink term is $k_3 = 0.00155$ s^{-1}. The 95% confidence intervals correspond to 3%, 5%, and 10% of the parameter value for k_1, k_2, and k_3, respectively. Regarding the availability of binding sites, 92.02% of the mAb starting concentration was used for the mAb with two available binding sites, 7.1% for one available binding site, and 0.89% for no active binding site.
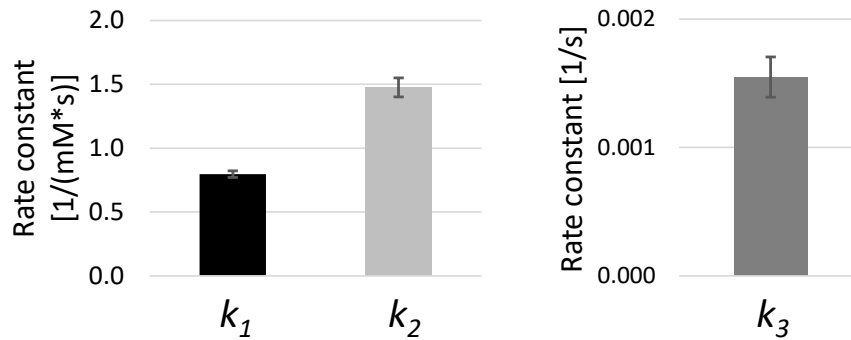
Figure 5.3: Rate constants of model 5 with 95% confidence intervals. k_1 gives the rate for the first attachment of NPM to mAb, k_2 for the second attachment. k_3 is the rate constant for the lumped drug depletion.

The model calibration for model 5 yielded an R^2 of 0.970 over the calibration data set of 12 runs. In Figure 5.4, one experiment at 1.5 g/L and NPM ratio of 3 is shown as an example. Model and experimental concentrations of un-, mono-, and di-conjugated mAb over 30 min reaction time are shown. Un-conjugated mAb is decreasing, mono-conjugated mAb is increasing during the first 45 s before it starts decreasing, and bi-conjugated mAb is continuously increasing. All concentrations are approaching a threshold corresponding to the starting values for mAb with zero, one and two active binding sites. The other experiments including the model fit can be found in the supplementary material.
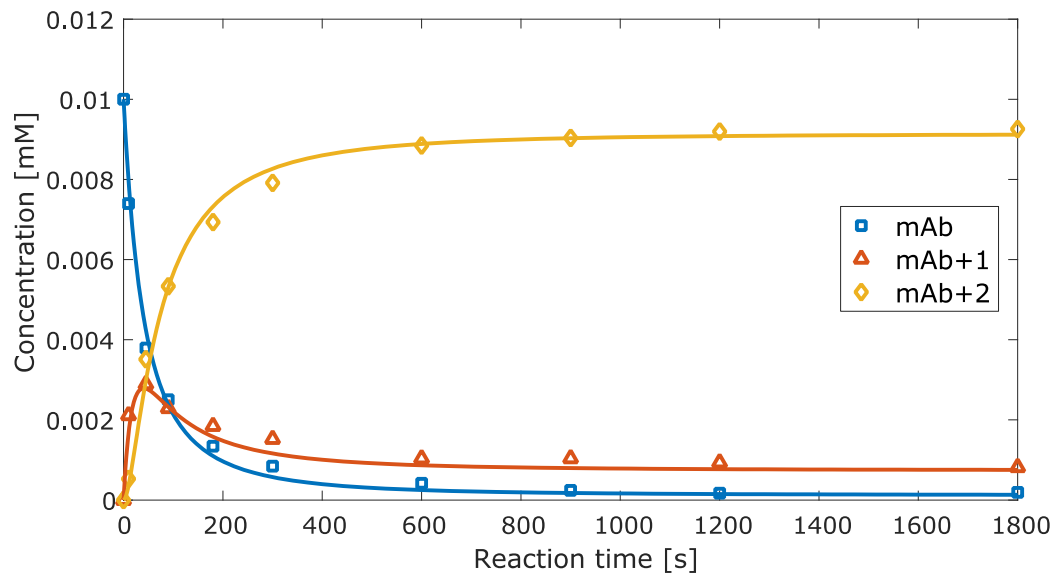
Figure 5.4: Example of conjugation run from the calibration set at 1.5 g/L and NPM ratio of 3. The markers are experimental data, the straight lines the fit for model 5. The blue square markers are the un-conjugated mAb, the red triangles the mono-conjugated mAb, and the yellow diamonds the bi-conjugated mAb.

73

5.4.3 Validation of selected models

An external validation data set consisting of 9 experiments at 1.75 g/L and 2.5 g/L (outside the calibration range of 1-2 g/L) was used to validate model 5. Using the starting concentrations for mAb and NPM, the course of the conjugation reaction was predicted by the model and compared to the experimental data. R^2 of prediction was at 0.978 and *RMSEP* at 0.00070 mM, which is in the same range as for the cross-validation with 4 CV groups. The results of the experiments and model 5 prediction are shown in Figure 5.5 for all 9 validation runs. Model predictions are closely following experimental data for all concentrations which is reflected in the R^2 of prediction. The conjugations at an NPM ratio of 2 do not reach an as high degree of conjugation as is obtained with a ratio of 3 or 4. Higher concentrations of mAb and NPM lead to a faster conjugation.
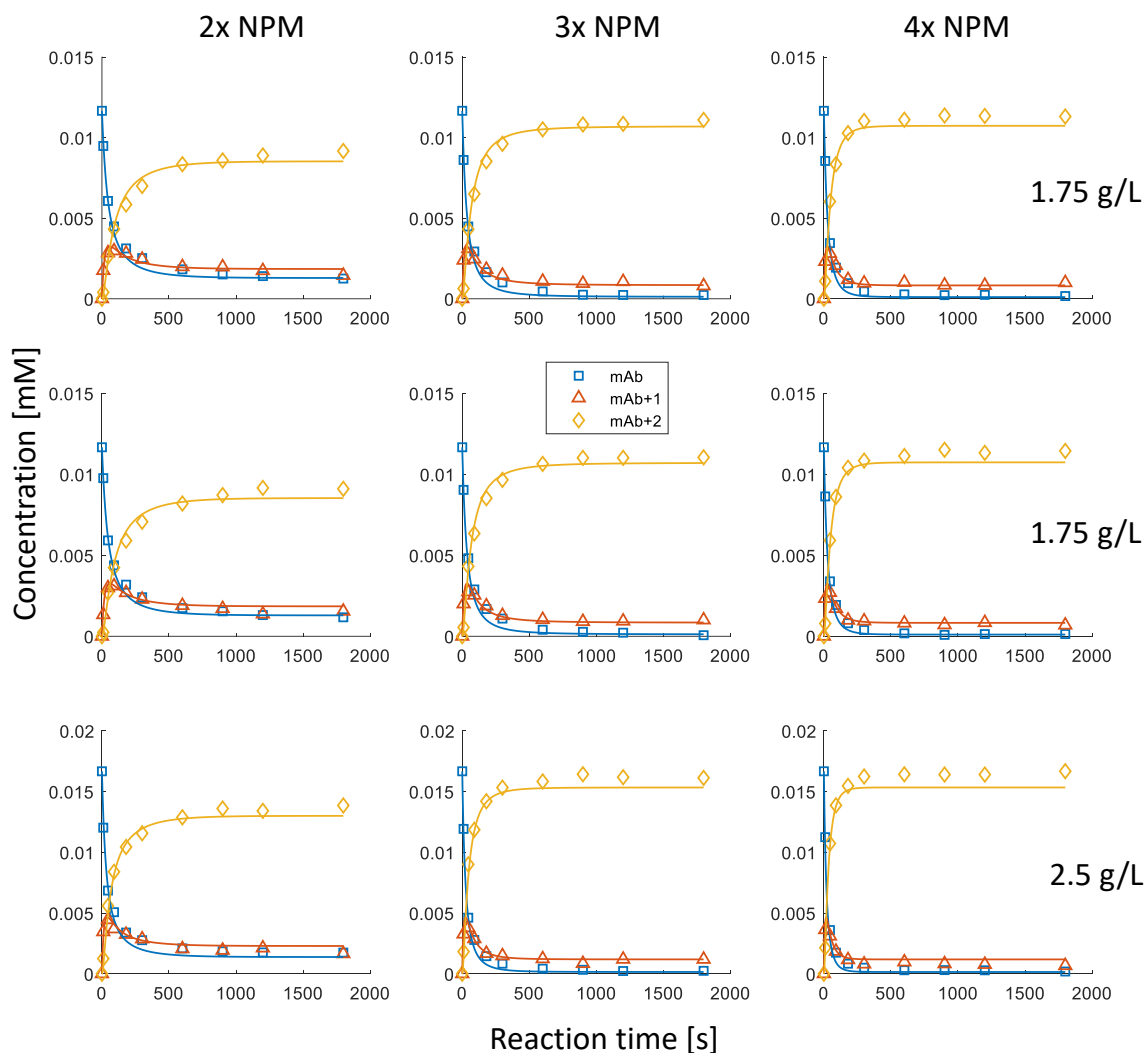
Figure 5.5: Results of model 5 prediction for the 9 validation experiments. The markers are experimental data and the respective model predictions are shown by straight lines. The blue square markers are the un-conjugated mAb, the red triangles the mono-conjugated mAb, and the yellow diamonds the bi-conjugated mAb. R^2 of prediction was at 0.978 and RMSEP at 0.00070 mM. The data at 2.5 g/L is outside the calibration range of the model (1-2 g/L).

5.4.4 Investigation of salt effects on rate constants

For investigating the influence of hydrophobicity and ionic strength on the rate of the conjugation reaction, varying concentrations of ammonium sulfate (AS), sodium chloride (NaCl), and guanidine hydrochloride (GuHCl) were added to the buffer. Model 5 was then newly fit to each of the salt runs and new rate constants were calculated for each salt and concentration. The results are shown in Figure 5.6. In general, the addition of salt leads to an increase in the reaction rate of the conjugation (k_1 and k_2). The effect of AS is stronger than the effect of NaCl and GuHCl. A higher concentration of the same salt, leads to

a faster conjugation, except in the case of 1 M AS, where the effect is lower than at 600 mM. At 1 M AS, the fit (R^2 = 0.924) was also worse than for the other runs (R^2 > 0.963) and the degree of conjugation was lower at the end of the reaction. With GuHCl, only k_1 is increasing with rising salt concentration. k_2 is about 35% higher than for the original model 5, but does not change between the different salt concentrations. Also regarding the drug sink term, the addition of salt leads to a higher rate constant. k_3 is about 10 times higher for 1 M AS and also 200 mM and 600 mM AS have a stronger effect than the other salts. For NaCl, k_3 is increased between 36% and 66% and for GuHCl between 10% and 25% with wide parameter confidence intervals.
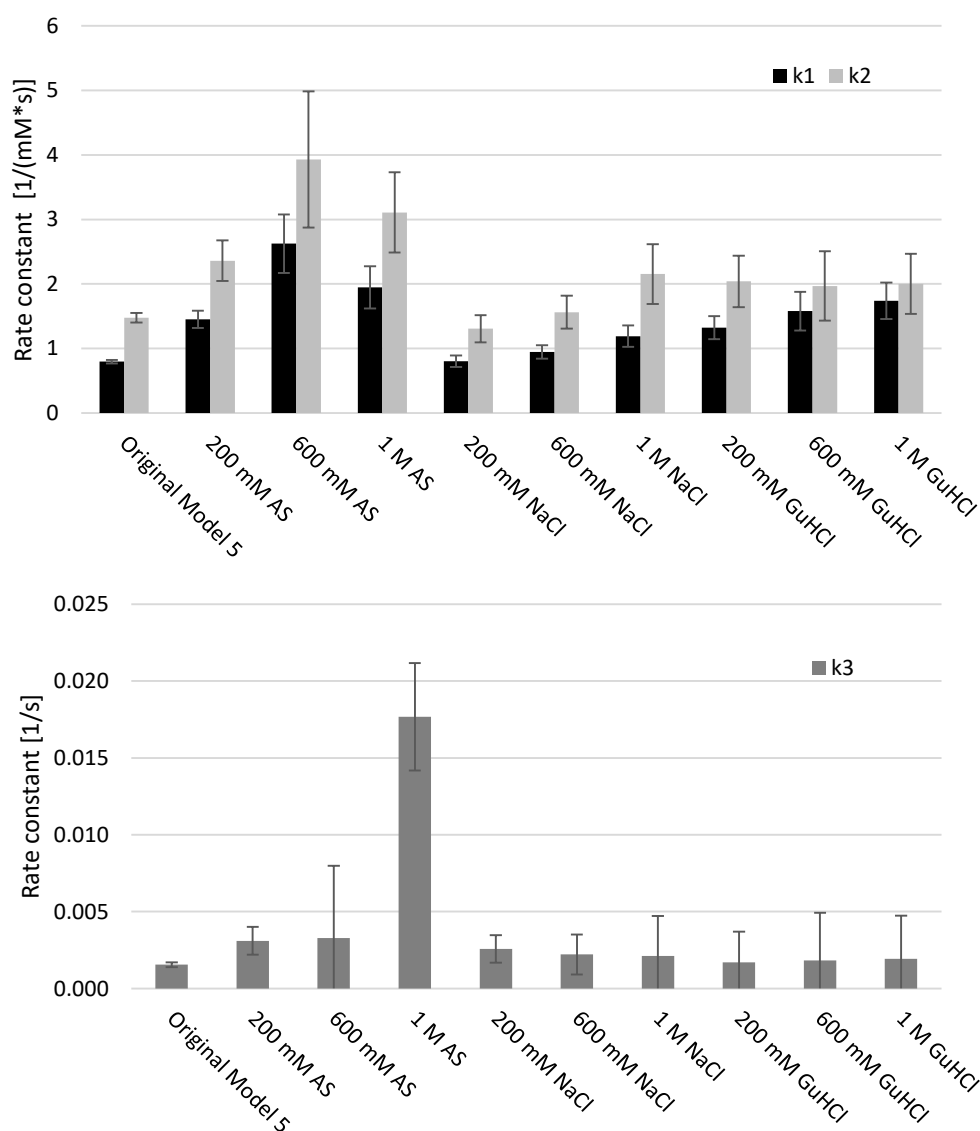

Figure 5.6: Effect of ammonium sulfate (AS), sodium chloride (NaCl), and guanidine hydrochloride (GuHCl) on model 5 rate constants. 200 mM, 600 mM, and 1 M of salt were tested. 95% confidence intervals are shown for the parameters. k_1 and k_2 values are shown in the top graph, k_3 values in the bottom graph.

5.4.5 Application of the kinetic model for process optimization

For applying the kinetic model as an *in silico* decision support in selecting the best process conditions, we conducted – as potential case study – an *in silico* screening and optimized the process for a short reaction time and a DAR close to 2. As described in detail in paragraph 5.3.3.2, different mAb concentrations and NPM ratios were screened. At each of over 200,000 points, the reaction time was optimized according to the objective function, maximizing bi-conjugated antibody and minimizing reaction time. The resulting color maps are shown in Figure 5.7. In the left graph, the optimal reaction times are shown. The higher the mAb concentration and the NPM excess, the lower the optimal reaction time, with the exception of an NPM excess between about 2.5 and 2. Here, a lower NPM excess requires a lower reaction time. In the right graph, the fraction of bi-conjugated mAb which is achieved at the optimal reaction time is visualized. Higher mAb concentrations and higher NPM ratios yield higher bi-conjugated fractions. The shaded area in both graphs represents a bi-conjugated fraction of over 91.5%. The lowest possible NPM ratio to reach this fraction depends on the mAb concentration and lies between about 2.65 and 3.85. Higher mAb concentrations need a lower drug excess.
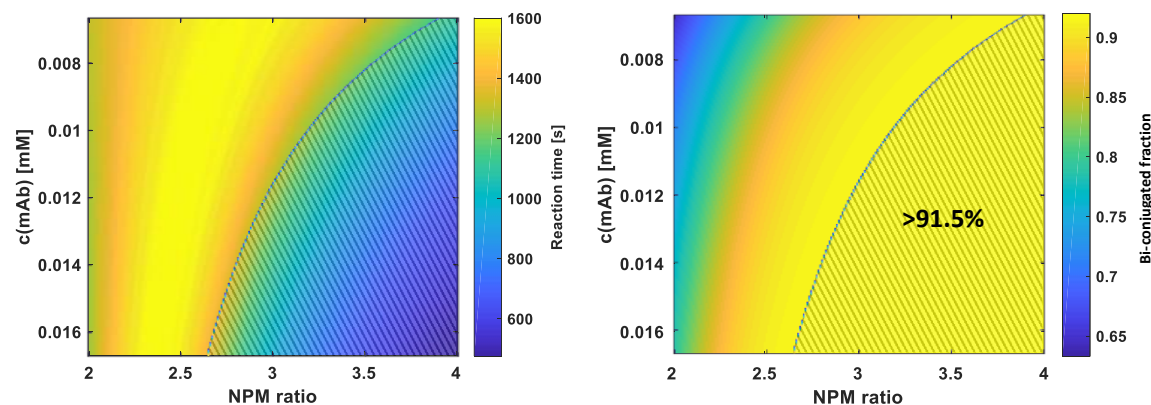
Figure 5.7: Results of in silico screening and optimization. Color maps show optimal reaction times (left) for screened mAb and NPM concentrations and the resulting fraction of bi-conjugated component (right). The shaded area in both graphs indicates a bi-conjugated fraction of greater than 91.5%.

5.4.6 Application of the kinetic model to support process monitoring

The established kinetic modeling approach was also applied to extend the capabilities of a previously developed PAT tool for conjugation reactions[2]. The tool consists of a calibrated PLS model which is able to calculate the reaction progress (amount of conjugated drug) directly from UV/Vis spectra recorded during the conjugation reaction. Here, we calibrated the PLS model, as well as the kinetic model with two conjugation runs at a 20 mL scale and 2 g/L of mAb

with a NPM ratio of 2. The concentration of conjugated drug over the reaction time was then predicted for a third run with both models. In Figure 5.8, this workflow is illustrated and the predictions are plotted together with the offline data of run 3. Both predictions are in agreement with the offline data and can be used for online process assessment by comparing PLS monitoring based on spectra with kinetic model prediction (based on starting concentrations).
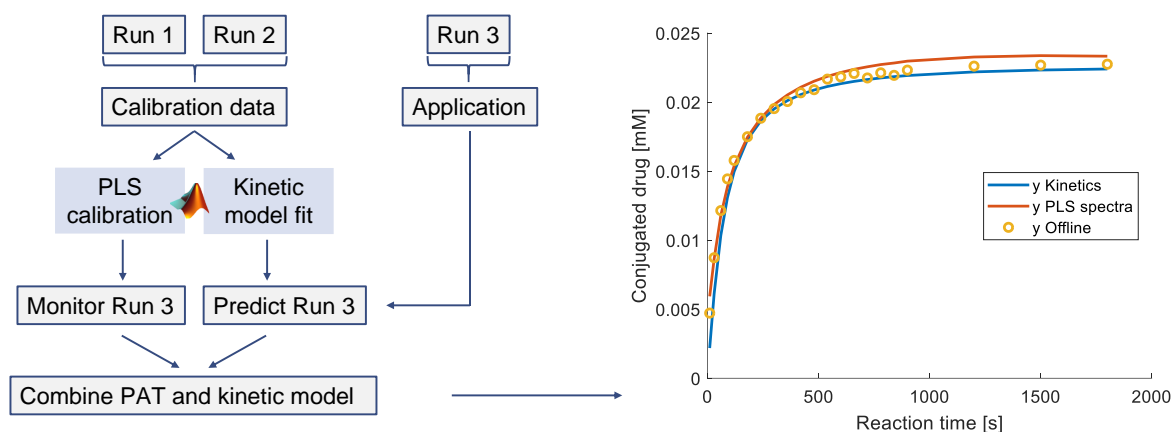
Figure 5.8: On the left, the workflow for supporting the UV/Vis-based reaction monitoring approach with the kinetic reaction model is illustrated. On the right, model predictions and offline data for the amount of conjugated drug over reaction time for run 3 are shown. The models were calibrated with the data of run 1 and 2. The blue line shows the course predicted by the kinetic model based on the starting concentrations. PLS model prediction based on UV/Vis spectra is represented by the red line. The yellow circles give the offline concentrations measured by RP-UHPLC.

5.5 Discussion

5.5.1 Model structure and model selection

For setting up a mechanistic model, some basic assumptions have to be made. First of all, we assumed the nucleophilic attachment of drug to mAb to be of the first order for both reactants, yielding a second-order reaction. This assumption should be valid since no reactant is present in great excess, which would result in a pseudo-first-order reaction. Based on previous analytical results, we assumed the absence of any higher-order components like tri- and n-conjugated antibodies. Experiments with no or a short re-oxidation showed, that the analytical RP method is able to detect higher-order components, if they are present (results not shown). Since the NPM molecules are reacting with two binding sites on one mAb, the question arises, if there are differences between the binding sites and if the first attachment influences the second. In order to answer these questions, three different model structures (models 1-3) were developed with their own set of rate laws and different rate constants

(Figure 5.2). Additionally, these models were extended by incorporating a lumped drug sink term, yielding models 4-6. The principal reason for a decrease in NPM content independently of the conjugation probably lies in its unspecific adsorption to the walls of the tubes. Since this was not studied in detail and there are other possible causes like a chemical inactivation, a lumped drug sink term was used. In the cross-validation, the models with drug sink term perform far better than their counterparts without the sink term, which seems to be a good extension of the model. Also in experiments containing no protein, a depletion of NPM over time was measured by a decrease in UV signal (supplementary material), which underlines the plausibility of including this term. This is supported by a low parameter uncertainty of k_3 (Figure 5.3). RMSEP and Q^2 results of all models in the CV point towards model 5 as the best model in the set and show that the basic model structure of model 2 and model 5 describes closest the underlying mechanism. Model 5 performed best for all amounts of CV groups and model 2 and model 4 share the second place. Since the binding sites are in the same place on identical heavy chains, no effect caused by different binding sites (model 3 and model 6) was expected. Still, this structure was included to investigate a possible influence of 3D structure. The poor performance of both of these models in the CV indicates that the binding sites can be treated as equal. An influence of the first binding on the second, on the other hand (model 2 and model 5), is backed by the results. A possible cause could be the hydrophobicity introduced by the first NPM molecule making the second attachment more feasible. The increased hydrophobicity can also be seen in the RP-UHPLC analytics, where the unconjugated mAb elutes first, before mono-conjugated and last bi-conjugated mAb (method introduced in a previous publication[1]). Dai *et al.* postulated hydrophobic interactions to be the driving force for reactivity and selectivity of their hydrophobic π-clamp binding site and showed a salt dependency following the Hofmeister series[144]. Since the cysteine binding sites for the NPM molecules are in the same position on the two heavy chains, an influence of the first binding on the second is possible. A possible fourth model basic structure combining model 2 and 3 in a structure where the binding sites are different and influence each other was discarded for two reasons: first, the poor performance of the models with different binding sites; second, to not unnecessarily increase the complexity of the models as model 5 already achieved excellent results.

The structure of the data and order of the runs can have an influence on CV results. When the arrangement of the runs for CV group assignment was changed, model 5 was still clearly the best model.

5.5.2 Model calibration and validation

All steps after model selection were done with model 5, while the other models were discarded. Parameters were estimated using the calibration set consisting of 12 experiments achieving a good model fit, shown by the alignment of model and experimental data in Figure 5.4 and the high R^2. The parameter uncertainty given by 95% confidence intervals (Figure 5.3) underlines the meaningfulness of the parameters included in the model structure. The model quality was then confirmed by the external validation, where 9 different experiments were used (R^2 of prediction of 0.978). All graphs in Figure 5.5 show a good alignment of model and experimental data. The incomplete conjugation for the runs with a NPM ratio of 2 is well represented by the model. Due to the NPM depletion, the reactive drug is used up before the maximum level of conjugation is reached. Here, the importance of including the drug sink term is highlighted once more. Also the behavior of the mono-conjugated component, which is first increasing and then going down, is captured well by the model. It is highly dependent on the ratio of k_1 and k_2. For most of the validation experiments, the bi-conjugated component is slightly underestimated by the model towards the end of the reaction. This is probably caused by the analytics because for the last samples, the measured concentration exceeded the adjusted concentration by around 4%. Taking into account that the starting concentrations are adjusted using UV/Vis measurements and the concentrations during the reaction are calculated from RP-UHPLC chromatograms, the deviation is acceptable. Overall, the calibration and validation of model 5 show excellent results and the model structure with the assumptions made seems to reflect the underlying principles very well.

One more thing that calls the attention is that k_2 is higher than k_1, so the second attachment is faster than the first. Since the binding sites structurally appear to be equal, the question is why this is the case. Here, the most probable cause might be the increased hydrophobicity that is introduced by the attachment of the first hydrophobic NPM molecule, which was discussed in the last paragraph. Lê-Quôc *et al.* found an increased reaction rate for N-substituted maleimides with increasing hydrophobicity[145]. They attributed this to a hydrophobic microenvironment of the binding site. Thus, an increased hydrophobicity of the microenvironment could be able to enhance the rate of the reaction in the case of the second NPM attachment. This said, the effect captured by the rate constant k_2 could also be caused by an increased local concentration of NPM in the binding region, caused by the increased hydrophobicity. By analyzing the influence of different salts on the rate constants, we intended to further investigate this effect and its inherent potential for improving the reaction.

5.5.3   Salt effects on the rate constants

It is known that the addition of kosmotropic salts promotes hydrophobic interactions, which for example is commonly used in hydrophobic interaction chromatography (HIC). AS and, to a lower extent, NaCl have this effect. In the conjugation experiments with added AS, the rate constants were strongly increased compared to corresponding runs without salt. For addition of 600 mM and 1 M of NaCl, rate constants were also higher, but the effect was a lot weaker than for AS. This again hints towards a strong impact of hydrophobicity on the reactivity of this conjugation reaction. At the same time, however, the addition of GuHCl, a chaotropic agent, also results in higher rate constants, even more so than NaCl, which suggests the involvement of other effects. For GuHCl, opposed to the other salts, only k_1 changes with salt concentration, while k_2, despite being higher than in the original model, stays at one level. On the one hand, the reaction rate can also be influenced by the ionic strength of the solution, which could be one factor. It was shown that already low concentrations of potassium chloride (< 50 mM) can enhance the reactivity of thiols in membrane proteins with a maleimide-functionalized fluorophore[146]. The effect increased with salt concentration, but stayed the same above 100 mM. On the other hand, there is the potential of GuHCl influencing protein conformation which could also have an impact. To get a clearer understanding of the underlying effects, a dedicated study will be necessary, but we can conclude that a hydrophobic effect probably is involved in the reactivity of the binding sites and that this knowledge can be employed for increasing the reaction rate by salt addition.

The strong effect of AS concentration on k_3 is an indicator of drug depletion being mainly caused by wall adsorption which is also hydrophobically driven. For 1 M of AS, the high k_3 value led to incomplete conjugation because all of the NPM was depleted. Regarding the influence of the other salts on k_3, it can be stated that they cause a very low increase compared to AS, but parameter uncertainty is high.

5.5.4   Model application

The selected model was applied to *in silico* screening, process optimization and as part of a soft sensor combining model description with PAT application.
In the screening, over 200,000 points were evaluated and the process was optimized for each one. The result in Figure 5.7 gives a range of conditions, in which the fraction of target component is over a specified threshold. Within this range, we can then select suitable conditions, where the needed drug excess is minimal. This is an important parameter, because excess free drug has to be removed afterwards. The optimal reaction time for the selected

condition is known from the left graph in Figure 5.7. The objective function of the optimization can be tuned according to the process development goals. Although the calibration range was between 1 g/L and 2 g/L, the screening range was set between 1 g/L and 2.5 g/L, because the validation showed that the model can extrapolate to 2.5 g/L. The decrease in optimal reaction time between a NPM ratio of about 2.5 and 2 shows that in this range, the drug is used up before conjugation is completed. These results show, that the kinetic model, applied effectively, contains detailed information on the conjugation process which can be leveraged in process development. It thus constitutes an efficient tool for *in silico* decision support.

For process monitoring, the tested combination of PAT tool and kinetic model is more accurate and flexible than just comparing the monitoring data to previous runs. What is also shown by the results is that we were able to fit the model also to data from a different setup in a different scale, which supports the selected model structure.

If root cause analysis is intended, the kinetic model should be expanded, e.g. towards more factors like pH, temperature and salt concentration.

5.6   Conclusion

In the present work, we developed a kinetic modeling approach and demonstrated how it can be applied as *in silico* decision support for the development of bioconjugation processes. The investigated reaction was the covalent attachment of hydrophobic maleimide-functionalized surrogate drugs to two engineered cysteines in a mAb. Six different model structures were proposed and the best one was selected by cross-validation, yielding additional insight into the underlying mechanism. The model provided evidence that the second binding is affected by the attachment of the first molecule, which was attributed to an increase in hydrophobicity in the environment of the binding site. The selected model was validated with an external validation set with high R^2 of prediction. Furthermore, an increased reaction rate was observed for the addition of different salts to the reaction. The application of the model to *in silico* screening and optimization showed its potential for enhancing efficiency in process development by evaluating over 200,000 conditions and calculating optimal reaction times. This enables the user to choose a condition where the target product yield is met with minimal use of drug excess and in the shortest reaction time possible. Finally, we presented an approach to combine the kinetic model with a previously developed PAT tool[2]. By extending the kinetic model, this approach could be used for online process assessment or root-cause analysis.

In summary, the proposed kinetic modeling approach has the potential to be used as a very versatile tool in the development of bioconjugation reactions. By shaping a further digitization of process development, tools like these are elementary for a more efficient process development.

Acknowledgments

Appendix B: Supplementary data

The supplementary data associated with this chapter contain the following information:

- Graphs of model 5 calibration experiments with model fit
- Rate laws for the other models
- Graph of NPM depletion over time independent of conjugation
- Formulae for model evaluation

6 Modeling of hydrophobic interaction chromatography for the separation of antibody-drug conjugates and its application towards quality by design

Sebastian Andris[a], Jürgen Hubbuch[a] *

[a] Institute of Process Engineering in Life Sciences, Section IV: Biomolecular Separation Engineering, Karlsruhe Institute of Technology, Fritz-Haber-Weg 2, 76131 Karlsruhe, Germany

* Corresponding author

Abstract

Antibody-drug conjugates (ADCs) are hybrid molecules based on monoclonal antibodies (mAbs) with covalently attached cytotoxic small-molecule drugs. Due to their potential for targeted cancer therapy, they form part of the diversifying pipeline of various biopharmaceutical companies, in addition to currently seven commercial ADCs. With other new modalities, ADCs contribute to the increasing complexity of biopharmaceutical development in times of growing costs and competition. Another challenge is the implementation of quality by design (QbD), which receives a lot of attention. In order to answer these challenges, mechanistic models are gaining interest as tools for enhanced process understanding and efficient process development.
The drug-to-antibody ratio (DAR) is a critical quality attribute (CQA) of ADCs. After the conjugation reaction, the DAR can still be adjusted by including a hydrophobic interaction chromatography (HIC) step. In this work, we developed a mechanistic model for the preparative separation of cysteine-engineered mAbs with different degrees of conjugation with a non-toxic surrogate drug. The model was successfully validated for varying load compositions with linear and optimized step gradient runs, applying conditions differing from the calibration runs. In two *in silico* studies, we then present

scenarios for how the model can be applied profitably to ensure a more robust achievement of the target DAR and for the efficient characterization of the design space. For this, we also used the model in a linkage study with a kinetic reaction model developed by us previously. The combination of the two models effectively widens system boundaries over two adjacent process steps.

We believe this work has great potential to help advance the incorporation of digital tools based on mechanistic models in ADC process development by illustrating their capabilities for efficient process development and increased robustness. Mechanistic models can support the implementation of QbD and eventually might be the basis for digital process twins able to represent multiple unit operations.

6.1 Introduction

Among antibody therapeutics in late-stage clinical studies by the end of November 2018, there were more molecules for cancer indications than for all non-cancer indications combined[27]. About one quarter of the 33 molecules for cancer indications were antibody-drug conjugates (ADCs), forming an important class of novel anti-cancer agents. Combining monoclonal antibodies (mAbs) and cytotoxic small-molecule drugs in one molecule, ADCs have the capacity for high selectivity and efficacy. The recent approval of trastuzumab deruxtecan by Daiichi Sankyo / AstraZeneca in December 2019 results in seven ADCs currently on the market.

With increasing complexity of therapeutic targets, new modalities like ADCs are diversifying the pipelines of pharmaceutical businesses, leading to increasing complexity and costs of pharmaceutical development[147]. At the same time, regulators are proposing the implementation of the quality-by-design (QbD) paradigm, which implies an enhanced knowledge regarding the relationship of product performance and process inputs in a wider range[10]. Among other things, this understanding facilitates an extended design space. This is beneficial, since, in contrast to conditions outside the design space, variations inside are not considered a process change. For implementing QbD as well as for coping with increased complexity and costs, the incorporation of digital tools like process modeling and simulation into process development may be essential. The use of mathematical models offers ways to improve process understanding and more efficiently characterize the process and the design space[54].

One critical quality attribute (CQA) of an ADC is its drug-to-antibody ratio (DAR), because it influences key factors like pharmacokinetics, efficacy, and tolerability of the product[45,111]. High-DAR species (DAR 9-10) exhibit a different behavior compared to components with less drug molecules attached

(DAR 2-6). Next to the average DAR, also the drug load distribution is relevant. The DAR is initially defined in the conjugation reaction, where the drug molecules are covalently attached to the mAb via a linker. In current literature, there are a few examples of kinetic models for protein conjugation reactions, predominantly PEGylation[58,143,148]. In our recent publication on conjugation reaction modeling, we developed a mechanistic model for the engineered cysteine-conjugation of two surrogate drugs to a mAb[3]. Apart from generating mechanistic insights, we applied the model for screening and optimizing the conjugation conditions towards achieving the target DAR in the most efficient way. This said, depending on the conjugation strategy, the reaction results in a rather broad or narrow distribution of components with different drug loadings. Only if a site-specific conjugation strategy like the conjugation to engineered cysteines is used, one has increased control over drug-loading and conjugation site[31,117]. In any case, it can be necessary to adjust the DAR and drug load distribution post conjugation, for example to remove unconjugated mAb, components with very high drug loading, or for troubleshooting purposes. Thus, a robust combination of conjugation and subsequent purification is necessary to achieve the target DAR. By establishing mechanistic models for both processes, linking and applying them towards increased process understanding, efficient process optimization, and process robustness, the implementation of QbD for ADC development could be advanced substantially. Since the small-molecule drugs, introduced into a comparably large protein, are generally very hydrophobic, the increased hydrophobicity can be exploited for separation of the components with different degrees of conjugation. Naturally, the most suitable method is hydrophobic interaction chromatography (HIC)[86–88]. It can be used to separate proteins under non-denaturing conditions depending on their interaction with hydrophobic ligands on the stationary phase. The retention of proteins in HIC is usually modulated by varying the ionic strength of the buffer. However, the influence of salt composition on protein retention is rather complex, and other factors like pH and temperature have an effect[149]. Due to the high level of hydrophobicity in ADCs, it can be necessary to include an organic solvent like isopropanol (IPA) in the running buffer.

The model-based characterization of the retention of proteins in HIC has been studied for many years[75,150–155]. While these models have extensively been used for facilitating a deeper understanding of the underlying mechanisms, there are fewer examples in the literature showcasing their beneficial application in process development. A mechanistic HIC model has, for example, been applied to optimizing the separation of an IgG from BSA as well as analyzing the robustness of the optimized process[154]. Borrmann *et al.* described how to develop a model for an antibody purification step enabling the prediction of process performance at different scales with varying operating conditions[156].

Close *et al.* developed a model for the HIC purification of a dimeric therapeutic protein with varying product form distribution[91]. Their intention was to use the model in further studies to explore the effect of the varying load on product quality. Finally, a mechanistic HIC model has been developed in order to lower the experimental effort in optimizing a mAb purification step[93]. Another example of a (non-HIC) chromatography model being used for handling variations in the feed composition has been presented for an ion-exchange step separating charge variants of a mAb[157].

For the preparative separation of different ADC species with HIC, no mechanistic model has been developed so far. As stated above, such a model could be effectively applied to process development and optimization and could support the implementation of QbD in ADC development by yielding process knowledge and facilitating a more robust realization of critical quality attributes like the DAR.

In this work, we use the transport-dispersive model (TDM) and the HIC adsorption isotherm developed by Mollerup *et al.*[75] to model the separation of mAbs conjugated with either zero, one, or two molecules of a non-toxic surrogate drug. The model is validated with linear gradient elution as well as optimized step gradient runs applying varying load compositions. Once validated, two *in silico* studies are conducted demonstrating the capabilities of the model in supporting the implementation of QbD in ADC development. The first study shows the application of the model to model-based process control, increasing robustness in achieving the target DAR. In the second study, a linkage study with a previously developed kinetic reaction model is presented. We believe that the model developed and the described applications represent an important step towards the intensified use of digital tools like mechanistic models for ADC process development, a trend that might eventually result in the creation of 'digital twins' for production processes.

6.2 Theory

6.2.1 Transport-dispersive model and boundary conditions

The TDM is a lumped-rate model describing convection, dispersion, and mass transfer inside a chromatography column[94]. It is based on mass balances that are one-dimensional in space, which means that the concentration of a solute i in the void volume c_i and bead pore volume $c_{p,i}$ are solely a function of the position along the column axis x and the time t. The system is described by a balance for the mobile phase (Equation 6.1) and a balance for the stationary phase (Equation 6.2):

$$\frac{\partial c_i}{\partial t} = -u_{\text{int}} \cdot \frac{\partial c_i}{\partial x} - \frac{1 - \varepsilon_{\text{int}}}{\varepsilon_{\text{int}}} \cdot \left(k_{\text{eff},i} \cdot \frac{3}{r_{\text{p}}} \cdot (c_i - c_{\text{p},i})\right) + D_{\text{ax}} \cdot \frac{\partial^2 c_i}{\partial x^2} \tag{6.1}$$

$$\varepsilon_{\text{p}} \cdot \frac{\partial c_{\text{p},i}}{\partial t} + \left(1 - \varepsilon_{\text{p}}\right) \frac{\partial q_i}{\partial t} = k_{\text{eff},i} \cdot \frac{3}{r_{\text{p}}} \cdot (c_i - c_{\text{p},i}) \tag{6.2}$$

The convective transport of the solutes is effected by the interstitial velocity of the solvent u_{int}. Rather than considering the concentration distribution inside the pores, the TDM employs a lumped coefficient, the effective film transfer coefficient k_{eff}. It lumps together film diffusion, pore diffusion, and surface diffusion. Besides k_{eff}, the mass transfer term depends on the interstitial porosity ε_{int}, the radius of the porous particles r_{p}, and the difference between the concentration in the void volume c_i and the pore concentration $c_{\text{p},i}$. In the last term of Equation 6.1, the impact of hydrodynamic effects on band broadening, for example caused by packing nonidealities, is described using the axial dispersion coefficient D_{ax}. The balance for the stationary phase (Equation 6.2) relates the mass transfer term to the change in pore concentration $c_{\text{p},i}$ and concentration adsorbed to the solid phase q_i, depending also on the particle porosity ε_{p}. The system of differential equations was solved using the software ChromX. ChromX uses Danckwerts' boundary conditions for column inlet and outlet, given by Equation 6.3 and Equation 6.4, where $c_{\text{in},i}$ means the applied inlet concentration[158]:

$$c_i(t, x = 0) = c_{\text{in},i}(t) + \frac{D_{\text{ax}}}{u_{\text{int}}} \cdot \frac{\partial c_i(t, x = 0)}{\partial x} \tag{6.3}$$

$$\frac{\partial c_i(t, x = L)}{\partial x} = 0 \tag{6.4}$$

The TDM does not account for adsorption kinetics, assuming an equilibrium between concentration in the pores and adsorbed concentration.

6.2.2 Isotherm model

For a description of the adsorption equilibrium, we used the HIC isotherm developed by Mollerup *et al.*[75]. Equation 6.5 shows the kinetic formulation of the isotherm as implemented in ChromX:

$$k_{\text{kin},i} \cdot \frac{\partial q_i}{\partial t} = k_{\text{eq},i} \cdot \left(1 - \sum_{j=1}^{N} \frac{q_j}{q_{\text{max},j}}\right)^{n_i} \cdot \exp\left(k_{\text{s},i} \cdot c_{\text{p,salt}} + k_{\text{p},i} \cdot c_{\text{p},i}\right) \cdot c_{\text{p},i} - q_i \tag{6.5}$$

where N represents the number of proteins, $k_{\text{kin},i}$ denotes the kinetic constant, and $k_{\text{eq},i}$ is the equilibrium constant. The saturation capacity $q_{\text{max},j}$ of the adsorber for component j depends on the ligand density, steric shielding, and the stoichiometric parameter n_j (number of ligands bound per protein). Finally,

$c_{p,salt}$ stands for the salt concentration in the pores, and $k_{s,i}$ and $k_{p,i}$ are parameters describing the effect of salt concentration and protein concentration, respectively, on the activity coefficient.

Within the linear adsorption range ($q \ll q_{max}$), Equation 6.5 can be simplified to:

$$k_{kin,i} \cdot \frac{\partial q_i}{\partial t} = k_{eq,i} \cdot \exp(k_{s,i} \cdot c_{p,salt}) \cdot c_{p,i} - q_i \qquad (6.6)$$

For these dilute conditions, the dependence of the activity coefficient on the protein concentration is negligible[159].

6.3 Materials and Methods

6.3.1 Chemicals, buffers, and proteins

Purified IgG1 mAb stock solution in PBS (+5 mM EDTA, pH 7.2) was kindly provided by AstraZeneca. The antibodies' disulfides were reduced with tris(2-carboxyethyl)phosphine hydrochloride (TCEP, Merck KGaA, #C4706). (L)-dehydroascorbic acid (DHA, Merck KGaA, #261556) was used for partial re-oxidation. The nontoxic compound 7-diethylamino-3-(4′-maleimidylphenyl)-4-methylcoumarin (CPM, Merck KGaA, #C1484) was employed as a substitute for small-molecule drugs used in ADCs. For dissolving CPM and DHA, dimethyl sulfoxide (DMSO, Merck KGaA, #472301) was used. The reaction was stopped by adding N-acetyl cysteine (NAC, Merck KGaA, #A7250) to bind free CPM.

NaH_2PO_4 x 2 H_2O from VWR International GmbH was used for all buffers. Titration to the desired pH was done using 4 M NaOH (Merck KGaA). After preparation, all buffers were filtered through a 0.2 µm cellulose acetate membrane filter (Sartorius AG, Göttingen, Germany). During the conjugation process, a 50 mM sodium phosphate buffer at pH 7.2 was used for dilution and buffer exchange. For the HIC runs, the high-salt equilibration buffer contained 1 M of ammonium sulfate (AS, AppliChem GmbH, #A1032) and 50 mM of sodium phosphate. The low-salt elution buffer only contained 50 mM of sodium phosphate. Both, equilibration and elution buffer, were at pH 7 and both contained 5% (v/v) of IPA (Merck KGaA, #101040), which was added after pH adjustment. Acetonitrile from Carl Roth GmbH + Co. KG (#8825) and trifluoroacetic acid (TFA) from Thermo Scientific (#28904) were used for reversed-phase ultra-high performance liquid chromatography (RP-UHPLC). For tracer experiments, dextran (Dextran from Leuconostoc spp., ~2,000 kDa,

Sigma, #95771) and acetone (Acetone for LC, Merck KGaA, #1.00020) were used.

6.3.2 Conjugation process

The mAb contained two engineered cysteines as binding sites for the conjugation. Instead of cytotoxic small-molecule drugs, the non-toxic, maleimide-functionalized surrogate drug CPM was used.

Prior to the conjugation reaction, the binding sites on the antibody were prepared, performing a reduction and partial re-oxidation step in 50 mL centrifuge tubes (Corning, #352070).

At the beginning, the mAb stock solution was diluted with 50 mM sodium phosphate buffer at pH 7.2 to the desired concentration. A Nano Drop 2000c spectrometer (Thermo Scientific, Waltham, USA) was used for concentration measurements. For the reduction, the mAb concentration was set to 6.2 g/L and TCEP was added in a 40-fold molar excess over the mAb concentration. After incubating for 3 h at room temperature and at a 350 rpm orbital shaking rate (Thermo Mixer C, Eppendorf AG, Hamburg, Germany), the reduced mAb was dialyzed into 50 mM sodium phosphate buffer pH 7.2. Dialysis was done at 5 °C with a 10 kDa molecular weight cut-off cassette (Thermo Scientific, #87731-87733) to remove the reducing agent.

Interchain disulfide bonds were reformed by a partial re-oxidation with a 20-fold molar excess of DHA (8 mM stock solution in DMSO), which was conducted for 4 h at room temperature and 350 rpm orbital shaking.

The conjugation was started by addition of CPM dissolved in DMSO at a molar ratio of 3:1 (CPM : mAb). During the reaction, the DMSO content was set to 10% and the mAb concentration was 5.1 g/L. Finally, a 12-fold molar excess of NAC (over CPM) was added to bind residual free drug and stop the conjugation reaction. To create different DARs for the HIC runs, the reactions were stopped at different times. Like this, six loads with DARs of 0.76, 0.78, 1.26, 1.49, 1.63, and 1.84 were generated and stored at -80 °C.

6.3.3 System and column characterization

All chromatography experiments were performed with an Ettan liquid chromatography (LC) system consisting of pump unit P-905, dynamic single chamber mixer M-925 (90 µL mixer volume), UV-Vis monitor UV-900, and conductivity monitor pH/C-900 (all GE Healthcare, Uppsala, Sweden). A Repligen OPUS Minichrom column with a column volume (CV) of 2.5 mL (ID 8 mm, L 50 mm), pre-packed with TSKgel Phenyl-5PW (20 µm), was used (Repligen GmbH, Ravensburg, Germany).

The system and column parameters were determined by injections of

noninteracting tracers[94]. As non-pore-penetrating tracer, dextran (~2,000 kDa) was used in a 10 g/L solution in running buffer. As pore-penetrating tracer, a 1% solution of acetone in running buffer was used. The tracer experiments were done by injecting 100 μL samples of tracer through a sample loop, with and without column connected to the system. Each experiment was performed in triplicates for both high- and low-salt buffer and the results were averaged. After their determination, these system and column parameters were used to calculate other model parameters like porosities and volumes. The axial dispersion coefficient (D_{ax}) was estimated from the concentration profile of the non-penetrating tracer dextran using the software ChromX (Version 1.3.12.1, GoSilico GmbH, Karlsruhe, Germany).

6.3.4 HIC experiments

Prior to each run, the load was buffer-exchanged into the equilibration buffer using PD-10 desalting columns with Sephadex G-25 resin in the spin protocol (GE Healthcare, #17085101). This step also served to remove free CPM molecules.

The system was first equilibrated with high-salt buffer (ionic strength (IS) of 3.106 M), before 0.5 mL of sample were loaded through a sample loop. All loads were concentrated between 4 g/L and 5 g/L of protein with varying compositions of ADC components (see Table 6.1). After a wash of 2.3 CV with equilibration buffer, the elution was started. For the linear as well as the step gradient runs, IS was immediately decreased in a first step (IS between 1.6 M and 2.504 M). From the level of the first step, IS was then decreased to 0.095 M, either in a linear gradient or another step. The linear gradient length was varied between 15 and 25 CV. The step length of the second step was varied between 6 and 12 CV. All bind-and-elute runs are summed up in Table 6.1.

Table 6.1: Summary of HIC gradient runs conducted for model calibration and validation.

Run #	Load #	Load DAR	Gradient length [CV]	Ionic strength at gradient start / after 1st step [M]
Model calibration				
1	1	0.76	20	2.504
2	1	0.76	15	2.504
3	2	1.48	20	2.504
4	3	1.49	15	2.504
5	3	1.49	25	2.504
6	4	1.84	20	2.504
7	4	1.84	25	2.504
8	5	0.78	6 (Step)	1.785
9	5	0.78	10 (Step)	1.600
Model validation				
10	6	1.63	12 (Step)	2.054
11	7	1.26	9 (Step)	1.942
12	7	1.26	17.5	2.353

6.3.5 Reversed-phase analytical chromatography

The load material as well as all fractions were analyzed using RP-UHPLC as described previously[1]. The assay was applied for quantification of the conjugation states of the intact mAb without sample preparation.

6.3.6 HIC model calibration

For modeling the transport of solutes through the column, the transport-dispersive model was used. All experiments described in Section 6.3.4 are expected to be in the linear range of the isotherm. Consequently, Equation 6.6 was used for modeling the adsorption. The protein parameters, namely k_{eff}, k_{kin}, k_{eq}, and k_s, were determined by minimizing the sum of squared residuals between experimental data and model prediction using ChromX. Adaptive simulated annealing (ASA)[160] and Ceres Solver[161] were used as global and local optimizers, respectively. For finite-element spatial discretization, linear finite elements with 'Streamline-Upwind / Petrov-Galerkin-stabilization' (SUPG) were selected. As time-stepping scheme for the simulation, the so-called

fractional-step scheme was chosen[162]. Thirty axial cells and time steps of 1 s were used.

6.3.7   Process optimization and HIC model validation

After achieving a satisfying fit, the model was validated with one linear gradient run and two step gradient runs with conditions differing from the calibration runs in load composition, gradient length, and gradient starting concentration (see Table 6.1). The conditions of the step gradients were determined by using the calibrated model to optimize the process towards high purity and yield of the bi-conjugated component, a short process time, and a low pooling volume (meaning a high concentration in the pool). The optimization was done for the step gradients only, varying the ionic strength of the first step, the length of the second step, and the pooling criterion. In order to have strongly varying conditions for a thorough validation, we changed the penalty for a long process time between the optimization for run 9 and run 10 (two different loads).

6.3.8   *In silico* study for model-based process control

In order to demonstrate the potential of a validated HIC model for a more robust achievement of the target DAR, an *in silico* study was conducted. A theoretical load resulting from the conjugation process was generated (DAR = 1.88) and the HIC process was optimized for this load, yielding a final target DAR in the HIC pool. The outcome of this procedure was assumed to be the standard process. Due to a process variation in the conjugation, the output and thus the load for the HIC step can vary. In order to mimic this case, the load was varied to a lower DAR value of 1.5. In case the subsequent HIC process is sensitive to these variations in the load, the previously developed 'stiff' HIC process might lead to a situation where the target DAR is missed. In order to prevent this, the HIC model was used to adjust the HIC process (allowing a more flexible parameter setting, determined by the targeted outcome) towards achieving the final target DAR in the HIC pool. Thus, reaching the target DAR was weighted more heavily in the objective of the optimization.

6.3.9   Model-based linkage study of HIC purification and conjugation

Finally, we combined the validated HIC model with a previously established kinetic reaction model[3]. A schematic overview is shown in Figure 6.1. The kinetic model was initially developed for the conjugation of a maleimide-functionalized surrogate drug to two engineered cysteines in a mAb, the same reaction as applied in this work for the generation of the HIC load material.

The input to the kinetic model are the starting concentrations of mAb and drug and the reaction time and the output is the concentration of each conjugate species, defining the DAR of the product. These output concentrations of the conjugation model acted as the input needed for the HIC model in order to apply an optimized step gradient process and calculate the yield and final DAR in the HIC pool. To showcase the potential of such a model combination or 'digital twin', an *in silico* screening and optimization for the conjugation reaction was conducted (varying mAb and drug input concentrations, as described in our previous publication), feeding the output directly into the HIC model. The HIC model was then used to optimize the HIC step gradient process for the different loads coming from the conjugation and for directly calculating the total yield (protein output of HIC in pool / protein input of conjugation) and final DAR in the HIC pool. In summary, the two models were used to calculate the total yield and the final output of the HIC process from the input parameters of the conjugation process. For simplicity, the duration of the HIC process was not varied in the optimization and the length of the second step was set constant at 30 mL. Instead, only the ionic strength of the first step and the pooling criterion were optimized.
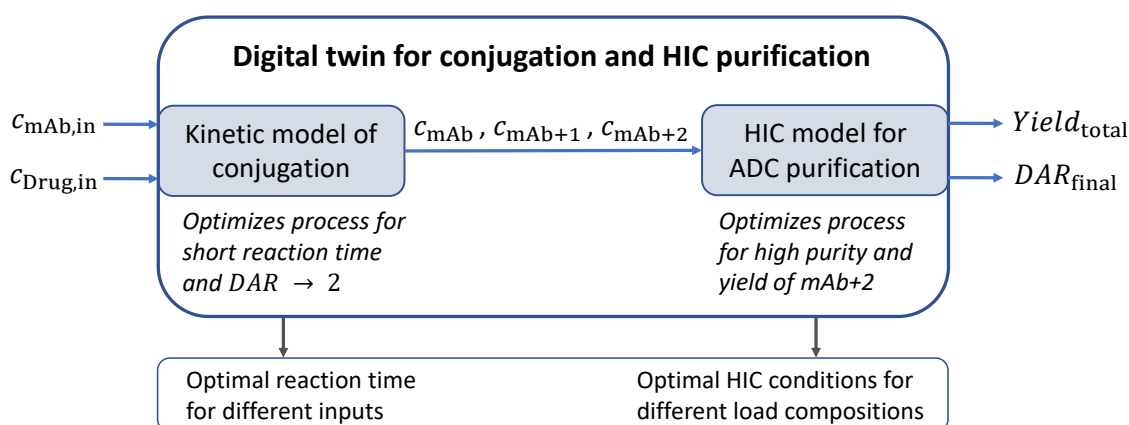
Figure 6.1: Schematic overview of the in silico linkage study between kinetic model for the conjugation and HIC model for the purification of ADCs. $c_{\mathrm{mab,in}}$ and $c_{\mathrm{Drug,in}}$ are the input concentrations of mAb and drug for the conjugation. c_{mAb}, $c_{\mathrm{mAb+1}}$ and $c_{\mathrm{mAb+2}}$ are the concentrations of un-, mono-, and di-conjugated mAb resulting from the conjugation, which form the input for the HIC model. $Yield_{\mathrm{total}}$ means the ratio of protein in the HIC pool to protein going into the conjugation. DAR_{final} is the DAR after the HIC step.

6.4 Results and Discussion

6.4.1 Model calibration

All parameters characterizing the system and column used herein are summarized in Table 6.1. The other model parameters of the TDM and the used adsorption isotherm (Equations 6.1, 6.2, 6.6) were determined by fitting the model to nine calibration experiments. Chromatograms showing the model fit together with the experimental data are presented in Figure 6.2. The unconjugated mAb is always the first component to elute, followed by the mono-conjugated and di-conjugated component. Retention times are well described by the model for all components in all runs. For the linear gradients, also peak shape and height are in good agreement. One exception is the tailing, especially of the bi-conjugated component, which is not as well described by the model. It has been reported repeatedly, that the interaction with the hydrophobic surface of the adsorber in HIC can lead to a partial unfolding of proteins [163–165]. The unfolded fraction of the protein is retained more strongly, which could lead to the tailing observed in Figure 6.2. Since this effect is not covered in the applied model, it would explain the deviation regarding the tailing. While we think that this is the most probable explanation, it is also possible that aggregates of the components are eluting in the end of the peak. Every attached CPM molecule adds hydrophobicity to the mAb, which can also be seen by the order of elution, so the bi-conjugated component is the most prone to aggregation. It might be possible to describe this effect by including a forth component for the aggregates, but the amount of aggregates would have to be quantified for all fractions with separate analytics. For the case of reversible on-column aggregation, this would not be possible. In the step runs, the isocratic part after the first step is also well described by the model, but the peak of the bi-conjugated component in the second step is wider and lower in the simulation. Nevertheless, the agreement of peak positions and peak shapes between experimental data and simulation was good, as visualized using parity plots. In Figure 6.3A, the retention volume V_R of the peak maximum is compared, giving a reference for the peak position. All markers are close to the parity line, which implies that the peak positions are well modeled for all components. This translates to an R^2 of 0.98 for the position of the peak maximum. By assessing the width at half of the peak height, a characterization of the peak shape is possible, because width as well as height of the peak are taken into account. Figure 6.3B shows that the simulated peaks have a tendency to be wider and/or lower than the ones in the experimental chromatograms, despite the generally good agreement between the shapes. The average difference is 0.86 mL, which is about 15% of the average width at half the peak height. This yields an R^2 of 0.83. In total, after parameter estimation, the model is able to describe the

experimental data very well, covering different linear gradient lengths, different load compositions as well as step gradients with varying step heights and lengths. We expect this approach to work in the same way using real cytotoxic drug molecules instead of surrogate drugs. The requirement is that sufficient recovery can be achieved and that the concentrations in the fractions can be quantified. Of course, the model development and calibration become more extensive, the more components with different DARs are present, which highly depends on the conjugation strategy.

Table 6.2: Parameters characterizing system and column.

Parameter	Symbol	Value	Unit	Determination
Column length	L	50	mm	Manufacturer
Column diameter	d	8	mm	Manufacturer
Bead radius	r_p	0.01	mm	Manufacturer
System dead volume	V_d	0.215	mL	Acetone tracer, no column
Retention volume acetone	V_{RAc}	2.370	mL	Acetone tracer, with column
Retention volume dextran	V_{RDex}	1.158	mL	Dextran tracer, with column
Superficial velocity	u	0.414	mm/s	Controlled
Column volume	V_c	2.500	mL	Manufacturer
Fluid volume	V_f	2.155	mL	$V_f = V_{RAc} - V_d$
Interstitial volume	V_{int}	0.943	mL	$V_{int} = V_{RDex} - V_d$
Total column porosity	ε_{tot}	0.862	-	$\varepsilon_{tot} = V_f/V_c$
Interstitial porosity	ε_{int}	0.377	-	$\varepsilon_{int} = V_{int}/V_c$
Particle porosity	ε_p	0.778	-	$\varepsilon_p = (V_f - V_{int})/(V_c - V_{int})$
Interstitial velocity	u_{int}	1.099	mm/s	$u_{int} = u/\varepsilon_{int}$
Axial dispersion	D_{ax}	0.133	mm²/s	Estimated from tracer

The results obtained from model calibration are based on the assumption that $q \ll q_{max}$, indicating a very low competition for binding sites. Furthermore, the effect of non-ideal protein behavior in the pores caused by protein-protein

interactions represented by the interaction parameter for protein k_p was neglected. All together, these assumptions result in a model only valid in the linear part of the adsorption isotherm. The adsorption behavior of the three components modeled is, in this case, only described by the equilibrium constant $k_{eq,i}$ and the kinetic rate constant $k_{kin,i}$ as well as the concentration of salt, its influence on protein activity being represented by $k_{s,i}$. In addition to these three parameters, the effective film diffusion coefficient $k_{eff,i}$ was estimated. A determination using empirical correlations was discarded due to the high salt concentration and the presence of IPA in the buffers, both increasing the viscosity of the solution[166] and thus influencing its mass transfer properties. The resulting parameters estimated for the un-conjugated, mono-conjugated, and bi-conjugated mAb are listed in Table 6.3. When compared to literature values for mAbs, the effective film diffusion coefficient $k_{eff,i}$ is in a plausible range[92,167]. An accurate comparison is difficult, however, as mass transfer inside the pores depends on many factors like pore size, pore tortuosity, and other conditions[168]. Furthermore, reports suggest that pore diffusion, as well as surface diffusion, play a strong part in the transport of proteins in HIC resins[155]. Since the components have approximately the same size, it is natural that their $k_{eff,i}$ are in the same range. All three estimated isotherm parameters were expected to increase with increasing hydrophobicity of the components, which is the case as shown in Table 6.3. $k_{s,i}$ covers the stronger effect of salt on more hydrophobic molecules, leading to a later elution of the higher conjugated species. The adsorption equilibrium $k_{eq,i}$ is also higher, meaning a higher affinity to the adsorber surface for more hydrophobic, more conjugated molecules. Apart from later elution, a higher $k_{eq,i}$ also impacts the peak shape. For the kinetic rate $k_{kin,i}$, the values range from 4.9×10^{-8} s to 39.62 s. Higher values lead to a slower change in adsorbed concentration, which causes the peaks to broaden. In this way, the wider peaks of the conjugated species can be described.

Organic solvents like the IPA present in the buffers also have an impact on the binding to the HIC adsorber. Since the concentration was 5% in all buffers at all times, this effect was not modeled separately. It is incorporated as a factor into the other model parameters and will not be further discussed.

Table 6.3: Estimated model parameters for the three modeled components unconjugated mAb (mAb), mono-conjugated mAb (mAb+1), and bi-conjugated mAb (mAb+2).

Parameter	mAb	mAb+1	mAb+2
$k_{\text{eff},i}$ [mm/s]	0.0013	0.0010	0.0015
$k_{\text{kin},i}$ [s]	4.9×10^{-8}	3.47	39.62
$k_{\text{eq},i}$ [-]	0.079	0.092	0.131
$k_{\text{s},i}$ [M^{-1}]	3.114	3.256	3.521
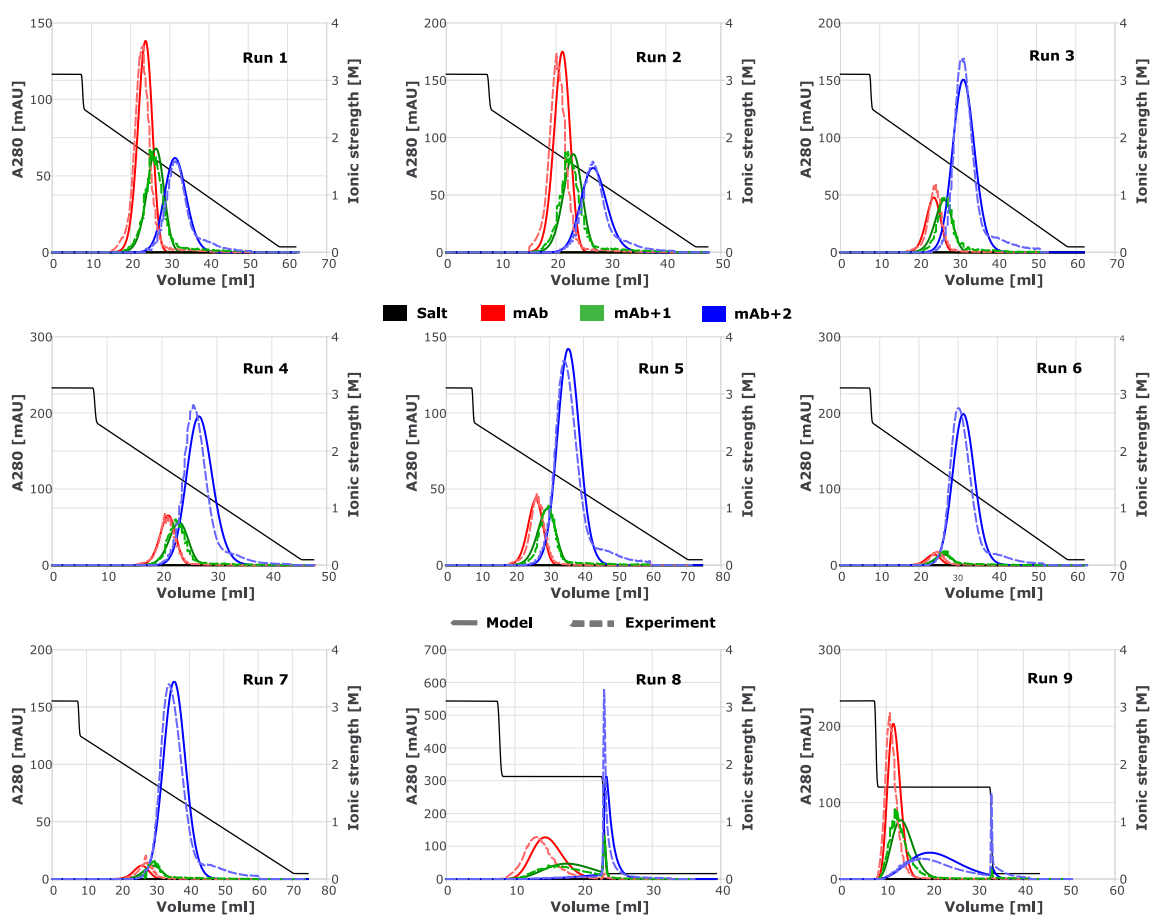
Figure 6.2: Overview of HIC gradient experiments used for parameter estimation. Absorption of the three mAb components at 280 nm (unconjugated in red, mono-conjugated in green, and bi-conjugated in blue) and ionic strength of the buffer (black) are plotted over the retention volume. The simulation is shown by the straight lines, the fraction data by the dashed lines. Load composition, gradient length, and step height were varied between the runs. The conditions of each run can be found in Table 6.1.
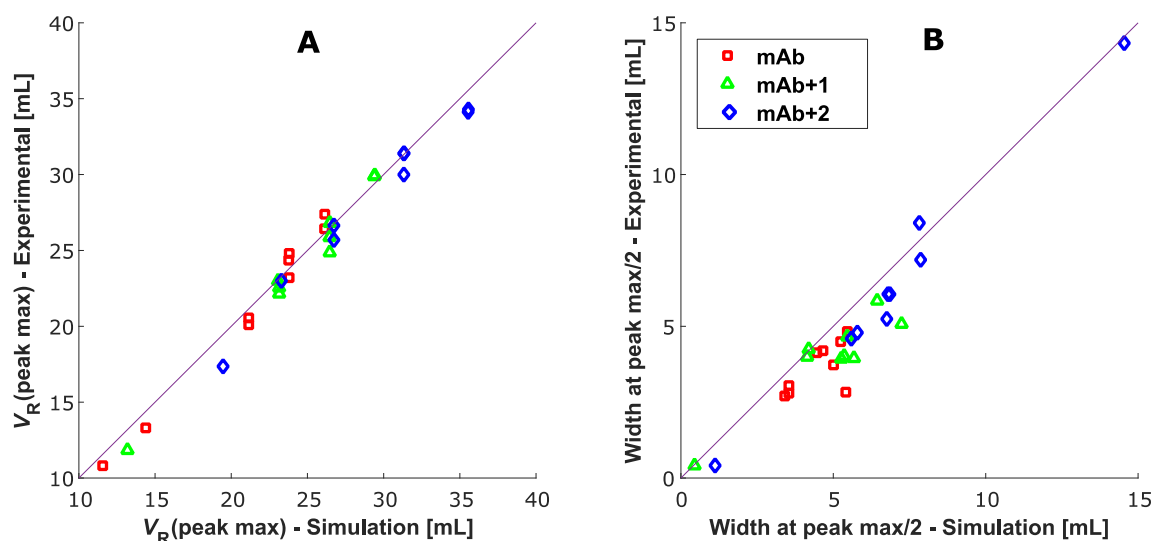
Figure 6.3: A: Parity plot for the retention volume (VR) of the peak maximum of experimental data and simulation in the calibration. B: Parity plot for the width at half peak height of experimental data and simulation in the calibration. Values on the line are equal in experiment and simulation. The red squares stand for the unconjugated mAb, the green triangles for the mono-conjugated mAb, and the blue diamonds for the bi-conjugated mAb.

6.4.2 Process optimization and model validation

After calibration of the chromatography model with 9 HIC experiments, the model was externally validated with three different experiments shown in Figure 6.4. The validation experiments consisted of one linear gradient run, where a different gradient length and a different gradient starting concentration were used, and two step gradient runs, where conditions optimized by the model were used (see Table 6.1). For the two step runs, two different load compositions were applied and the process was optimized based on the input, as described in more detail in Section 6.3.7. Prior to discussing the validation, the results of this process optimization for the steps are examined. The optimization resulted in different salt concentrations for the first step and different step lengths of the second step. Also pooling boundaries were optimized. With these optimized conditions, high experimental yields and a DAR close to the target DAR of 2 were achieved as can be seen in Table 6.4. The bi-conjugate yield is 98% for Run 10 and 96% for Run 11 compared to 93%, which was achieved in the long linear gradient in Run 5 (25 CV). While for the present optimization, yield and purity of the target bi-conjugated component were weighted equally, the objective function can be adjusted according to the preferences. Run 10 and Run 11 resulted in a DAR of 1.89 and 1.86 in the pool, the linear gradient of Run 5 gave a DAR of 1.89. While this is higher than in the optimized Run 11, it has to be taken into account that the load for Run 11 (DAR = 1.26) had a lower DAR than the one for Run 5 (DAR = 1.49), which

makes it more difficult to reach a high DAR in the HIC pool. Moreover, the concentration in the optimized step pools is 2.6 times higher than in Run 5 with a similar loaded mass, and the processing time is shorter.

Table 6.4: Predicted and experimental yield and DAR of optimized step runs (Run 10 and 11).

Run 10	Predicted	Experimental	Deviation [%]
Yield	0.97	0.98	0.6
DAR	1.96	1.89	3.4
Run 11	Predicted	Experimental	Deviation [%]
Yield	0.94	0.96	2.1
DAR	1.93	1.86	4.0

The data obtained from fractionation and the respective model prediction for the three validation runs are depicted in Figure 6.4. Model and experimental data are in good agreement for all three runs. Especially the elution during the linear gradient is very well described regarding both peak position as well as peak shape. As for the calibration runs, the bi-conjugated component deviates regarding the tailing. The probable cause was discussed in the previous section. The simulation of the step runs successfully describes the isocratic elution before the IS drop of the second step for all components, but it slightly underestimates the rest of unconjugated and mono-conjugated component that is eluting in the target product peak of the second step. For integrating the product peak, the pooling boundaries optimized by the model were used. It is highly important to the application of the model that the amount of the target bi-conjugated component in the pool is very well predicted, which is reflected by the good agreement of predicted and experimental yields (see Table 6.4; about 1.5% deviation). Due to the residual un- and mono-conjugated species in the product peak, the DAR in the HIC pool is overestimated by about 3.7%. In general, these results show the successful validation of the calibrated HIC model. Additionally, it could be demonstrated that the proposed HIC model is able to determine optimal conditions for a step gradient run for varying load compositions of conjugated components. This underlines the applicability of a mechanistic chromatography model for ADC process development and optimization. In the next two sections, this ability of the model to use concentrations of conjugated components as an input and identify optimized HIC parameters as an output is applied in two *in silico* studies to showcase its application in process control and model linkage.
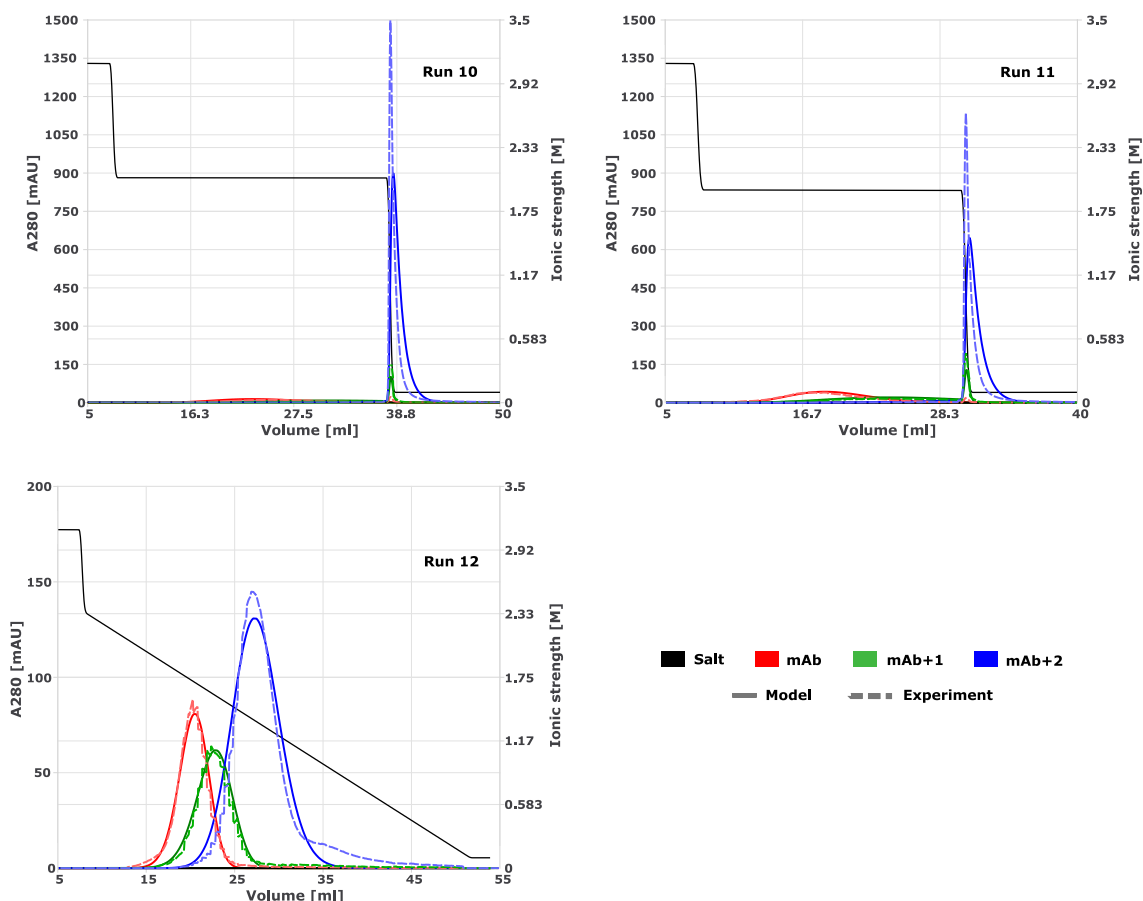
Figure 6.4: HIC gradient experiments used for model validation. The conditions for the step gradients in Run 10 and Run 11 were optimized using the calibrated model. For calculation of yield and DAR, the same optimized pooling boundaries were used for simulation and experimental data. Absorption of the three mAb components at 280 nm (unconjugated in red, mono-conjugated in green, and bi-conjugated in blue) and ionic strength of the buffer (black) are plotted over the retention volume. The simulation is shown by the straight lines, the fraction data by the dashed lines. The conditions of each run can be found in Table 6.1.

6.4.3 Robust DAR by model-based process control

In the introduction, the importance of the DAR as a CQA for ADCs was underlined. It is crucial to reach the specified value in a robust manner. While the DAR can, of course, depend on many factors, two processes are particularly important for reaching the target degree of conjugation, namely the conjugation reaction and the purification post-conjugation. This *in silico* study was designed to demonstrate the applicability of the HIC model in this context of reaching a target degree of conjugation in a controlled manner. A flow chart with the setup and the results of the study is displayed in Figure 6.5. The top sequence of steps represents the standard process, where a conjugation reaction at 5 g/L with a resulting DAR of 1.88 was assumed. Processing this load composition by using the standard HIC step (optimized for this load), gives

a DAR of 1.97 in the HIC pool with a yield of 98.1%.

A deviation from the specified process for the conjugation can potentially lead to a different output, in this case study a DAR of 1.5. This constitutes a varied load for the standard HIC process. Due to the inability of the stiff original HIC process to react on variation in the load, the final DAR in the pool dropped to 1.85. The process performance is apparently sensitive to different load compositions. For mitigating the impact of the deviation in the conjugation output, the HIC model was used for model-based process control. In the previous section, it was shown that the developed model can be used for process optimization and to predict yield and DAR for varying load compositions. In this study, we thus optimized the HIC process towards achieving the same DAR of 1.97 as in the standard process. As a consequence, the yield dropped from 98.1% to 91.2%, which is an acceptable price compared to losing the whole batch. In Table 6.5, the original and the adjusted HIC conditions are listed. Especially the volume of the second step was adjusted, from 30 mL to 44.46 mL in the adapted process. These results demonstrate how a mechanistic process model can help compensate variations in previous process steps in order to reach product specifications by model-based process control. This underlines the potential of mechanistic models for ADC development.
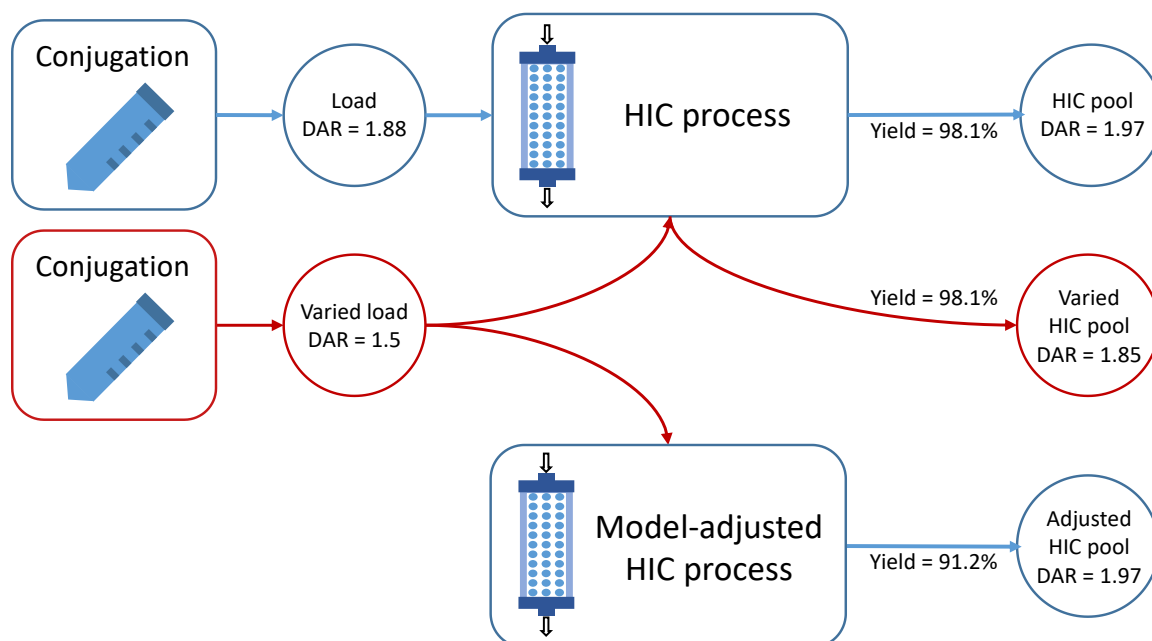

Figure 6.5: This flow chart shows how a mechanistic chromatography model can be applied for more robustly achieving the specified degree of conjugation in the pool. By adjusting the process using the model, one can react to a variation in a previous process step, here the conjugation reaction.

Table 6.5: HIC process parameters adjusted by model in reaction to variation in conjugation output.

Parameter	HIC standard	HIC adjusted
c_{step} [M]	2.078	2.093
V_{step} [mL]	30.00	44.46
Pool start [mL]	37.54	52.00
Pool end [mL]	43.90	57.30

6.4.4   Model-based linkage study of conjugation reaction and HIC purification

In the last part of this work, we performed an *in silico* linkage by combining the validated HIC model with a previously established kinetic reaction model for the conjugation[3]. The goal was to investigate the potential of the linked models to act as 'digital twin' and thus to exploit the possibility to establish a flexible design space over two adjacent unit operations. In Figure 6.6, the results of this linkage study are presented. The overall objective was reaching a DAR of 2 with high yield.

As described in Section 6.3.9, the input to the kinetic model consisted of the mAb concentration and the ratio of CPM to mAb concentration. Graph A in Figure 6.6 shows the DAR, which is achieved with different starting concentrations, when optimizing the conjugation for a DAR of 2 and a short reaction time (with the DAR being the primary objective). The DAR is calculated from the individual component concentrations. At each data point, this output was then used as input for the HIC model, in order to optimize the HIC settings on the basis of the different load compositions. Graphs B and C in Figure 6.6 give the optimal ionic strength of the first step and the volume at the end of the pool, respectively. The lower the incoming DAR from the conjugation, the more the salt concentration has to be lowered in the first step and the lower is the pool volume. For simplicity, the volume of the second step was not varied in the optimization. For each screened condition, the final yield was calculated as amount of protein in the HIC pool divided by amount of mAb going into the conjugation reaction. Yield and DAR in the HIC pool are shown in graphs D and E of Figure 6.6. It can be seen that good DAR values between 1.94 and 1.97 can be achieved with the optimized HIC steps, working with incoming DARs as low as 1.46. This is facilitated by the model by adjusting the HIC process according to the load composition. As is to be expected, the yield drops lower, the lower the DAR is after conjugation. For the condition with the lowest degree of conjugation, the yield is 64% compared to 93% for the condition with the highest DAR.

This case study shows how two mechanistic models can be used in combination to screen inputs of the conjugation reaction and directly assess the output of the subsequent purification step *in silico*. Prior to a running process, such combination can help to investigate questions like how low the drug excess can be set in the conjugation while still achieving the target DAR with a good yield after purification. Furthermore, it is not only possible to optimize the second process step for the best set of parameters in the first process step, but for a range of parameter sets. Finally, the combination of adjacent process models widens system boundaries over more than one individual process step and thus the established 'digital twin' might lead to an overall flexible design space.
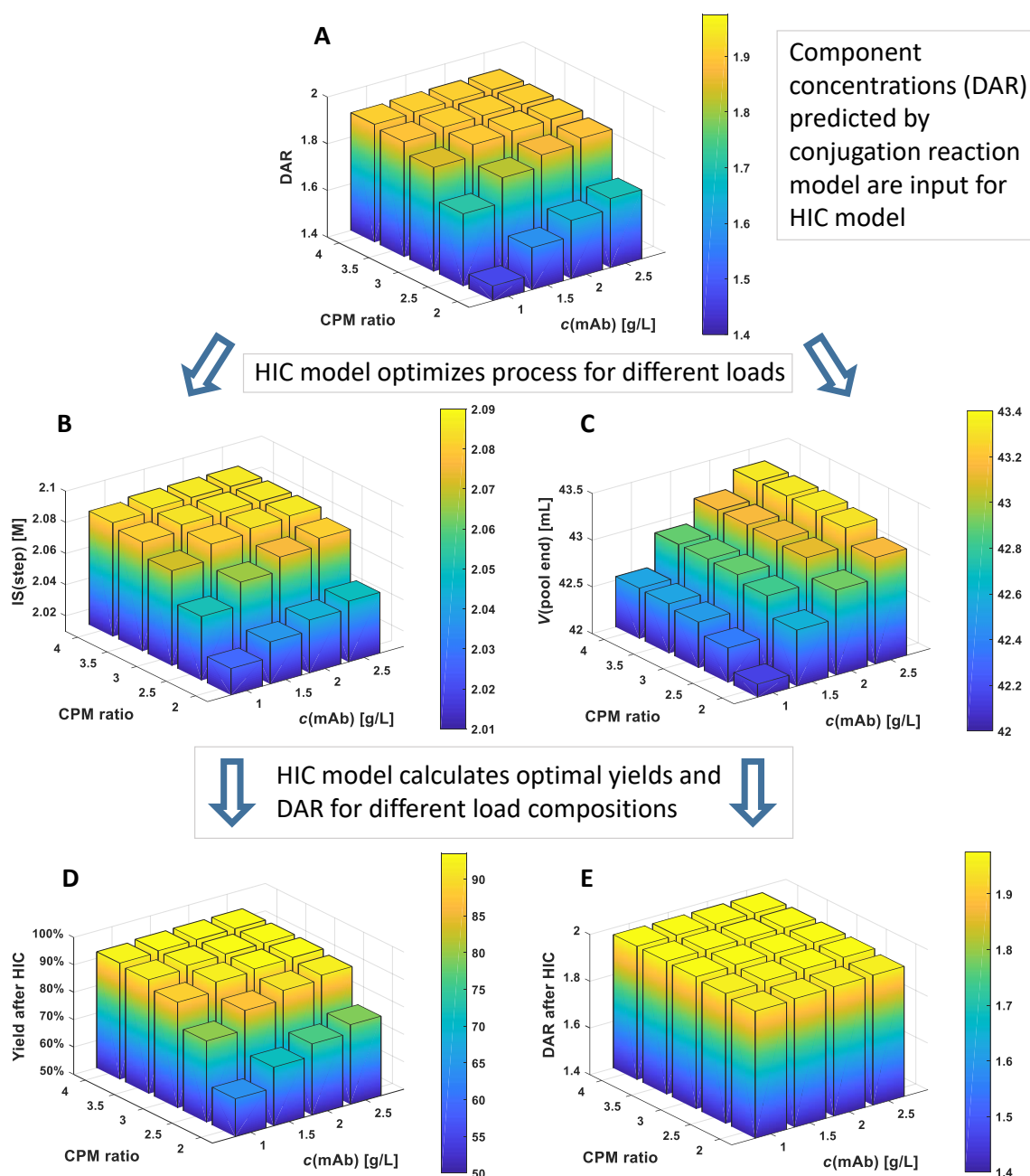
Figure 6.6: Results of linkage study of kinetic reaction model and HIC model for engineered-cysteine conjugation and subsequent HIC purification. A: DAR after conjugation for different input concentrations of mAb and CPM. B: Optimal ionic strength of the first step in HIC depending on output from the conjugation reaction. Each screened condition in the conjugation is a new load composition for HIC. C: Optimal pooling end volume in HIC depending on output from the conjugation reaction. D: Final yield after HIC. E: DAR after HIC. Yield and DAR after HIC are determined by the two models directly from the input concentrations of the conjugation.

6.5   Conclusion

A mechanistic HIC model for the preparative separation of ADC species with different degrees of conjugation was successfully developed and its benefit for ADC development was demonstrated in two *in silico* case studies. The model was validated with one linear and two step gradient experiments, in which gradient starting concentration, gradient length, and load composition were changed. With the *in silico*-optimized step runs, a higher yield and similar purity of the target bi-conjugated component in a shorter processing time and with a higher concentration in the pool was achieved compared to a gradient run with similar load. Yield and DAR of these runs were predicted by the model with relative errors between 1% and 4%. After validating the ability of the model to find optimal HIC process conditions for different load compositions, an *in silico* study was conducted to show how this can be applied to ensure a robust achievement of the target DAR, a critical quality attribute of ADCs. By adjusting the HIC purification according to the model, it was possible to react to a variation in the conjugation reaction, which had affected the DAR of the load. Next to model-based process control, the HIC model was used in an *in silico* linkage study, combining it with a kinetic reaction model developed by us previously[3]. The combination illustrates the application of mechanistic models for efficient characterization of a wider design space. Both case studies elucidate, how mechanistic modeling could pave the way from stiff processes unable to react to variations in previous steps towards more flexible processing approaches.

Going further, the chromatographic model should be extended to higher load concentrations by including experiments beyond the linear range of the isotherm. However, the model developed in this work serves its purpose of demonstrating how model description can be used in the implementation of QbD for ADC development and how the incorporation of modeling and simulation tools can support a more efficient characterization of process and design space in times of increasing complexity and costs.

We believe that the concepts presented in this work could help fertilize the ground for a further implementation of QbD in biopharmaceutical development and eventually for the emergence of digital process twins mirroring whole chains of unit operations.

Acknowledgments

7 Conclusion and Outlook

This thesis contributes to finding answers to some of the current challenges in biopharmaceutical development, and in ADC development in particular. One objective was establishing tools for highly efficient process development in order to cope with increasing complexity and costs. Furthermore, it was intended to promote the implementation of QbD for conjugation processes by providing enhanced process understanding, techniques for process monitoring, and efficient ways to characterize the design space. To this end, the potential of different high-throughput, analytical, and digital tools for ADC process development was evaluated (Chapters 3-6). Several such methods were developed for the process of site-specifically attaching two maleimide-functionalized surrogate drugs to a cysteine-engineered mAb. After validating the methods, it was demonstrated how they can be applied to dealing with the mentioned challenges and different ADC-related problems like achieving the target DAR.

The first part of this work (Chapter 3) was dedicated to establishing a high-throughput process development platform for site-specific ADC conjugations comprising the whole conjugation process as well as high-throughput compatible analytics. All process steps including a buffer exchange and the subsequent protein quantification were successfully transferred to a robotic liquid handling station. A high-throughput compatible RP-UHPLC method with a runtime of 7 min was developed to assess conjugation results efficiently. Combining high-throughput screening with DoE, the platform was applied to conjugation experiments and the results were presented using response surface modeling. Finally, the comparability to a manual setup was shown. The developed platform facilitates efficient parameter screening for site-specific conjugation strategies, which often require multiple reaction steps leading to a wide range of parameters. The degree of automation and parallelization that high-throughput platforms offer could be essential for finding optimal parameters for the next generation of ADCs.

In the second part of the thesis (Chapter 4), a UV/Vis-based on-line monitoring method for ADC conjugation reactions utilizing multivariate data analysis was created. First, a spectral change caused by the conjugation of the surrogate drug to the mAb was successfully identified. It can most probably be ascribed

to solvatochromism. By using PLS regression, the change in the UV/Vis signal was then correlated to the amount of conjugated drug in the solution as determined by RP-UHPLC. The calibrated PLS model allowed to follow the reaction progress solely by measuring UV/Vis absorption, a fast and noninvasive technique. The approach was successfully validated by using either cross-validation or external data for two different surrogate drugs and two setups with different detectors. This on-line monitoring tool could be applied to assessing the DAR of ADCs during the conjugation reaction, possibly reducing an analytical bottleneck. Additionally, the monitoring of this critical quality attribute is the first step in implementing a PAT-based control strategy as promoted by QbD.

The DAR is also pivotal in the third part of this PhD thesis (Chapter 5), where a kinetic reaction model for site-specific ADC conjugations was developed, which is able to predict the DAR at each point of the reaction from the starting concentrations. Six model structures, each a set of ODEs, were proposed and the best model was selected by cross-validation. This model suggests that the binding to the second of two equal binding sites is influenced by the first attachment in the way that it has an increased reaction rate. The effect was attributed to the hydrophobicity introduced by the first attached drug. Additionally, it was shown that the addition of different salts, especially ammonium sulfate, can have a strong, positive effect on the reaction rate. The selected model was subsequently validated by predicting an external data set, including data outside the calibration range. In order to determine starting concentrations yielding the target DAR in the shortest reaction time possible, the investigated process was optimized performing an *in silico* screening and optimization. It also enables the selection of conditions where optimal results are achieved with minimal drug excess, an important criterion due to high toxicity and cost of the drug molecules. Finally, an idea for the extension of the monitoring approach developed in Chapter 4 was presented, combining it with the kinetic reaction model. This combination can help identify process deviations on-line. The demonstrated capabilities make the established kinetic modeling approach a valuable tool for ADC conjugation development benefiting efficiency and process understanding.

In the final study (Chapter 6), a mechanistic chromatography model for the preparative separation of ADC components was developed and its application to efficient process development and model-based process control was demonstrated. The HIC purification of the surrogate ADCs was described using a model for the transport of solutes through the column (TDM) and for the adsorption equilibrium. Calibration and validation showed good agreement of model and experimental data for linear and step gradient runs. The model was

able to find optimized step gradient conditions for loads with different compositions of ADC components and to successfully predict DAR and yield of the optimized runs. In a first *in silico* case study, this ability of the HIC model was used for the controlled achievement of the target DAR, reacting to process variations in the conjugation. An *in silico* linkage study for conjugation and HIC purification applying both the HIC model as well as the kinetic reaction model from Chapter 5 demonstrated the potential of mechanistic models for efficient process characterization. The linked models form a 'digital process twin' which might enable a flexible design space over the two adjacent unit operations. The presented study illustrates how a mechanistic HIC model could benefit ADC process development by facilitating efficient characterization of the design space and model-based process control. Both are important elements in the implementation of QbD.

Overall, the tools and ideas developed in this thesis constitute a valuable contribution to shaping the process development for the next generation of ADCs. The increased efficiency needed to cope with rising complexity and costs could be delivered by high-throughput experimentation and mechanistic modeling approaches. Enhanced process understanding and control enabled by PAT and mechanistic modeling procedures will help forwarding QbD-focused process development. By applying techniques like mechanistic modeling to ADC-specific problems like DAR control or low drug usage, the potential of these techniques for ADC processing was demonstrated. Combinations of two mechanistic models or different tools like PAT and a mechanistic model give an idea of the opportunities which these digital tools might offer in the future, possibly paving the way to real digital process twins.

Bibliography

1. Andris S, Wendeler M, Wang X, Hubbuch J. Multi-step high-throughput conjugation platform for the development of antibody-drug conjugates. J Biotechnol 2018; 278:48–55. doi: 10.1016/j.jbiotec.2018.05.004

2. Andris S, Rüdt M, Rogalla J, Wendeler M, Hubbuch J. Monitoring of antibody-drug conjugation reactions with UV/Vis spectroscopy. J Biotechnol 2018; 288:15–22. doi: 10.1016/j.jbiotec.2018.10.003

3. Andris S, Seidel J, Hubbuch J. Kinetic reaction modeling for antibody-drug conjugate process development. J Biotechnol 2019; 306:71–80. doi: 10.1016/j.jbiotec.2019.09.013

4. Andris S, Hubbuch J. Modeling of hydrophobic interaction chromatography for the separation of antibody-drug conjugates and its application towards quality by design. J Biotechnol 2020; 317:48–58. doi: 10.1016/j.jbiotec.2020.04.018

5. Jagschies G, Lindskog E, Łacki K, Galliher P. Biopharmaceutical Processing: Development, Design, and Implementation of Manufacturing Processes. Elsevier; 2018.

6. Walsh G. Biopharmaceutical benchmarks 2018. Nat Biotechnol 2018; 36:1136–45. doi: 10.1038/nbt.4305

7. Nagel KM. Introduction to Biologic and Biosimilar Product Development and Analysis. AAPS; 2018.

8. Kiss R, Gottschalk U, Pohlscheidt M. New Bioprocessing Strategies: Development and Manufacturing of Recombinant Antibodies and Proteins. Springer International Publishing; 2018.

9. Carter PJ, Lazar GA. Next generation antibody drugs: Pursuit of the "high-hanging fruit." Nat Rev Drug Discov 2018; 17:197–223. doi: 10.1038/nrd.2017.227

10. ICH. Q8(R2) Pharmaceutical development. 2009;

11. Hemmerich J, Noack S, Wiechert W, Oldiges M. Microbioreactor Systems for Accelerated Bioprocess Development. Biotechnol J 2018; 13:1–9. doi: 10.1002/biot.201700141

12. McDonald P, Tran B, Williams CR, Wong M, Zhao T, Kelley BD, Lester P. The rapid identification of elution conditions for therapeutic antibodies from cation-exchange chromatography resins using high-throughput screening. J Chromatogr A 2016; 1433:66–74. doi: 10.1016/j.chroma.2015.12.071

13. Bhambure R, Kumar K, Rathore AS. High-throughput process

development for biopharmaceutical drug substances. Trends Biotechnol 2011; 29:127–35. doi: 10.1016/j.tibtech.2010.12.001

14. Chhatre S, Titchener-Hooker NJ. Review: Microscale methods for high-throughput chromatography development in the pharmaceutical industry. J Chem Technol Biotechnol 2009; 84:927–40. doi: 10.1002/jctb.2125

15. Narayanan H, Luna MF, Stosch M von, Bournazou MNC, Polotti G, Morbidelli M, Butté A, Sokolov M. Bioprocessing in the Digital Age – the Role of Process Models. Biotechnol J 2020; 15. doi: 10.1002/jssc.201200569

16. Chen W, Chen X, Gandhi R, Mantri R V., Sadineni V, Saluja A. Application of Mechanistic Models for Process Design and Development of Biologic Drug Products. J Pharm Innov 2016; 11:200–13. doi: 10.1007/s12247-016-9250-0

17. Strebhardt K, Ullrich A. Paul Ehrlich's magic bullet concept: 100 years of progress. Nat Rev cancer 2008; 8:473–80. doi: 10.1038/nrc2394

18. Ehrlich P, Morgenroth J. Die Seitenkettentheorie der Immunität. Anleitung zu Hyg Untersuchungen nach den im Hyg Inst der königl Ludwig-Maximilians-Universität zu München üblichen Methoden zusammengestellt 1902; 3:381–94.

19. Ehrlich P. Aus Theorie und Praxis der Chemotherapie. Folia Serol 1911; 7:698–714.

20. Goodman LS, Wintrobe MM, Dameshek W, Goodman MJ, Gildman A, McLennan M. Nitrogen mustard therapy. JAMA 1946; 132:126–32.

21. Gilman A. The initial clinical trial of nitrogen mustard. Am J Surg 1963; 105:574–8. doi: 10.1016/0002-9610(63)90232-0

22. Carter P. Improving the efficacy of antibody-based cancer therapies. Nat Rev Cancer 2001; 1:118–29.

23. Little M, Kipriyanov SM, Le Gall F, Moldenhauer G. Of mice and men: Hybridoma and recombinant antibodies. Immunol Today 2000; 21:364–70. doi: 10.1016/S0167-5699(00)01668-6

24. Scott AM, Wolchok JD, Old LJ. Antibody therapy of cancer. Nat Rev Cancer 2012; 12:278–87. doi: 10.1038/nrc3236

25. Slamon DJ, Godolphin W, Jones LA, Holt JA, Wong SG, Keth DE, Levin WJ, Stuart SG, Udove J, Ullrich A, et al. HER-2/neu Proto-oncogene in human breast and ovarian cancer. Science (80-) 1989; 244:707–12.

26. Slamon DJ, Clark GM, Wong SG, Levin WJ, Ullrich A, Mcguire WL. Human Breast Cancer: Correlation of Relapse and Survival with Amplification of the HER-2/neu Oncogene. Science (80-) 1987; 235:177–

82.

27. Kaplon H, Reichert JM. Antibodies to watch in 2019. MAbs 2019; 11:219–38. doi: 10.1080/19420862.2018.1556465

28. Rossin R, Versteegen RM, Wu J, Khasanov A, Wessels HJ, Steenbergen EJ, Ten Hoeve W, Janssen HM, Van Onzen AHAM, Hudson PJ, et al. Chemically triggered drug release from an antibody-drug conjugate leads to potent antitumour activity in mice. Nat Commun 2018; 9:1–11. doi: 10.1038/s41467-018-03880-y

29. Gébleux R, Stringhini M, Casanova R, Soltermann A, Neri D. Non-internalizing antibody–drug conjugates display potent anti-cancer activity upon proteolytic release of monomethyl auristatin E in the subendothelial extracellular matrix. Int J Cancer 2017; 140:1670–9. doi: 10.1002/ijc.30569

30. Ryman JT, Meibohm B. Pharmacokinetics of monoclonal antibodies. CPT Pharmacometrics Syst Pharmacol 2017; 6:576–88. doi: 10.1002/psp4.12224

31. Agarwal P, Bertozzi CR. Site-specific antibody-drug conjugates: the nexus of bioorthogonal chemistry, protein engineering, and drug development. Bioconjug Chem 2015; 26:176–92. doi: 10.1021/bc5004982

32. Malik P, Phipps C, Edginton A, Blay J. Pharmacokinetic Considerations for Antibody-Drug Conjugates against Cancer. Pharm Res 2017; doi: 10.1007/s11095-017-2259-3

33. Fu Y, Ho M. DNA Damaging Agent Based Antibody-Drug Conjugates for Cancer Therapy. Antib Ther 2018; 1:33–43. doi: 10.1093/abt/tby007/5086672

34. Lambert J. Antibody-drug conjugates: targeted delivery and future prospects. Ther Deliv 2016; 7:279–82. doi: 10.1002/9781118903681

35. Chari RVJ. Expanding the Reach of Antibody–Drug Conjugates. ACS Med Chem Lett 2016; 7:974–6. doi: 10.1021/acsmedchemlett.6b00312

36. Damelin M, Bankovich A, Park A, Aguilar J, Anderson W, Santaguida M, Aujay M, Fong S, Khandke K, Pulito V, et al. Anti-EFNA4 calicheamicin conjugates effectively target triple-negative breast and ovarian tumor-initiating cells to result in sustained tumor regressions. Clin Cancer Res 2015; 21:4165–73. doi: 10.1158/1078-0432.CCR-15-0695

37. Hamilton GS. Antibody-drug conjugates for cancer therapy: The technological and regulatory challenges of developing drug-biologic hybrids. Biologicals 2015; 43:318–32. doi: 10.1016/j.biologicals.2015.05.006

38. Zhang D, Le H, Cruz-Chuh J dela, Bobba S, Guo J, Staben L, Zhang C, Ma Y, Kozak KR, Lewis Phillips GD, et al. Immolation of p -Aminobenzyl

Ether Linker and Payload Potency and Stability Determine the Cell-Killing Activity of Antibody–Drug Conjugates with Phenol-Containing Payloads. Bioconjug Chem 2018; 29:267–74. doi: 10.1021/acs.bioconjchem.7b00576

39.   Bakhtiar R. Antibody drug conjugates. Biotechnol Lett 2016; 38:1655–64. doi: 10.1007/s10529-016-2160-x

40.   Gébleux R, Casi G. Antibody-drug conjugates: Current status and future directions. Pharmacol Ther 2016; 167:48–59. doi: 10.1016/j.drudis.2013.11.004

41.   Kim MT, Chen Y, Marhoul J, Jacobson F. Statistical modeling of the drug load distribution on trastuzumab emtansine (Kadcyla), a lysine-linked antibody drug conjugate. Bioconjug Chem 2014; 25:1223–32. doi: 10.1021/bc5000109

42.   Jackson DY. Processes for Constructing Homogeneous Antibody Drug Conjugates. Org Process Res Dev 2016; 20:852–66. doi: 10.1021/acs.oprd.6b00067

43.   Chudasama V, Maruani A, Caddick S. Recent advances in the construction of antibody–drug conjugates. Nat Chem 2016; doi: 10.1038/NCHEM.2415

44.   Junutula JR, Raab H, Clark S, Bhakta S, Leipold DD, Weir S, Chen Y, Simpson M, Tsai SP, Dennis MS, et al. Site-specific conjugation of a cytotoxic drug to an antibody improves the therapeutic index. Nat Biotechnol 2008; 26:925–32. doi: 10.1038/nbt.1480

45.   Sun X, Ponte JF, Yoder NC, Laleau R, Coccia J, Lanieri L, Qiu Q, Wu R, Hong E, Bogalhas M, et al. Effects of Drug-Antibody Ratio on Pharmacokinetics, Biodistribution, Efficacy, and Tolerability of Antibody-Maytansinoid Conjugates. Bioconjug Chem 2017; 28:1371–81. doi: 10.1021/acs.bioconjchem.7b00062

46.   Strop P, Liu S-H, Dorywalska M, Delaria K, Dushin RG, Tran T-T, Ho W-H, Farias S, Casas MG, Abdiche Y, et al. Location Matters: Site of Conjugation Modulates Stability and Pharmacokinetics of Antibody Drug Conjugates. Chem Biol 2013; 20:161–7. doi: 10.1016/j.chembiol.2013.01.010

47.   Ohri R, Bhakta S, Fourie-O'Donohue A, Dela Cruz-Chuh J, Tsai SP, Cook R, Wei B, Ng C, Wong AW, Bos AB, et al. High-Throughput Cysteine Scanning to Identify Stable Antibody Conjugation Sites for Maleimide- and Disulfide-Based Linkers. Bioconjug Chem 2018; 29:473–85. doi: 10.1021/acs.bioconjchem.7b00791

48.   Su D, Kozak KR, Sadowsky J, Yu SF, Fourie-O'Donohue A, Nelson C, Vandlen R, Ohri R, Liu L, Ng C, et al. Modulating Antibody-Drug Conjugate Payload Metabolism by Conjugation Site and Linker

Modification. Bioconjug Chem 2018; 29:1155–67. doi: 10.1021/acs.bioconjchem.7b00785

49. Shen B-Q, Xu K, Liu L, Raab H, Bhakta S, Kenrick M, Parsons-Reponte KL, Tien J, Yu S-F, Mai E, et al. Conjugation site modulates the in vivo stability and therapeutic activity of antibody-drug conjugates. Nat Biotechnol 2012; 30:184–9. doi: 10.1038/nbt.2108

50. Großhans S, Rüdt M, Sanden A, Brestrich N, Morgenstern J, Heissler S, Hubbuch J. In-line Fourier-transform infrared spectroscopy as a versatile process analytical technology for preparative protein chromatography. J Chromatogr A 2018; 1547:37–44. doi: 10.1016/j.chroma.2018.03.005

51. Furuki K, Toyo'oka T. Determination of thiol-to-protein ratio and drug-to-antibody ratio by in-line size exclusion chromatography with post-column reaction. Anal Biochem 2017; 527:33–44. doi: 10.1016/j.ab.2017.04.008

52. Garg M, Roy M, Chokshi P, Rathore AS. Process Development in the QbD Paradigm: Mechanistic Modeling of Antisolvent Crystallization for Production of Pharmaceuticals. Cryst Growth Des 2018; 18:3352–9. doi: 10.1021/acs.cgd.8b00055

53. Rüdt M, Briskot T, Hubbuch J. Advances in downstream processing of biologics – Spectroscopy: An emerging process analytical technology. J Chromatogr A 2017; 1490:2–9. doi: 10.1016/j.chroma.2016.11.010

54. Chatterjee S, Moore CM V, Nasr MM. An Overview of the Role of Mathematical Models in Implementation of Quality by Design Paradigm for Drug Development and Manufacture. In: Gintaras V. Reklaitis, Seymour C, García-Munoz S, editors. Comprehensive Quality by Design for Pharmaceutical Product Development and Manufacture. John Wiley & Sons, Inc.; 2017. page 9–24.

55. Gronemeyer P, Ditz R, Strube J. Trends in upstream and downstream process development for antibody manufacturing. Bioengineering 2014; 1:188–212. doi: 10.3390/bioengineering1040188

56. Awotwe-Otoo D, Agarabi C, Wu GK, Casey E, Read E, Lute S, Brorson KA, Khan MA, Shah RB. Quality by design: Impact of formulation variables and their interactions on quality attributes of a lyophilized monoclonal antibody. Int J Pharm 2012; 438:167–75. doi: 10.1016/j.ijpharm.2012.08.033

57. Rathore AS, Sharma C, Persad A. Use of computational fluid dynamics as a tool for establishing process design space for mixing in a bioreactor. Biotechnol Prog 2012; 28:382–91. doi: 10.1002/btpr.745

58. Xiaojiao S, Corbett B, Macdonald B, Mhaskar P, Ghosh R. Modeling and Optimization of Protein PEGylation. Ind Eng Chem Res 2016; 55:11785–

94. doi: 10.1021/acs.iecr.6b03122

59. Hahn T, Baumann P, Huuk T, Heuveline V, Hubbuch J. UV absorption-based inverse modeling of protein chromatography. Eng Life Sci 2016; 16:99–106. doi: 10.1002/elsc.201400247

60. Zurdo J. Developability assessment as an early de-risking tool for biopharmaceutical development. Pharm Bioprocess 2013; 1:29–50. doi: 10.4155/pbp.13.3

61. I. Razinkov V, J. Treuheit M, W. Becker G. Methods of High Throughput Biophysical Characterization in Biopharmaceutical Development. Curr Drug Discov Technol 2013; 10:59–70. doi: 10.2174/157016313804998915

62. Coffman JL, Kramarczyk JF, Kelley BD. High-throughput screening of chromatographic separations: I. method development and column modeling. Biotechnol Bioeng 2008; 100:605–18. doi: 10.1002/bit.21904

63. Kramarczyk JF, Kelley BD, Coffman JL. High-throughput screening of chromatographic separations: II. Hydrophobic interaction. Biotechnol Bioeng 2008; 100:707–20. doi: 10.1002/bit.21907

64. Kiesewetter A, Menstell P, Peeck LH, Stein A. Development of pseudo-linear gradient elution for high-throughput resin selectivity screening in RoboColumn® Format. Biotechnol Prog 2016; 32:1503–19. doi: 10.1002/btpr.2363

65. Brenac Brochier V, Ravault V. High throughput development of a non protein A monoclonal antibody purification process using mini-columns and bio-layer interferometry. Eng Life Sci 2016; 16:152–9. doi: 10.1002/elsc.201400244

66. Baumann P, Hahn T, Hubbuch J. High-throughput micro-scale cultivations and chromatography modeling: Powerful tools for integrated process development. Biotechnol Bioeng 2015; 112:2123–33. doi: 10.1002/bit.25630

67. Baumgartner K, Galm L, Nötzold J, Sigloch H, Morgenstern J, Schleining K, Suhm S, Oelmeier SA, Hubbuch J. Determination of protein phase diagrams by microbatch experiments: Exploring the influence of precipitants and pH. Int J Pharm 2015; 479:28–40. doi: 10.1016/j.ijpharm.2014.12.027

68. Chai Q, Shih J, Weldon C, Phan S, Jones BE. Development of a high-throughput solubility screening assay for use in antibody discovery. MAbs 2019; 11:747–56. doi: 10.1080/19420862.2019.1589851

69. Catcott KC, McShea MA, Bialucha CU, Miller KL, Hicks SW, Saxena P, Gesner TG, Woldegiorgis M, Lewis ME, Bai C, et al. Microscale screening of antibody libraries as maytansinoid antibody-drug conjugates. MAbs 2016; 8:513–23. doi: 10.1080/19420862.2015.1134408

70. Puthenveetil S, Musto S, Loganzo F, Tumey LN, O'Donnell CJ, Graziani E. Development of Solid-Phase Site-Specific Conjugation and Its Application toward Generation of Dual Labeled Antibody and Fab Drug Conjugates. Bioconjug Chem 2016; 27:1030–9. doi: 10.1021/acs.bioconjchem.6b00054

71. Antony J. Fundamentals of Design of Experiments. In: Design of experiments for engineers and scientists. Elsevier Ltd.; 2014. page 7–18.

72. Yang T, Sundling MC, Freed AS, Breneman CM, Cramer SM. Prediction of pH-dependent chromatographic behavior in ion-exchange systems. Anal Chem 2007; 79:8927–39. doi: 10.1021/ac071101j

73. Hämmerling F, Ladd Effio C, Andris S, Kittelmann J, Hubbuch J. Investigation and prediction of protein precipitation by polyethylene glycol using quantitative structure-activity relationship models. J Biotechnol 2017; 241:87–97. doi: 10.1016/j.jbiotec.2016.11.014

74. Rüdt M, Brestrich N, Rolinger L, Hubbuch J. Real-time monitoring and control of the load phase of a protein A capture step. Biotechnol Bioeng 2017; 114:368–73. doi: 10.1002/bit.26078

75. Mollerup JM, Hansen TB, Kidal S, Staby A. Quality by design-Thermodynamic modelling of chromatographic separation of proteins. J Chromatogr A 2008; 1177:200–6. doi: 10.1016/j.chroma.2007.08.059

76. Hu X, Bortell E, Kotch FW, Xu A, Arve B, Freese S. Development of Commercial-Ready Processes for Antibody Drug Conjugates. Org Process Res Dev 2017; 21:601–10. doi: 10.1021/acs.oprd.7b00023

77. FDA. Guidance for Industry - PAT - A Framework for Innovative Pharmaceutical Development, Manufacturing and Quality Assurance. 2004;

78. Kessler W. Multivariate Datenanalyse. Wiley-VCH Verlag GmbH & Co. KGaA; 2007.

79. Wold S, Esbensen K, Geladi P. Principal component analysis. Chemom Intell Lab Syst 1987; 2:37–52. doi: 10.1016/0169-7439(87)80084-9

80. Wold S, Sjöström M, Eriksson L. PLS-regression: A basic tool of chemometrics. Chemom Intell Lab Syst 2001; 58:109–30. doi: 10.1016/S0169-7439(01)00155-1

81. Brestrich N, Briskot T, Osberghaus A, Hubbuch J. A tool for selective inline quantification of co-eluting proteins in chromatography using spectral analysis and partial least squares regression. Biotechnol Bioeng 2014; 111:1365–73. doi: 10.1002/bit.25194

82. Schmidt-Traub H, Schulte M, Seidel-Morgenstern A. Preparative Chromatography. Wiley-VCH Verlag GmbH & Co. KGaA; 2012.

83. Unger KK, Ditz R, Machtejevas E, Skudas R. Liquid chromatography-its development and key role in life science applications. Angew Chemie - Int Ed 2010; 49:2300–12. doi: 10.1002/anie.200906976

84. Marcus Y. Effect of ions on the structure of water. Pure Appl Chem 2009; 109:1346–70. doi: 10.1351/PAC-CON-09-07-02

85. Mollerup JM. Applied thermodynamics: A new frontier for biotechnology. Fluid Phase Equilib 2006; 241:205–15. doi: 10.1016/j.fluid.2005.12.037

86. Godwin A, Bryant P, Pabst M, Badescu G, Bird M, McDowell W, Jamieson E, Swierkosz J, Jurlewicz K, Tommasi R, et al. In vitro and in vivo evaluation of cysteine rebridged trastuzumab-MMAE antibody drug conjugates with defined drug-to-antibody ratios. Mol Pharm 2015; 12:1872–9. doi: 10.1021/acs.molpharmaceut.5b00116

87. Kudirka R, Barfield RM, McFarland J, Albers AE, De Hart GW, Drake PM, Holder PG, Banas S, Jones LC, Garofalo AW, et al. Generating site-specifically modified proteins via a versatile and stable nucleophilic carbon ligation. Chem Biol 2015; 22:293–8. doi: 10.1016/j.chembiol.2014.11.019

88. Drake PM, Albers AE, Baker J, Banas S, Barfield RM, Bhat AS, De Hart GW, Garofalo AW, Holder P, Jones LC, et al. Aldehyde tag coupled with HIPS chemistry enables the production of ADCs conjugated site-specifically to different antibody regions with distinct in vivo efficacy and PK outcomes. Bioconjug Chem 2014; 25:1331–41. doi: 10.1021/bc500189z

89. Pirrung SM, van der Wielen LAM, van Beckhoven RFWC, van de Sandt EJAX, Eppink MHM, Ottens M. Optimization of biopharmaceutical downstream processes supported by mechanistic models and artificial neural networks. Biotechnol Prog 2017; 33:696–707. doi: 10.1002/btpr.2435

90. Wang G, Briskot T, Hahn T, Baumann P, Hubbuch J. Root cause investigation of deviations in protein chromatography based on mechanistic models and artificial neural networks. J Chromatogr A 2017; 1515:146–53. doi: 10.1016/j.chroma.2017.07.089

91. Close EJ, Salm JR, Bracewell DG, Sorensen E. Modelling of industrial biopharmaceutical multicomponent chromatography. Chem Eng Res Des 2014; 92:1304–14. doi: 10.1016/j.cherd.2013.10.022

92. Huuk TC, Hahn T, Doninger K, Griesbach J, Hepbildikler S, Hubbuch J. Modeling of complex antibody elution behavior under high protein load densities in ion exchange chromatography using an asymmetric activity coefficient. Biotechnol J 2017; 12. doi: 10.1002/biot.201600336

93. Shekhawat LK, Chandak M, Rathore AS. Mechanistic modeling of hydrophobic interaction chromatography for monoclonal antibody purification: process optimization in the quality by design paradigm. J

Chem Technol Biotechnol 2018; 93:2784. doi: 10.1002/jctb.5742

94. Seidel-Morgenstern A, Schmidt-Traub H, Michel M, Epping A, Jupke A. Modeling and model parameters. In: Preparative Chromatography. Wiley-VCH Verlag GmbH & Co. KGaA; 2012. page 312–418.

95. Mollerup JM. A review of the thermodynamics of protein association to ligands, protein adsorption, and adsorption isotherms. Chem Eng Technol 2008; 31:864–74. doi: 10.1002/ceat.200800082

96. Wang G, Hahn T, Hubbuch J. Water on Hydrophobic Surfaces: Mechanistic Modeling of Hydrophobic Interaction Chromatography. J Chromatogr A 2016; 1465:71–8. doi: 10.1016/j.chroma.2016.07.085

97. Brooks CA, Cramer SM. Steric mass-action ion exchange: Displacement profiles and induced salt gradients. AIChE J 1992; 38:1969–78. doi: 10.1002/aic.690381212

98. Beck A, Goetsch L, Dumontet C, Corvaia N. Strategies and challenges for the next generation of therapeutic antibodies. Nat Rev Drug Discov 2017; 16:315–37. doi: 10.1038/nrd.2016.268

99. Lhospice F, Brégeon D, Belmant C, Dennler P, Chiotellis A, Fischer E, Gauthier L, Boedec A, Rispaud H, Savard-Chambard S, et al. Site-Specific Conjugation of Monomethyl Auristatin E to Anti-CD30 Antibodies Improves Their Pharmacokinetics and Therapeutic Index in Rodent Models. Mol Pharm 2015; 12:1863–71. doi: 10.1021/mp500666j

100. Pillow TH, Tien J, Parsons-reponte KL, Bhakta S, Li H, Staben LR, Li G, Chuh J, Donohue AF, Darwish M, et al. Site-Specific Trastuzumab Maytansinoid Antibody − Drug Conjugates with Improved Therapeutic Activity through Linker and Antibody Engineering. J Med Chem 2014; 57:7890–9. doi: 10.1021/jm500552c

101. Treier K, Hansen S, Richter C, Diederich P, Hubbuch J, Lester P. High-throughput methods for miniaturization and automation of monoclonal antibody purification processes. Biotechnol Prog 2012; 28:723–32. doi: 10.1002/btpr.1533

102. Maiser B, Dismer F, Hubbuch J. Optimization of random PEGylation reactions by means of high throughput screening. Biotechnol Bioeng 2014; 111:104–14. doi: 10.1002/bit.25000

103. Oelmeier S, Ladd Effio C, Hubbuch J. High throughput screening based selection of phases for aqueous two-phase system-centrifugal partitioning chromatography of monoclonal antibodies. J Chromatogr A 2012; 1252:104–14. doi: 10.1016/j.chroma.2012.06.075

104. Wendeler M, Grinberg L, Wang X, Dawson PE, Baca M. Enhanced catalysis of oxime-based bioconjugations by substituted anilines. Bioconjug Chem 2014; 25:93–101. doi: 10.1021/bc400380f

105. Burke PJ, Hamilton JZ, Pires TA, Setter JR, Hunter JH, Cochran JH, Waight AB, Gordon KA, Toki BE, Emmerton KK, et al. Development of Novel Quaternary Ammonium Linkers for Antibody–Drug Conjugates. Mol Cancer Ther 2016; 15:938–45. doi: 10.1158/1535-7163.MCT-16-0038

106. Vink M, Derr K, Love J, Stokes DL, Ubarretxena-Belandia I. A high-throughput strategy to screen 2D crystallization trials of membrane proteins. J Struct Biol 2007; 160:295–304. doi: 10.1016/j.jsb.2007.09.003

107. Bailey MJ, Hooker AD, Adams CS, Zhang S, James DC. A platform for high-throughput molecular characterization of recombinant monoclonal antibodies. J Chromatogr B 2005; 826:177–87. doi: 10.1016/j.jchromb.2005.08.021

108. Zimmerman ES, Heibeck TH, Gill A, Li X, Murray CJ, Madlansacay MR, Tran C, Uter NT, Yin G, Rivers PJ, et al. Production of Site-Specific Antibody−Drug Conjugates Using Optimized Non-Natural Amino Acids in a Cell-Free Expression System. Bioconjug Chem 2014; 25:351–61. doi: 10.1021/bc400490z

109. Staben LR, Koenig SG, Lehar SM, Vandlen R, Zhang D, Chuh J, Yu S-F, Ng C, Guo J, Liu Y, et al. Targeted drug delivery through the traceless release of tertiary and heteroaryl amines from antibody–drug conjugates. Nat Chem 2016; 8:1112–9. doi: 10.1038/nchem.2635

110. Christie RJ, Fleming R, Bezabeh B, Woods R, Mao S, Harper J, Joseph A, Wang Q, Xu ZQ, Wu H, et al. Stabilization of cysteine-linked antibody drug conjugates with N-aryl maleimides. J Control Release 2015; 220:660–70. doi: 10.1016/j.jconrel.2015.09.032

111. Hamblett KJ, Senter PD, Chace DF, Sun MMC, Lenox J, Cerveny CG, Kissler KM, Bernhardt SX, Kopcha AK, Zabinski RF, et al. Effects of Drug Loading on the Antitumor Activity of a Monoclonal Antibody Drug Conjugate. Clin cancer Res 2004; 10:7063–70. doi: 10.1158/1078-0432.CCR-04-0789

112. Sun MMC, Beam KS, Cerveny CG, Hamblett KJ, Blackmore RS, Torgov MY, Handley FGM, Ihle NC, Senter PD, Alley SC. Reduction-Alkylation Strategies for the Modification of Specific Monoclonal Antibody Disulfides. Bioconjug Chem 2005; 16:1282–90. doi: 10.1021/bc050201y

113. Xu Y, Jiang G, Tran C, Li X, Heibeck TH, Masikat MR, Cai Q, Steiner AR, Sato AK, Hallam TJ, et al. RP-HPLC DAR Characterization of Site-Specific Antibody Drug Conjugates Produced in a Cell Free Expression System. Org Process Res Dev 2016; 20:1034–43. doi: 10.1021/acs.oprd.6b00072

114. Lyon RP, Bovee TD, Doronina SO, Burke PJ, Hunter JH, Neff-LaFord HD, Jonas M, Anderson ME, Setter JR, Senter PD. Reducing hydrophobicity of homogeneous antibody-drug conjugates improves pharmacokinetics and therapeutic index. Nat Biotechnol 2015; 33:733–6.

doi: 10.1038/nbt.3212

115. Jain N, Smith SW, Ghone S, Tomczuk B. Current ADC Linker Chemistry. Pharm Res 2015; 32:3526–40. doi: 10.1007/s11095-015-1657-7

116. Junutula JR, Gerber H-P. Next-Generation Antibody-Drug Conjugates (ADCs) for Cancer Therapy. ACS Med Chem Lett 2016; 7:972–3. doi: 10.1021/acsmedchemlett.6b00421

117. Schumacher D, Hackenberger CPR, Leonhardt H, Helma J. Current Status: Site-Specific Antibody Drug Conjugates. J Clin Immunol 2016; 36:100–7. doi: 10.1007/s10875-016-0265-6

118. Wakankar A, Chen Y, Gokarn Y, Jacobson FS. Analytical methods for physicochemical characterization of antibody drug conjugates. MAbs 2011; 3:161–72. doi: 10.4161/mabs.3.2.14960

119. Chari RVJ, Martell BA, Gross JL, Cook SB, Shah SA, Blättler WA, McKenzie SJ, Goldmacher VS. Immunoconjugates Containing Novel Maytansinoids: Promising Anticancer Drugs. Cancer Res 1992; 52:127–31.

120. Tang Y, Tang F, Yang Y, Zhao L, Zhou H, Dong J, Huang W. Real-Time Analysis on Drug-Antibody Ratio of Antibody-Drug Conjugates for Synthesis, Process Optimization, and Quality Control. Sci Rep 2017; 7:7763–73. doi: 10.1038/s41598-017-08151-2

121. Bakeev KA. Process Analytical Technology: Spectroscopic Tools and Implementation Strategies for the Chemical and Pharmaceutical Industries. 2nd ed. John Wiley & Sons; 2010.

122. Bakeev KA. Process Analytical Technology. Blackwell Publishing Ltd; 2005.

123. Simon LL, Pataki H, Marosi G, Meemken F, Hungerbühler K, Baiker A, Tummala S, Glennon B, Kuentz M, Steele G, et al. Assessment of recent process analytical technology (PAT) trends: A multiauthor review. Org Process Res Dev 2015; 19:3–62. doi: 10.1021/op500261y

124. Hansen SK, Jamali B, Hubbuch J. Selective high throughput protein quantification based on UV absorption spectra. Biotechnol Bioeng 2013; 110:448–60. doi: 10.1002/bit.24712

125. Quinn AC, Gemperline PJ, Baker B, Zhu M, Walker DS. Fiber-optic UV/visible composition monitoring for process control of batch reactions. Chemom Intell Lab Syst 1999; 45:199–214. doi: 10.1016/S0169-7439(98)00105-1

126. Gurden SP, Westerhuis JA, Smilde AK. Monitoring of batch processes using spectroscopy. AIChE J 2002; 48:2283–97. doi: 10.1002/aic.690481018

127. Suppan P. Invited review solvatochromic shifts: The influence of the medium on the energy of electronic states. J Photochem Photobiol A Chem 1990; 50:293–330. doi: 10.1016/1010-6030(90)87021-3

128. Reichardt C, Welton T. Solvents and solvent effects in organic chemistry. John Wiley & Sons; 2011.

129. Jiskoot W, Crommelin D, editors. Methods for structural analysis of protein pharmaceuticals. American Association of Pharmaceutical Scientists; 2005.

130. de Jong S. SIMPLS: An alternative approach to partial least squares regression. Chemom Intell Lab Syst 1993; 18:251–63. doi: 10.1016/0169-7439(93)85002-X

131. Savitzky A, Golay MJE. Smoothing and differentiation of data by simplified least squares procedures. Anal Chem 1964; 36:1627–39.

132. Deep K, Singh KP, Kansal ML, Mohan C. A real coded genetic algorithm for solving integer and mixed integer optimization problems. Appl Math Comput 2009; 212:505–18. doi: 10.1016/j.amc.2009.02.044

133. Ragone R, Colonna G, Balestrieri C, Servillo L, Irace G. Determination of tyrosine exposure in proteins by second-derivative spectroscopy. Biochem 1984; 23:1871–5.

134. Mach H, Middaugh CR. Simultaneous monitoring of the environment of tryptophan, tyrosine, and phenylalanine residues in proteins by near-ultraviolet second-derivative spectroscopy. Anal Biochem 1994; 222:323–31. doi: 10.1006/abio.1994.1499

135. Tedaldi LM, Aliev AE, Baker JR. [2 + 2] Photocycloadditions of thiomaleimides. Chem Commun 2012; 48:4725–7. doi: 10.1039/C2CC31673K

136. Lambert JM, Berkenblit A. Antibody-Drug Conjugates for Cancer Treatment. Annu Rev Med 2018; 69:191–207. doi: 10.1146/annurev-med-061516-121357

137. Lu J, Jiang F, Lu A, Zhang G. Linkers Having a Crucial Role in Antibody–Drug Conjugates. Int J Mol Sci 2016; 17:561. doi: 10.3390/ijms17040561

138. Akkapeddi P, Azizi S-A, Freedy A, Cal PMSD, Gois PMP, Bernardes GJL. Construction of Homogeneous Antibody-drug Conjugates using Site-selective Protein Chemistry. Chem Sci 2016; doi: 10.1039/C6SC00170J

139. Tumey LN, Li F, Rago B, Han X, Loganzo F, Musto S, Graziani EI, Puthenveetil S, Casavant J, Marquette K, et al. Site Selection: a Case Study in the Identification of Optimal Cysteine Engineered Antibody Drug Conjugates. AAPS J 2017; doi: 10.1208/s12248-017-0083-7

140. Tolcher AW. Antibody drug conjugates: lessons from 20 years of clinical experience. Ann Oncol 2016; :1–5. doi: 10.1093/annonc/mdw424

141. Gikanga B, Adeniji NS, Patapoff TW, Chih HW, Yi L. Cathepsin B Cleavage of vcMMAE-Based Antibody-Drug Conjugate Is Not Drug Location or Monoclonal Antibody Carrier Specific. Bioconjug Chem 2016; 27:1040–9. doi: 10.1021/acs.bioconjchem.6b00055

142. Westerberg K, Broberg Hansen E, Degerman M, Budde Hansen T, Nilsson B. Model-based process challenge of an industrial ion-exchange chromatography step. Chem Eng Technol 2012; 35:183–90. doi: 10.1002/ceat.201000560

143. Moosmann A, Blath J, Lindner R, Müller E, Böttinger H. Aldehyde PEGylation kinetics: A standard protein versus a pharmaceutically relevant single chain variable fragment. Bioconjug Chem 2011; 22:1545–58. doi: 10.1021/bc200090x

144. Dai P, Zhang C, Welborn M, Shepherd JJ, Zhu T, Van Voorhis T, Pentelute BL. Salt effect accelerates site-selective cysteine bioconjugation. ACS Cent Sci 2016; 2:637–46. doi: 10.1021/acscentsci.6b00180

145. Lé-Quóc K, Le-Quóc D, Gaudemer Y. Evidence for the Existence of Two Classes of Sulfhydryl Groups Essential for Membrane-Bound Succinate Dehydrogenase Activity. Biochemistry 1981; 20:1705–10. doi: 10.1021/bi00510a001

146. Ohyashiki T, Taka M, Mohri T. The Effects of Ionic Strength on the Protein Conformation and the Fluidity of Porcine Intestinal Brush Border Membranes. J Biol Chem 1985; 260:6857–61.

147. Kukura JL, Thien MP. Current Challenges and Opportunities in the Pharmaceutical Industry. In: Chemical Engineering in the Pharmaceutical Industry. 2019. page 19–26.

148. Pfister D, Ulmer N, Klaue A, Ingold O, Morbidelli M. Modeling the Kinetics of Protein Conjugation Reactions. Chemie-Ingenieur-Technik 2016; 88:1598–608. doi: 10.1002/cite.201600046

149. Tomaz C. Hydrophobic interaction chromatography. In: Liquid chromatography. Elsevier Inc.; 2017. page 171–90.

150. Melander WR, Corradini D, Horváth C. Salt-mediated retention of proteins in hydrophobic-interaction chromatography. Application of solvophobic theory. J Chromatogr A 1984; 317:67–85. doi: 10.1016/S0021-9673(01)91648-6

151. Geng X, Guo L, Chang J. Study of the retention mechanism of proteins in hydrophobic interaction chromatography. J Chromatogr A 1990; 507:1–23. doi: 10.1016/S0021-9673(01)84176-5

152. Staby A, Mollerup J. Solute retention of lysozyme in hydrophobic interaction perfusion chromatography. J Chromatogr A 1996; 734:205–12. doi: 10.1016/0021-9673(95)01161-7

153. Perkins TW, Mak DS, Root TW, Lightfoot EN. Protein retention in hydrophobic interaction chromatography: Modeling variation with buffer ionic strength and column hydrophobicity. J Chromatogr A 1997; 766:1–14. doi: 10.1016/S0021-9673(96)00978-8

154. Jakobsson N, Degerman M, Nilsson B. Optimisation and robustness analysis of a hydrophobic interaction chromatography step. J Chromatogr A 2005; 1099:157–66. doi: 10.1016/j.chroma.2005.09.009

155. Nagrath D, Xia F, Cramer SM. Characterization and modeling of nonlinear hydrophobic interaction chromatographic systems. J Chromatogr A 2011; 1218:1219–26. doi: 10.1016/j.chroma.2010.12.111

156. Borrmann C, Helling C, Lohrmann M, Sommerfeld S, Strube J. Phenomena and modeling of hydrophobic interaction chromatography. Sep Sci Technol 2011; 46:1289–305. doi: 10.1080/01496395.2011.561515

157. Kumar V, Rathore AS. Mechanistic Modeling Based PAT Implementation for Ion-Exchange Process Chromatography of Charge Variants of Monoclonal Antibody Products. Biotechnol J 2017; 12:1–9. doi: 10.1002/biot.201700286

158. Danckwerts P V. Continuous flow systems - Distribution of residence times. Chem Eng Sci 1953; 2:1–13. doi: 10.1016/0009-2509(96)81810-0

159. To BCS, Lenhoff AM. Hydrophobic interaction chromatography of proteins. II. Solution thermodynamic properties as a determinant of retention. J Chromatogr A 2007; 1141:235–43. doi: 10.1016/j.chroma.2006.12.022

160. Ingber L. Adaptive simulated annealing. In: Stochastic Global Optimization & Its Applications. 2012. page 33–62.

161. Agarwal S, Mierle K. Ceres Solver.

162. Glowinski R. Handbook of numerical analysis. 9th ed. 2003.

163. Jungbauer A, Machold C, Hahn R. Hydrophobic interaction chromatography of proteins: III. Unfolding of proteins upon adsorption. J Chromatogr A 2005; 1079:221–8. doi: 10.1016/j.chroma.2005.04.002

164. Jones TT, Fernandez EJ. Hydrophobic interaction chromatography selectivity changes among three stable proteins: Conformation does not play a major role. Biotechnol Bioeng 2004; 87:388–99. doi: 10.1002/bit.20123

165. Jones TT, Fernandez EJ. A-Lactalbumin Tertiary Structure Changes on Hydrophobic Interaction Chromatography Surfaces. J Colloid Interface

Sci 2003; 259:27–35. doi: 10.1016/S0021-9797(02)00180-7

166. Park J-G, Lee S-H, Ryu J-S, Hong Y-K, Kim T-G, Busnaina AA. Interfacial and Electrokinetic Characterization of IPA Solutions Related to Semiconductor Wafer Drying and Cleaning. J Electrochem Soc 2006; 153:G811. doi: 10.1149/1.2214532

167. Briskot T, Stückler F, Wittkopp F, Williams C, Yang J, Konrad S, Doninger K, Griesbach J, Bennecke M, Hepbildikler S, et al. Prediction uncertainty assessment of chromatography models using Bayesian inference. J Chromatogr A 2019; 1587:101–10. doi: 10.1016/j.chroma.2018.11.076

168. Guiochon G, Felinger A, Shirazi DG, Katti AM. Fundamentals of preparative and nonlinear chromatography. 2nd ed. Elsevier Inc.; 2006.

Abbreviations

AC	Affinity chromatography
ADC	Antibody-drug conjugates
ADCC	Antibody-dependent cellular cytotoxicity
API	Active pharmaceutical ingredient
ASA	Adaptive simulated annealing
CDC	Complement-dependent cytotoxicity
CDR	Complementarity-determining regions
CEX	Cation exchange
CFD	Computational fluid dynamics
CPM	7-Diethylamino-3-(4'-maleimidylphenyl)-4-methylcoumarin
CPP	Critical process parameter
CQA	Critical quality attribute
CV	Cross-validation
DAD	Diode array detector
DAR	Drug-to-antibody ratio
DBC	Dynamic binding capacity
DHA	(L)-Dehydroascorbic acid
DMSO	Dimethyl sulfoxide
DoE	Design of experiments
EMA	European Medicines Agency
FDA	Food and Drug Administration (USA)
GuHCl	Guanidine hydrochloride
HCCF	Harvested cell culture fluid
HIC	Hydrophobic interaction chromatography
HTC	High-throughput conjugation
HTS	High-throughput screening
IC_{50}	Half maximal inhibitory concentration
ICH	International conference on harmonization of technical requirements for registration of pharmaceuticals for human use
IEX	Ion exchange chromatography
IgG	Immunoglobulin G
IPA	Isopropanol

|	
IS	Ionic strength
LC	Liquid chromatography
mAb	Monoclonal antibody
MLR	Multiple linear regression
MVDA	Multivariate data analysis
MWCO	Molecular weight cut-off
NAC	N-Acetyl-cysteine
NHS	N-hydroxysuccinimide
NPM	N-(1-Pyrenyl)maleimide
NPM ratio	Molar ratio of NPM over mAb at start of reaction
ODE	Ordinary differential equation
PAT	Process analytical technology
PBS	Phosphate-buffered saline
PC	Principal component
PCA	Principal component analysis
PLS	Partial least squares
PP	Polypropylene
PRESS	Predictive residual sum of squares
QbD	Quality by design
QSAR	Quantitative structure-activity relationships
QTPP	Quality target product profile
RMSECV	Root mean square error of cross-validation
RMSEP	Root mean square error of prediction
RP-UHPLC	Reversed-phase ultra-high performance liquid chromatography
RPC	Reversed-phase chromatography
SEC	Size-exclusion chromatography
TCEP	Tris(2-carboxyethyl)phosphine hydrochloride
TDM	Transport-dispersive model
TFA	Trifluoroacetic acid
UHPLC	Ultra-high performance liquid chromatography

Symbols

a	Number of principal components in T
c	Chapter 3: Protein concentration
c_i	Molar concentration of component i in the mobile phase
$c_{\text{in},i}$	Applied inlet concentration
$C_{\text{mAb}_{0c}}$	Molar concentration of mAb with zero free thiols
$C_{\text{mAb}_{0c}\text{NPM}}$	Molar concentration of mAb with zero free thiols and one NPM attached
$C_{\text{mAb}_{0c}\text{NPM}_a}$	Molar concentration of mAb with zero free thiols and one NPM attached to binding site a
$C_{\text{mAb}_{0c}\text{NPM}_b}$	Molar concentration of mAb with zero free thiols and one NPM attached to binding site b
$C_{\text{mAb}_{0c}(\text{NPM})_{ab}}$	Molar concentration of mAb with zero free thiols and one NPM attached to binding site a and b
$C_{\text{mAb}_{0c}(\text{NPM})_2}$	Molar oncentration of mAb with zero free thiols and two NPM attached
$C_{\text{mAb}_{1c}}$	Molar concentration of mAb with one free thiol
$C_{\text{mAb}_{1c}\text{NPM}}$	Molar concentration of mAb with one free thiol and one NPM attached
$C_{\text{mAb}_{2c}}$	Molar concentration of mAb with two free thiols
C_{mAb_a}	Molar concentration of mAb with one free thiol at binding site a
$C_{\text{mAb}_{ab}}$	Molar concentration of mAb with one free thiol at binding site a and one free thiol at binding site b
$C_{\text{mAb}_a\text{NPM}_b}$	Molar concentration of mAb with one free thiol at binding site a and one NPM attached at binding site b
C_{mAb_b}	Molar concentration of mAb with one free thiol at binding site b
$C_{\text{mAb}_b\text{NPM}_a}$	Molar concentration of mAb with one free thiol at binding site b and one NPM attached at binding site a
C_{NPM}	Molar concentration of NPM
$c_{\text{p},i}$	Molar concentration of component i in the pores
$c_{\text{p,salt}}$	Molar salt concentration in the pores
c_{step}	Ionic strength of first step
$c(mAb)$	Molar concentration of mAb
d	Inner column diameter

| D_{ax} | Axial dispersion coefficient |
d_c	Inner column diameter
E	Residual matrix in PCA or PLS
IC_{50}	Half maximal inhibitory concentration
k	Rate constant of NPM attachment in model 1 and 4
k_1	Rate constant of first NPM attachment in model 2 and 5
k_2	Rate constant of second NPM attachment in model 2 and 5
$k_1{}'$	Rate constant of NPM attachment to first binding site in model 3 and 6
$k_2{}'$	Rate constant of NPM attachment to second binding site in model 3 and 6
k_3	Rate constant of NPM depletion in kinetic models
$k_{eff,i}$	Effective mass transfer coefficient of component i
$k_{eq,i}$	Equilibrium constant in adsorption isotherm
$k_{kin,i}$	Kinetic constant in adsorption isotherm
$k_{p,i}$	Parameter describing the effect of protein concentration on activity coefficient of component i
$k_{s,i}$	Parameter describing effect of salt concentration on activity coefficient of component i
L	Column length
m	Number of variables in X
mAb	Unconjugated monoclonal antibody
$mAb+0$	mAb with zero surrogate drugs attached
$mAb+1$	mAb with one surrogate drugs attached
$mAb+2$	mAb with two surrogate drugs attached
$mAbNPM_1$	Monoclonal antibody with one NPM attached
$mAbNPM_2$	Monoclonal antibody with two NPM attached
N	Number of components
n	Number of observations in X
n_j	Number of ligands bounds per protein j
NPM	N-(1-Pyrenyl)maleimide
P	Loadings matrix of X-data in PCA
p_i	i^{th} vector in P
Q	Loadings matrix of Y-data in PLS
Q^2	Coefficient of determination of cross-validation
q_i	Section 1.3: i^{th} vector in Q

q_i	Section 1.4 and Chapter 6: Molar protein concentration adsorbed to solid phase
$q_{max,j}$	Saturation capacity of adsorber for component j
R^2	Coefficient of determination
R^2_{pred}	R^2 of prediction
r_p	Particle / bead radius
RMSECV	Root mean square error of cross-validation
RMSEP	Root mean square error of prediction
T	Scores matrix of X in PCA or PLS
t	Time
t_i	i^{th} vector in T
U	Scores matrix of Y in PLS
u	Superficial velocity
u_i	Vector with greatest Euclidean norm out of the columns of Y
u_{int}	Interstitial velocity of mobile phase
$\dot{V}$	Volumetric flow rate
V_{ads}	Volume of the stationary phase
V_c	Column volume
V_d	System dead volume
V_f	Fluid volume
V_{int}	Interstitial volume
V_{pore}	Pore volume
V_R	Retention volume
V_{RAc}	Retention volume of acetone
V_{RDex}	Retention volume of dextran
V_{sol}	Volume of stationary phase
V_{step}	Volume of second step (before decrease in IS)
W	Weighted loadings matrix in PLS
w_i	i^{th} vector in W
X	Data matrix for PCA or PLS
x	Position along the column length
Y	Matrix containing target variables in PLS
y_i	i^{th} vector of Y
ε_{int}	Interstitial porosity
ε_p	Porosity of the stationary phase

|	
ε_{tot}	Total column porosity
λ_{max}	Wavelength of maximal absorbance

Suppl. Figure 1: Raw spectra of all calibration samples. The spectra are colored according to the reaction progress from blue to red. The microplate experiments are depicted in the top row, while the bottom row shows the spectra recorded in the lab-scale setup. Since the lab-scale experiments were performed at the same nominal mAb concentration, the different runs are artificially offset by 50 mAU. The left column shows experiments with NPM, the right column shows experiments with CPM.
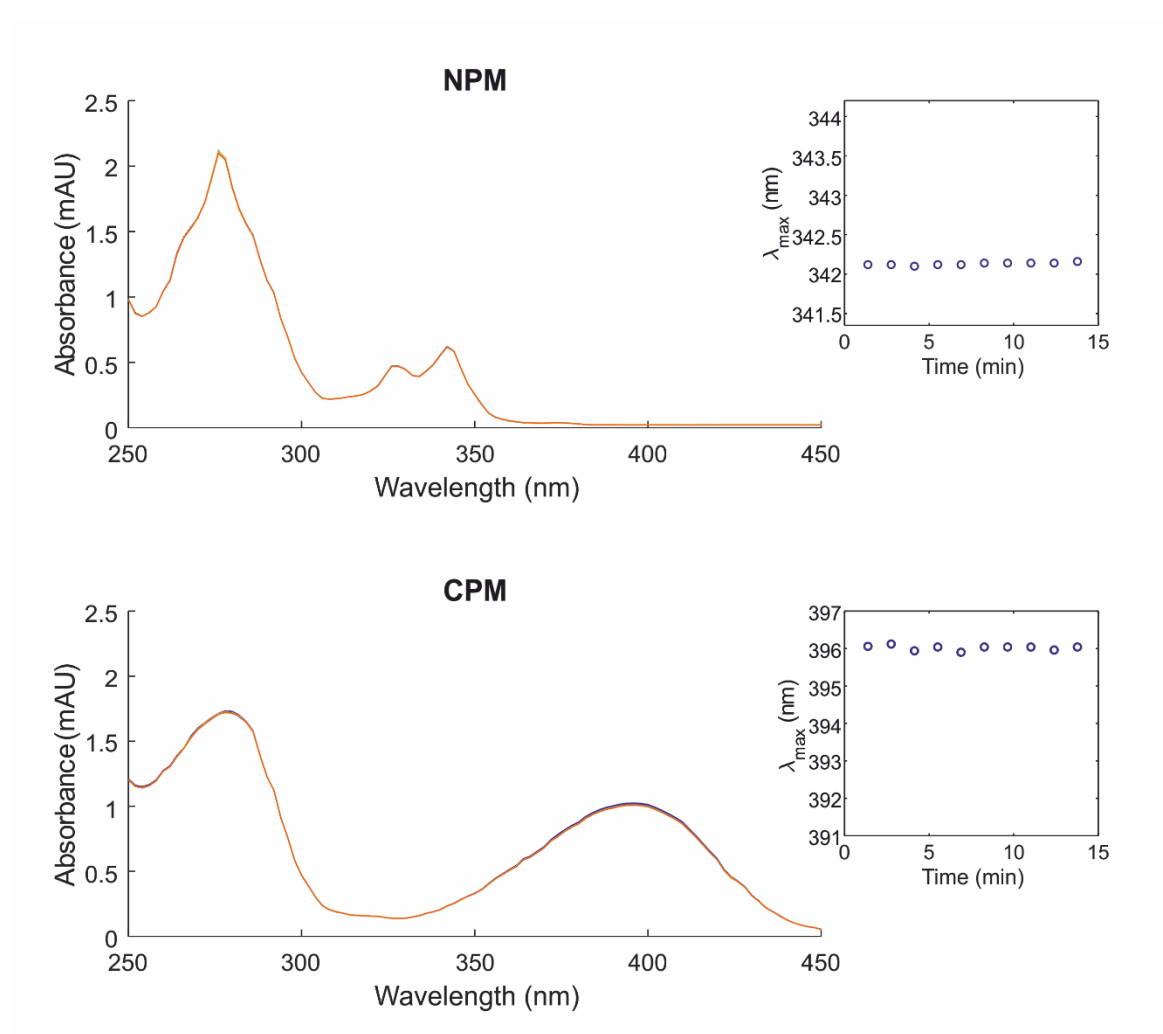
Suppl. Figure 2: Raw spectra of a mixture of 5T4 mAb and quenched drug recorded over the course of 15 min. The spectra are colored according to reaction time from blue to red. mAb, drug and NAC concentrations are the same as in the lab-scale experiments. The surrogate drugs were quenched prior to addition to the mAb solution in order to prevent the conjugation reaction. DMSO content is 10% as in the other experiments. The evolution of the band maxima of the drugs over time is shown on the right side. No shift in band maxima is observed.
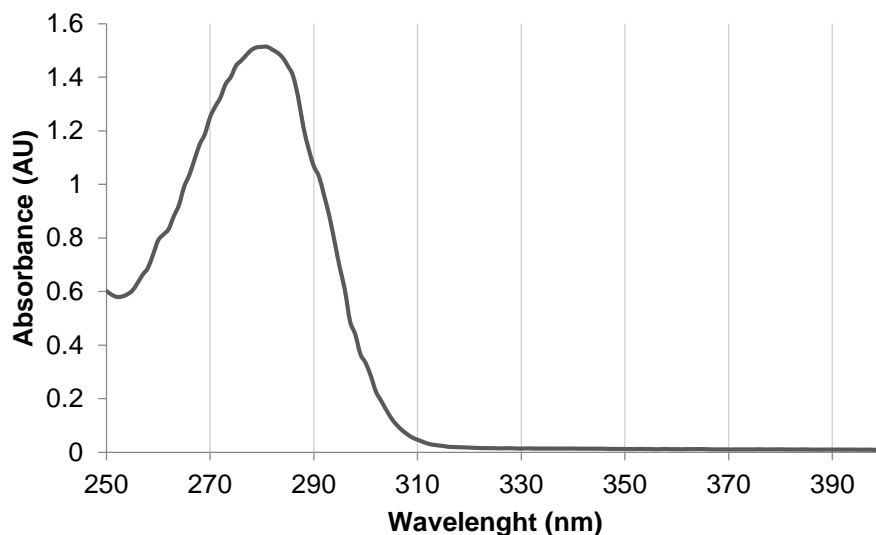
Suppl. Figure 3: Pure component UV/Vis absorbance spectrum of 5T4 mAb measured in Tecan plate reader M200 Pro at a concentration of 2 mg/mL (in 50 mM sodium phosphate buffer).
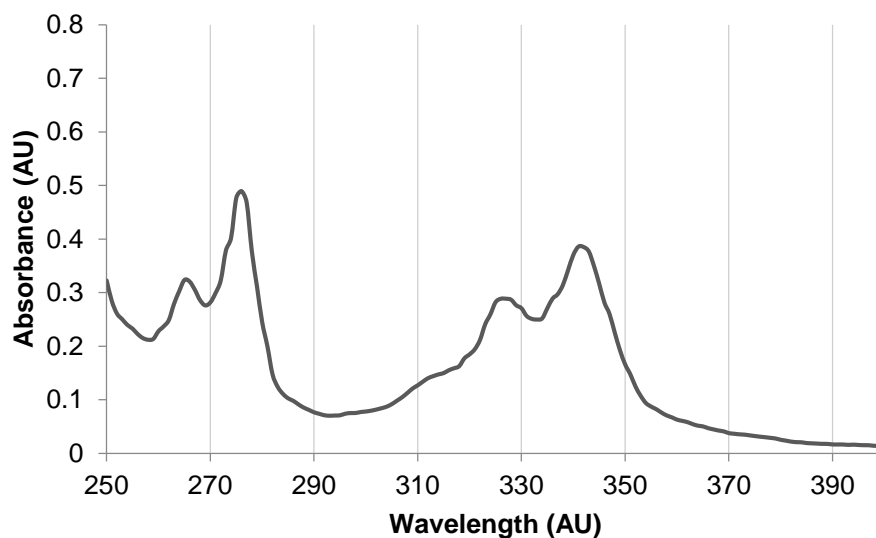
Suppl. Figure 4: Pure component UV/Vis absorbance spectrum of NPM in phosphate buffer containing 10% of DMSO measured in Tecan plate reader M200 Pro.
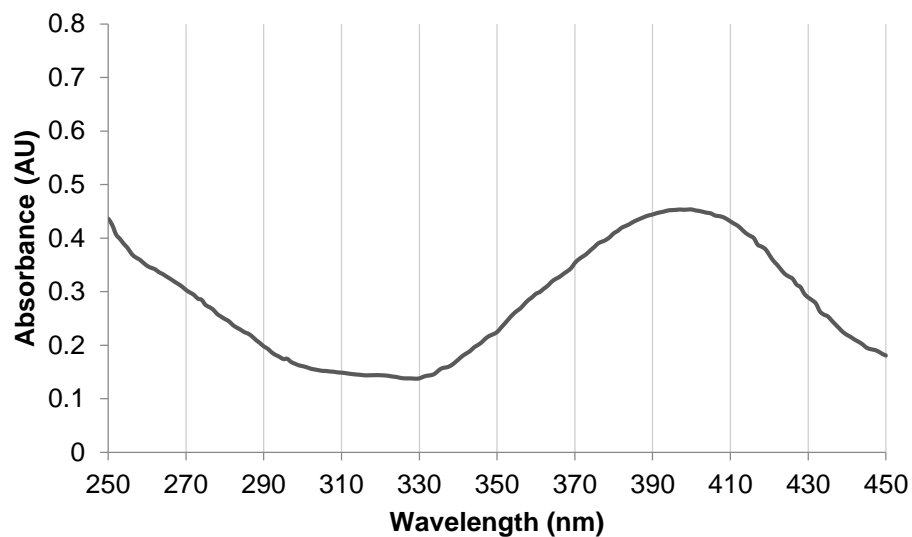
Suppl. Figure 5: Pure component UV/Vis absorbance spectrum of CPM in phosphate buffer containing 10% of DMSO measured in Tecan plate reader M200 Pro.

Appendix B   Supplementary data for Chapter 5
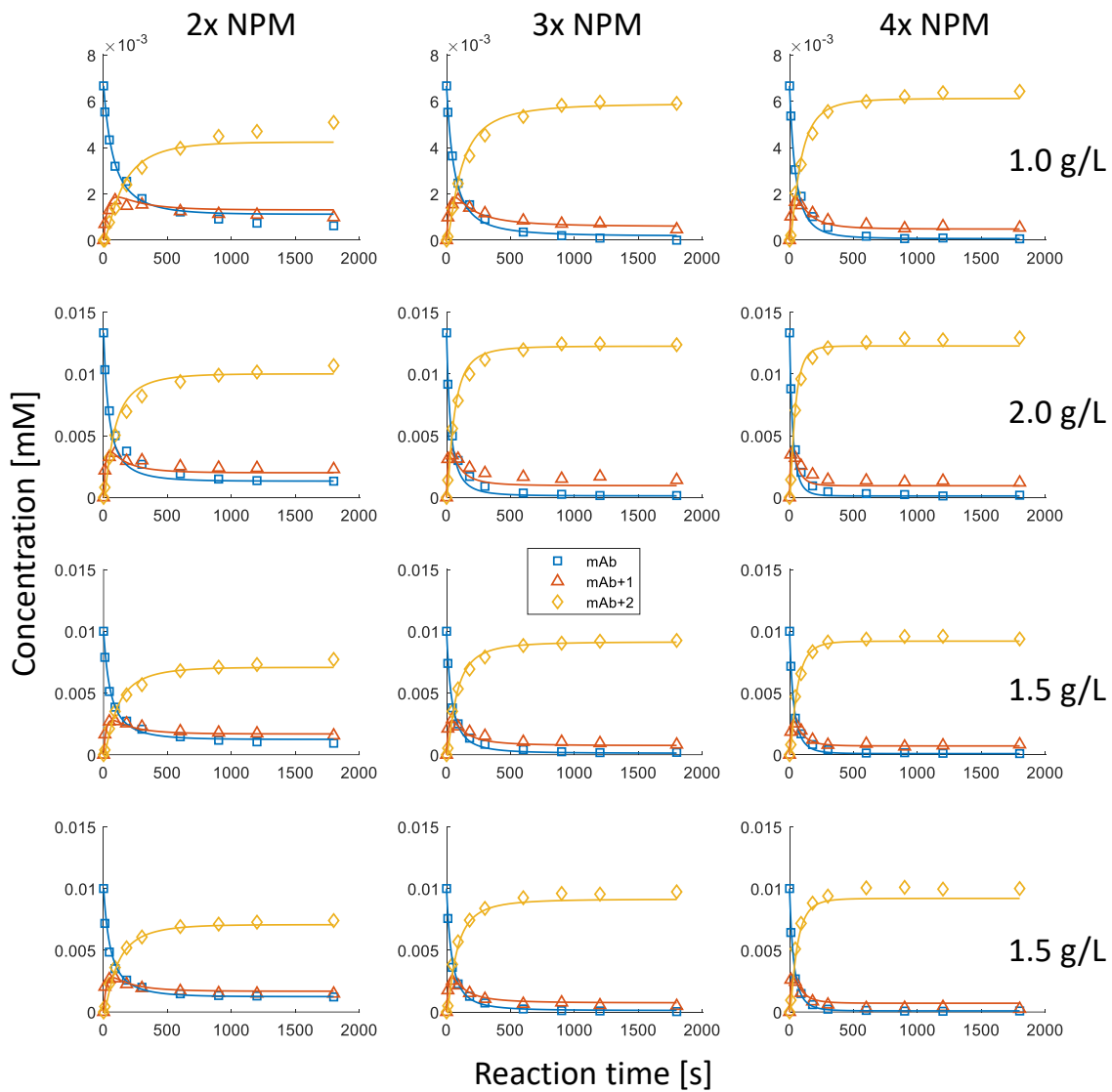
Suppl. Figure 6: Results of model 5 calibration for the 12 calibration experiments. Markers are experimental data and the respective model predictions are shown by straight lines. Blue square markers are the un-conjugated mAb, red triangles the mono-conjugated mAb and yellow diamonds the bi-conjugated mAb. R² was at 0.970.

Rate laws for model 4:

$$\frac{dC_{\text{mAb}_{2}\text{c}}}{dt} = -k_1 \cdot C_{\text{mAb}_{2}\text{c}} \cdot C_{\text{NPM}} \tag{A1}$$

$$\frac{dC_{\text{mAb}_{1}\text{c}}}{dt} = -k_1 \cdot C_{\text{mAb}_{1}\text{c}} \cdot C_{\text{NPM}} \tag{A2}$$

$$\frac{dC_{\text{mAb}_{0}\text{c}}}{dt} = 0 \tag{A3}$$

$$\frac{dC_{\text{mAb}_{1}\text{cNPM}}}{dt} = k_1 \cdot C_{\text{mAb}_{2}\text{c}} \cdot C_{\text{NPM}} - k_1 \cdot C_{\text{mAb}_{1}\text{cNPM}} \cdot C_{\text{NPM}} \tag{A4}$$

$$\frac{dC_{\text{mAb}_{0}\text{cNPM}}}{dt} = k_1 \cdot C_{\text{mAb}_{1}\text{c}} \cdot C_{\text{NPM}} \tag{A5}$$

$$\frac{dC_{\text{mAb}_{0}\text{c(NPM)}_2}}{dt} = k_1 \cdot C_{\text{mAb}_{1}\text{cNPM}} \cdot C_{\text{NPM}} \tag{A6}$$

$$\frac{dC_{\text{NPM}}}{dt} = -k_1 \cdot C_{\text{mAb}_{2}\text{c}} \cdot C_{\text{NPM}} - k_1 \cdot C_{\text{mAb}_{1}\text{c}} \cdot C_{\text{NPM}} - k_1 \cdot C_{\text{mAb}_{1}\text{cNPM}} \cdot C_{\text{NPM}} \\ - k_3 \cdot C_{\text{NPM}} \tag{A7}$$

The rate laws for model 1 are the same without the NPM sink term in equation A7 ($-k_3 \cdot C_{\text{NPM}}$).

Rate laws for model 6:

$$\frac{dC_{\text{mAb}_{\text{ab}}}}{dt} = -k_{1'} \cdot C_{\text{mAb}_{\text{ab}}} \cdot C_{\text{NPM}} - k_{2'} \cdot C_{\text{mAb}_{\text{ab}}} \cdot C_{\text{NPM}} \tag{A8}$$

$$\frac{dC_{\text{mAb}_{\text{a}}}}{dt} = -k_{1'} \cdot C_{\text{mAb}_{\text{a}}} \cdot C_{\text{NPM}} \tag{A9}$$

$$\frac{dC_{\text{mAb}_{\text{b}}}}{dt} = -k_{2'} \cdot C_{\text{mAb}_{\text{b}}} \cdot C_{\text{NPM}} \tag{A10}$$

$$\frac{dC_{\text{mAb}_{0c}}}{dt} = 0 \tag{A11}$$

$$\frac{dC_{\text{mAb}_{\text{a}}\text{NPM}_{\text{b}}}}{dt} = -k_{1'} \cdot C_{\text{mAb}_{\text{a}}\text{NPM}_{\text{b}}} \cdot C_{\text{NPM}} + k_{2'} \cdot C_{\text{mAb}_{\text{ab}}} \cdot C_{\text{NPM}} \tag{A12}$$

$$\frac{dC_{\text{mAb}_{\text{b}}\text{NPM}_{\text{a}}}}{dt} = k_{1'} \cdot C_{\text{mAb}_{\text{ab}}} \cdot C_{\text{NPM}} - k_{2'} \cdot C_{\text{mAb}_{\text{b}}\text{NPM}_{\text{a}}} \cdot C_{\text{NPM}} \tag{A13}$$

$$\frac{dC_{\text{mAb}_{0c}\text{NPM}_{\text{a}}}}{dt} = k_{1'} \cdot C_{\text{mAb}_{\text{a}}} \cdot C_{\text{NPM}} \tag{A14}$$

$$\frac{dC_{\text{mAb}_{0c}\text{NPM}_{\text{b}}}}{dt} = k_{2'} \cdot C_{\text{mAb}_{\text{b}}} \cdot C_{\text{NPM}} \tag{A15}$$

$$\frac{dC_{\text{mAb}_{0c}(\text{NPM})_{\text{ab}}}}{dt} = k_{1'} \cdot C_{mAb_aNPM_b} \cdot C_{\text{NPM}} + k_{2'} \cdot C_{\text{mAb}_{\text{b}}\text{NPM}_{\text{a}}} \cdot C_{\text{NPM}} \tag{A16}$$

$$\frac{dC_{\text{NPM}}}{dt} = -k_{1'} \cdot C_{\text{mAb}_{\text{ab}}} \cdot C_{\text{NPM}} - k_{2'} \cdot C_{\text{mAb}_{\text{ab}}} \cdot C_{\text{NPM}} - k_{1'} \\ \cdot C_{\text{mAb}_{\text{a}}} \cdot C_{\text{NPM}} - k_{2'} \cdot C_{\text{mAb}_{\text{b}}} \cdot C_{\text{NPM}} - k_{1'} \cdot C_{\text{mAb}_{\text{a}}\text{NPM}_{\text{b}}} \\ \cdot C_{\text{NPM}} - k_{2'} \cdot C_{\text{mAb}_{\text{b}}\text{NPM}_{\text{a}}} \cdot C_{\text{NPM}} - k_3 \cdot C_{\text{NPM}} \tag{A17}$$

The rate laws for model 3 are the same without the NPM sink term in equation A17 ($-k_3 \cdot C_{\text{NPM}}$).

Rate laws for model 2:

$$\frac{dC_{\mathrm{mAb_{2c}}}}{dt} = -k_1 \cdot C_{\mathrm{mAb_{2c}}} \cdot C_{\mathrm{NPM}} \tag{A18}$$

$$\frac{dC_{\mathrm{mAb_{1c}}}}{dt} = -k_1 \cdot C_{\mathrm{mAb_{1c}}} \cdot C_{\mathrm{NPM}} \tag{A19}$$

$$\frac{dC_{\mathrm{mAb_{0c}}}}{dt} = 0 \tag{A20}$$

$$\frac{dC_{\mathrm{mAb_{1c}NPM}}}{dt} = k_1 \cdot C_{\mathrm{mAb_{2c}}} \cdot C_{\mathrm{NPM}} - k_2 \cdot C_{\mathrm{mAb_{1c}NPM}} \cdot C_{\mathrm{NPM}} \tag{A21}$$

$$\frac{dC_{\mathrm{mAb_{0c}NPM}}}{dt} = k_1 \cdot C_{\mathrm{mAb_{1c}}} \cdot C_{\mathrm{NPM}} \tag{A22}$$

$$\frac{dC_{\mathrm{mAb_{0c}(NPM)_2}}}{dt} = k_2 \cdot C_{\mathrm{mAb_{1c}NPM}} \cdot C_{\mathrm{NPM}} \tag{A23}$$

$$\frac{dC_{\mathrm{NPM}}}{dt} = -k_1 \cdot C_{\mathrm{mAb_{2c}}} \cdot C_{\mathrm{NPM}} - k_1 \cdot C_{\mathrm{mAb_{1c}}} \cdot C_{\mathrm{NPM}} - k_2 \cdot C_{\mathrm{mAb_{1c}NPM}} \cdot C_{\mathrm{NPM}} \tag{A24}$$
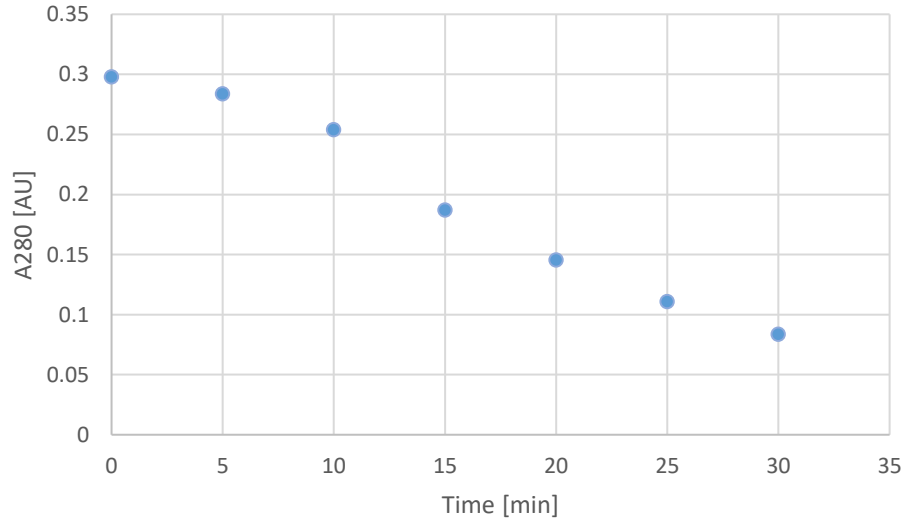
Suppl. Figure 7: Absorption at 280 nm over time measured in Tecan plate reader for a 0.04 mM NPM solution in 50 mM sodium phosphate buffer containing 10% DMSO. The solution was held in a shaken 2 mL Eppendorf Safelock Tube and 200 µL samples were taken every 5 min and measured in a Greiner UV-star microplate.

$$R^2 = 1 - \frac{\sum_i^n (y_i - \hat{y}_i)^2}{\sum_i^n (y_i - \bar{y}_i)^2} \tag{A25}$$

$$SSE = \sum_i^n (y_i - \hat{y}_i)^2 \tag{A26}$$

$$RMSEP = \sqrt{\frac{SSE}{n}} \tag{A27}$$

$$SSE_{\text{tot}} = \sum_j^n SSE_j \tag{A28}$$

$$RMSECV = \sqrt{\frac{SSE_{\text{tot}}}{n}} \tag{A29}$$

$$Q^2 = 1 - \frac{SSE_{\text{tot}}}{\sum_i^n (y_i - \bar{y}_i)^2} \tag{A30}$$